CIRCUIT MODELS WITH MIXED LUMPED AND DISTRIBUTED ELEMENTS FOR PASSIVE ONE-PORT DEVICES

METİN ŞENGÜL

IŞIK UNIVERSITY
2006

CIRCUIT MODELS WITH MIXED LUMPED AND DISTRIBUTED ELEMENTS FOR PASSIVE ONE-PORT DEVICES

METİN ŞENGÜL

Submitted to the Graduate School of Science and Engineering

in partial fulfillment of the requirements for the degree of

Doctor of Philosophy

in

Electronics Engineering

IŞIK UNIVERSITY
2006

CIRCUIT MODELS WITH MIXED LUMPED AND DISTRIBUTED ELEMENTS FOR PASSIVE ONE-PORT DEVICES

APPROVED BY:

Prof. Ahmet AKSEN   Işık University
(Thesis Supervisor)

Prof. Sıddık B. YARMAN   Istanbul University
(Thesis Supervisor)

Prof. Yorgo ISTEFANOPULOS   Işık University

Prof. Avni MORGÜL   Boğaziçi University

Prof. Ercan TOPUZ   Istanbul Technical University

Assoc. Prof. Uluğ BAYAZIT   Işık University

APPROVAL DATE: 23 January 2006

CIRCUIT MODELS WITH MIXED LUMPED AND DISTRIBUTED ELEMENTS
FOR PASSIVE ONE-PORT DEVICES

Abstract

In this thesis, to model measured data obtained from an actual passive one-port device, a circuit modeling method with mixed lumped and distributed elements is proposed. Namely, measured data is modelled by means of its Darlington equivalent, in other words, as a lossless two-port terminated with a resistance. Two network topologies are examined. The first topology is ladder networks connected with unit elements and the second one is cascaded separate lumped and distributed networks. In the proposed modeling method, analytic expression of the input reflection coefficient of the two-port model is obtained by using gradient method, and then, after synthesizing this two-variable function, the model is reached. Thus, for the first time in the literature, a two-variable circuit modeling method is presented.

PASİF TEK KAPILILARIN KARIŞIK TOPLU VE DAĞILMIŞ ELEMANLI
DEVRE MODELLERİ

Özet

Bu doktora tezinde, fiziksel, pasif tek kapılı bir devreye/elemana ilişkin, bir frekans bandında ölçülmüş saçılma parametresi verisinin, bir direnç ile sonlandırılmış kayıpsız, karışık toplu ve dağılmış elemanlar içeren iki kapılı bir devre ile modelleme yöntemi önerilmiştir. İncelenen model topolojilerinden birincisi, birim elemanlarla bağlanmış merdiven devreler, diğeri ise ardarda bağlanmış sadece toplu ve sadece dağılmış elemanlar içeren devrelerdir. Önerilen modelleme yönteminde, gradyan metodundan yararlanılarak, iki kapılı kayıpsız modelin giriş saçılma parametresinin analitik ifadesi elde edilmiş, daha sonra, bu iki-değişkenli analitik giriş fonksiyonu sentezlenerek modele ulaşılmıştır. Böylece literatüre ilk kez iki-değişkenli devre modelleme yöntemi sunulmaktadır.

To my mother Gülhanım Şengül

and

My fiancée Melek Yılmaz

Acknowledgements

Table of Contents

List of Tables

List of Figures

List of Symbols

σ : Real part of complex frequency variable p

ω : Imaginary part of complex frequency variable p

λ : Richards variable, $\lambda = \tanh p\tau = \Sigma + j\Omega$

τ : Delay length of a Unit Element

Σ : Real part of Richards variable

Ω : Imaginary part of Richards variable

∇ : Del operator

Γ_{in} : Input reflection coefficient

E_r : Dielectric constant

E_e : Effective dielectric constant

f_n : Normalization frequency

I : Unity matrix

p : Complex frequency variable, $p = \sigma + j\omega$

P_d : Dissipated power

$R(p)$: Real part of $Z(p)$ impedance

R_L : Real part of load impedance

R_S : Real part of source impedance

R_n : Normalization resistance

S : Scattering matrix of a lossless two-port

T : Transfer scattering matrix of a lossless two-port

t : Thickness of metal conductor on the substrate

Th	: Height of substrate
$X(p)$	: Imaginary part of $Z(p)$ impedance
X_L	: Imaginary part of load impedance
X_S	: Imaginary part of source impedance
W	: Width of the metal conductor on the substrate
$Z(p)$	: Impedance as a function of complex variable p
Z_C	: Characteristics impedance
Z_{in}	: Input impedance
Z_L	: Load impedance
Z_S	: Source impedance
$\det[\cdot]$	: Determinant of a matrix
$Ev\{\cdot\}$	: Even part of a polynomial
$Im\{\cdot\}$	: Imaginary part of a complex number
$Max\{\cdot\}$	: Maximum value of $\{\cdot\}$
$Re\{\cdot\}$	: Real part of a complex number
$\dfrac{\partial(\cdot)}{\partial x}$	: Partial derivative with respecto to x
$\lvert \cdot \rvert$	: Magnitude of a complex number
$(\cdot)^*$	: Conjugate of a complex number
$(\cdot)^T$	: Transpose of a matrix or a vector
$(\cdot)^{*T} = (\cdot)^+$	: Conjugate transpose of a matrix or a vector
$(\cdot)_*$	: Paraconjugate of a complex variable polynomial

List of Abbreviations

ADS   : Advanced design system

AWR   : Advanced wave research

BR   : Bounded real

CPS   : Coplanar strip line

CPW   : Coplanar waveguide

HFSS   : High frequency structure simulator

LHP   : Left half plane

LPLU   : Low-pass ladder network connected with UEs

MIC   : Monolithic integrated circuit

PRF   : Positive real function

RFT   : Real frequency technique

RHP   : Right half plane

TL   : Transmission line

TPG   : Transducer power gain

UE   : Unit element

VLSI   : Very large scale integration

Chapter 1
Introduction

In communication systems design, one of the most common problems is to obtain circuit models of the components that are defined by numerical data. Especially, in the systems working at microwave frequencies, front-end, inter-stage and back-end blocks such as high-frequency transistors, antennas and amplifiers are characterized by their measured data. In such high frequency systems that contain these kinds of blocks, to design filter and matching circuits by using the known analytic and semi-analytic methods to control the power flow between the stages, it is necessary to model the numerically defined components by realizable circuit functions or circuit components. From this point of view, to be able to use the present analytic design methods, it is very important to model the numerically defined devices via lossy or lossless components.

One of the typical fields that needs circuit modeling is the broadband impedance matching circuit design [1-3]. In this problem, it is desired to obtain a lossless two-port network between the given source and the load to transfer maximum power over the possible broadest frequency band [4-7]. Here, source and load impedances can be regarded as complex one-port networks and they are defined by numerical data. In impedance matching problem, power transfer level between source and load can be determined via Analytic Gain-Bandwidth Theory [1,8-11]. To be able to use this theory, it is necessary to know the one-port models of the complex source and load impedances.

In literature, there are valuable works about data modeling [12-16]. But, because of the difficulties in modeling by the existing methods in literature and the lack of

1

accuracy in matching problems, numerical or semi-analytic computer aided methods which use numerically defined loads are proposed. The method called Real Frequency Technique (RFT), developed by Carlin [11] and Yarman [17], is improved by many researchers and overcame the difficulties in modeling that is inevitable in analytic methods [18-27]. But, new, efficient and accurate data modeling and matching network design via analytic methods are unanswered fundamental problems for researchers.

In practice, a load can be defined by the amplitude-phase or real-imaginary pairs of impedance or reflection parameters measured in the desired frequency band. While modeling these kinds of numerical data, realizability conditions of circuit functions must be considered. In this work, a physical device defined by numerical data is modeled as a lossy one-port or a lossless two-port network (Darlington equivalent [28]).
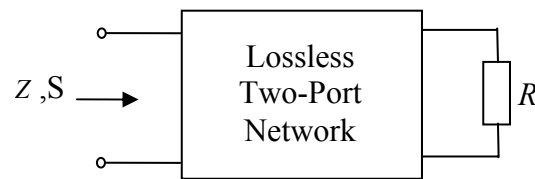
Figure 1.1 Darlington equivalent network.

In literature, two methods are widely used to model the given impedance data:

1. A network topology is selected and the best suitable components values are designated.
2. An impedance or reflection function which is suitable for the data is determined and the model is obtained by synthesizing the function.

In the first method, after selecting the network topology, an optimization tool is used to define the suitable component values [29,30]. Although this is a very simple and straightforward method, it contains some difficulties: Optimization process is highly nonlinear with respect to the component values, can reach a local minimum or can diverge. So to get a satisfactory result after the optimization process, initial values must be selected properly. But it is not so easy to get suitable initial values.

In addition to this difficulty, what is the network topology for the given data? This is not clear. So the modeler will try lots of network topologies and select the best suitable one. Or the problem will be unanswered.

Lots of methods are proposed to model the given impedance or reflection data. In the simplest one, impedance data are represented by a rational function and the coefficients of the function are determined by interpolation. Such a rational function $Z(p)$ is given in (1.1),

$$Z(p) = \frac{\sum_{i=0}^{n-1} a_i p^i}{\sum_{i=0}^{n-1} b_i p^i} \tag{1.1}$$

where $p = \sigma + j\omega$ is the usual complex frequency variable, a_i and b_i $(i = 0,1,\ldots,(n-1))$ are positive real coefficients. But at the end of this method, a positive real function cannot be reached.

In [31], two modeling tools are given. These methods use input impedance or scattering parameters of the device. In the first method, called Immittance Approach, impedance or admittance data are used. Real part of the input impedance is approximated by a minimum reactance function, then after removing minimum reactive data, the remaining imaginary data is modelled by a Foster function. In the second method, called Reflection Parameter Approach, measured reflection coefficient data are modelled by a bounded real function.

All the modeling methods in the literature use only lumped (or distributed) elements in the models. So in this study, the objective is to develop new modeling methods which use mixed lumped and distributed elements in the models.

In the second chapter of this dissertation, some fundamental network theoretical concepts relevant to this study are reviewed in a brief manner.

In Chapter 3, after discussing modeling concept and gradient method, proposed reflection coefficient based method to obtain mixed models for passive one-port devices is explained.

In Chapter 4, algorithms, flow charts and numerical aspects of the proposed modeling method are given.

Chapter 5 is devoted to the applications of the mixed modeling method. To illustrate the utilization of the method, antenna modeling, lumped to mixed filter transformation and single stage microwave amplifier design examples are examined.

Chapter 2

Fundamental Properties of Lossless Two-Ports

Circuit components can be characterized as having two or more terminals. Components that are connected together in some manner are known as networks. In Figure 2.1, a network and its external terminals which provide access to the network can be seen. Generally a mathematical representation determined from the external terminals is interested and used to predict the response for any source or load connected to the network.
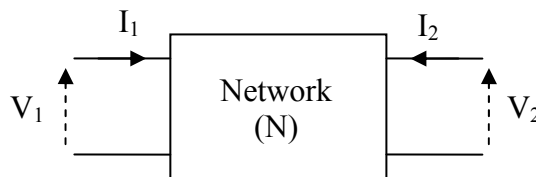
Figure 2.1 General four-terminal network.

The pair of external terminals used to connect a termination is known as a port, and a network with n ports is named an n-port network. The n-port network does not necessarily have 2n terminals; a terminal can be common to more than one port. The voltage and current definition at each port is shown in Figure 2.1.

2.1 Scattering Parameters

The network parameters (such as Z or Y parameters) require open and short circuits to obtain the coefficients. But at higher frequencies, it is difficult to realize an open or short circuit, and the accuracy of any measurements is dependent on how well the

terminations can be realized. In addition, many active devices oscillate at open and short circuit terminations, and any measurements made under these conditions are meaningless.

A useful network representation developed to characterize microwave circuits is scattering, or S-parameters. The S-parameters can be measured using any convenient termination. Perhaps the most important feature is that these parameters can be measured at very high frequencies accurately.
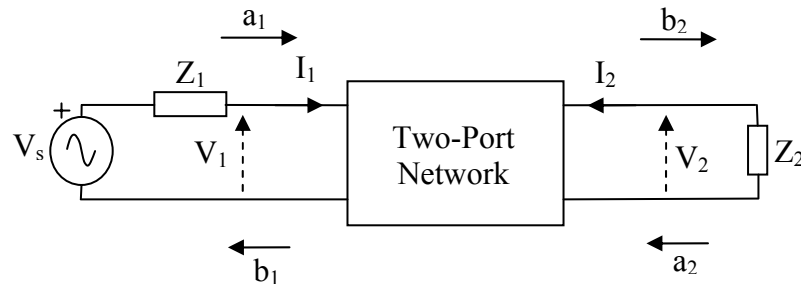
Figure 2.2 General two-port network [32].

Figure 2.2 shows a two-port network which is driven at port 1 by a $Z_1\Omega$ voltage source and terminated at port 2 by a $Z_2\Omega$ load. Z_1 and Z_2, are known as the reference impedances and can be any value, although 50Ω is the most common value. The voltage and current definitions are shown in Figure 2.2, and two new parameters which are functions of V_i, I_i and Z_i can be defined as [32]

$$a_i = \frac{V_i + Z_i I_i}{2\sqrt{|\mathrm{Re}\,Z_i|}}$$

(2.1.a)

and

$$b_i = \frac{V_i - Z_i^* I_i}{2\sqrt{|\mathrm{Re}\,Z_i|}}$$

(2.1.b)

6

where Z_i^* is the complex conjugate of Z_i, and $\mathrm{Re}\, Z_i$ is the real part of the reference impedance. If b_i is selected as the dependent variable and a_i as the independent variable, it can be written for the two-port in Figure 2.2

$$\begin{aligned}
b_1 &= S_{11}a_1 + S_{12}a_2 \\
b_2 &= S_{21}a_1 + S_{22}a_2
\end{aligned} \tag{2.2}$$

(2.2) can be expressed in matrix form as [32],

$$b = S\,a \tag{2.3}$$

for any n-port network.

The coefficients of the S-matrix can be evaluated by setting $a_2 = 0$ and $a_1 = 0$, then solving for S_{11}, S_{21} and S_{12}, S_{22} respectively. Using Figure 2.2, it is seen that the output voltage is $(-I_2 Z_2)$. Then if this is substituted into (2.1.a):

$$a_2 = \frac{V_2 + Z_2 I_2}{2\sqrt{|\mathrm{Re}\, Z_2|}} = \frac{-I_2 Z_2 + Z_2 I_2}{2\sqrt{|\mathrm{Re}\, Z_2|}} = 0$$

Namely a_i is always zero at any port not connected to a source and terminated with the reference impedance. Thus, the S-parameters of any network can easily be measured by connecting a source to one port at a time.

From transmission line theory, it can be written that [32]

$$V_i = V_{iI} + V_{iR}$$

and

7

$$I_i = \frac{V_{iI}}{Z_i} - \frac{V_{iR}}{Z_i}$$

where the subscripts I and R denote the incident and reflected components of voltage, respectively. If Z_i is assumed to be real, and substituting into (2.1.a)

$$a_i = \frac{V_i + Z_i I_i}{2\sqrt{|\mathrm{Re}\,Z_i|}} = \frac{(V_{iI} + V_{iR}) + Z_i\left(\dfrac{V_{iI}}{Z_i} - \dfrac{V_{iR}}{Z_i}\right)}{2\sqrt{|\mathrm{Re}\,Z_i|}} = \frac{V_{iI}}{\sqrt{|\mathrm{Re}\,Z_i|}}$$

and into (2.1.b)

$$b_i = \frac{V_i - Z_i^* I_i}{2\sqrt{|\mathrm{Re}\,Z_i|}} = \frac{(V_{iI} + V_{iR}) - Z_i^*\left(\dfrac{V_{iI}}{Z_i} - \dfrac{V_{iR}}{Z_i}\right)}{2\sqrt{|\mathrm{Re}\,Z_i|}} = \frac{V_{iR}}{\sqrt{|\mathrm{Re}\,Z_i|}}$$

which shows that a_i is a function of the incident voltage and b_i is a function of reflected voltages. It is also can be seen that both parameters are the square root of power, namely

$$|a_i|^2 = \frac{|V_{iI}|^2}{|\mathrm{Re}\,Z_i|} \qquad |b_i|^2 = \frac{|V_{iR}|^2}{|\mathrm{Re}\,Z_i|}.$$

Thus, a_i is an incident wave, $|a_i|^2$ is incident power, b_i is a reflected wave, and $|b_i|^2$ is reflected power. From (2.2), it is seen that the reflected wave at each port is the sum of the incident waves from all ports modified by coefficients of the S-parameter matrix.

$|a_1|^2$ can be written as by using Figure 2.2,

$$|a_1|^2 = \left| \frac{V_1 + Z_1 \left(\frac{V_s - V_1}{Z_1} \right)}{2\sqrt{|\mathrm{Re}\, Z_1|}} \right|^2 = \frac{|V_s|^2}{4|\mathrm{Re}\, Z_1|}$$

and it is found that $|a_1|^2$ is the available power from the source. If the reflected power is subtracted from the available power from the source, it is obtained that

$$
\begin{aligned}
|a_i|^2 - |b_i|^2 &= a_i a_i^* - b_i b_i^* \\
&= \frac{(V_1 + Z_1 I_1)(V_1^* + Z_1^* I_1^*)}{4|\mathrm{Re}\, Z_1|} - \frac{(V_1 - Z_1^* I_1)(V_1^* - Z_1 I_1^*)}{4|\mathrm{Re}\, Z_1|} \\
&= \frac{2Z_1 (V_1 I_1^* + V_1^* I_1)}{4|\mathrm{Re}\, Z_1|} \\
&= \frac{Z_1}{|\mathrm{Re}\, Z_1|} \mathrm{Re}(V_1 I_1^*)
\end{aligned}
$$

which is the delivered power to the network. When the source is connected to port 1, $|a_2|^2$ is zero and $|b_2|^2$ can be written as

$$|b_2|^2 = \left| \frac{V_2 - Z_2^* I_2}{2\sqrt{|\mathrm{Re}\, Z_2|}} \right|^2 = |\mathrm{Re}\, Z_2||I_2|^2$$

which is the delivered power to the load.

S-parameter matrix coefficients (S_{ij}) are all ratios of reflected-to-incident waves, which is a very convenient representation for microwave circuits. When a generator with available power $|a_i|^2$ is connected to port i, a at port i and b at all ports can be measured. At port i,

$$S_{ii} = \frac{b_i}{a_i} = \frac{V_i - Z_i^* I_i}{V_i + Z_i I_i} = \frac{Z_{in} I_i - Z_i^* I_i}{Z_{in} I_i + Z_i I_i} = \frac{Z_{in} - Z_i^*}{Z_{in} + Z_i}$$

where Z_{in} is the input impedance at port i. Thus,

$$S_{ii} = \Gamma_{in} = \text{Reflection coefficient at port } i$$

and

$$|S_{ii}|^2 = \frac{|b_i|^2}{|a_i|^2} = \text{Reflected power from the input / available power from the source} =$$

Return loss at port i.

At any port j, where $i \neq j$,

$$|S_{ji}|^2 = \frac{|b_j|^2}{|a_i|^2} = \text{Delivered power to the load / Available power from the source} =$$

Transducer power gain.

According to the conservation of energy, the total power incident at all ports of a passive network equal the power absorbed by the network, plus power emerging from the network. So the power dissipated in the network is the difference between incident and reflected power, namely $|a_i|^2 - |b_i|^2$. Total dissipated power can be written as the sum of the dissipated power at each port [32]:

$$P_d = \sum_{i=1}^{n} \left(|a_i|^2 - |b_i|^2 \right) = \sum_{i=1}^{n} a_i a_i^* - \sum_{i=1}^{n} b_i b_i^*, \text{ or}$$

$$P_d = \left[a^* \right]^T a - \left[b^* \right]^T b \qquad\qquad (2.4.a)$$

where $[a^*]^T$ and $[b^*]^T$ are obtained by replacing each element of a and b with its complex conjugate and then by transposing. From (2.3),

$$b = S\,a$$

$$[b^*]^T = [S^*]^T [a^*]^T$$

which is substituted into (2.4.a):

$$P_d = [a^*]^T\,a - [S^*]^T [a^*]^T\,S\,a$$

and then rewritten as

$$P_d = [a^*]^T \left\{ I - [S^*]^T\,S \right\} a \qquad\qquad (2.4.b)$$

where I is the unit matrix. The term within braces in (2.4.b) determines whether the dissipated power is positive or negative. This term can be defined as [32]

$$Q = I - [S^*]^T\,S \qquad\qquad (2.5)$$

which is known as the dissipation matrix. When Q is nonnegative, the network is passive, or the dissipated power is greater than or equal to zero.

For a passive two-port [32],

$$|S_{11}|^2 + |S_{21}|^2 \le 1 \qquad\qquad (2.6.a)$$

and

$$|S_{22}|^2 + |S_{12}|^2 \le 1 \qquad\qquad (2.6.b)$$

Also if the two-port is lossless, then the dissipated power is zero and (2.5) can be written as

$$[S^*]^T S = I$$

or

$$\begin{bmatrix} S_{11}^* & S_{21}^* \\ S_{12}^* & S_{22}^* \end{bmatrix} \begin{bmatrix} S_{11} & S_{12} \\ S_{21} & S_{22} \end{bmatrix} = \begin{bmatrix} 1 & 0 \\ 0 & 1 \end{bmatrix}$$

which can be expanded as

$$S_{11}^* S_{11} + S_{21}^* S_{21} = 1 \qquad\qquad (2.7.a)$$

$$S_{11}^* S_{12} + S_{21}^* S_{22} = 0 \qquad\qquad (2.7.b)$$

$$S_{12}^* S_{11} + S_{22}^* S_{21} = 0 \qquad\qquad (2.7.c)$$

$$S_{12}^* S_{12} + S_{22}^* S_{22} = 1 \qquad\qquad (2.7.d)$$

From (2.7), it can be shown that

$$S_{11} S_{11}^* = S_{22} S_{22}^* \qquad\qquad (2.8.a)$$

$$S_{12} S_{12}^* = S_{21} S_{21}^* \qquad\qquad (2.8.b)$$

From these relations it can be concluded that the magnitudes of reflection and transmission coefficients are bounded by unity, i.e. $|S_{ji}| \leq 1$ for $p = j\omega$.

As a result of the discussions above, the fundamental properties of the scattering matrix of a lossless two-port can be summarized as [6,33]:

1. The elements of S-matrix are rational and real for real p.
2. S-matrix is analytic in $\operatorname{Re} p \geq 0$.

3. S-matrix is paraunitary and satisfies $S_*^T S = I \quad \forall p$.

4. If S-matrix is symmetric $(S_{12} = S_{21})$, then the lossless two-port is reciprocal.

One can easily obtain the corresponding impedance and admittance matrices, if the scattering matrix satisfies all the conditions summarized above and the realizability theory in immittance formalism can be established. It is usually expressed based on Darlington's approach and expressed via the driving point functions of a two-port terminated by a resistance at the output. At this point, it is meaningful to give the following fundamental properties with respect to the driving point reflectance and impedance functions [6,33]:

- The function $S_1(p)$ is said to be bounded real (BR) if

  1. $S_1(p)$ is real for p real,

  2. $S_1(p)$ is analytic in $\text{Re}\, p > 0$,

  3. $|S_1(j\omega)| \leq 1$ for all ω.

- By using the bounded real reflection function ($S_1(p)$) of a resistively terminated two-port defined above, the corresponding driving point input impedance is given by

$$Z_1(p) = \frac{1 + S_1(p)}{1 - S_1(p)} \tag{2.9}$$

  This impedance function is a positive real function (PRF.) and satisfies the followings,

  1. $Z_1(p)$ is real for p real,

  2. $\text{Re}\, Z_1(p) > 0$ for $\text{Re}\, p > 0$.

It can be concluded for the realizability of driving point functions as a resistively terminated two-port network that,
A rational positive real impedance function (or a bounded real reflection function) is realizable as a resistively terminated lossless two-port.

In dealing with cascade connected networks, usually the scattering transfer matrix is used instead of the scattering matrix. After rearranging the port variables a_i and b_i in the scattering equations (2.2), it is obtained that

$$\begin{bmatrix} b_1 \\ a_1 \end{bmatrix} = \begin{bmatrix} T_{11} & T_{12} \\ T_{21} & T_{22} \end{bmatrix} \begin{bmatrix} a_2 \\ b_2 \end{bmatrix} \tag{2.10}$$

which defines the scattering transfer matrix T. The elements of T-matrix are related to the elements of S-matrix as follows:

$$T_{11} = -\frac{\det S}{S_{21}}, \quad T_{21} = -\frac{S_{22}}{S_{21}}, \quad T_{12} = \frac{S_{11}}{S_{21}}, \quad T_{22} = \frac{1}{S_{21}} \tag{2.11}$$

where $\det[S]$ denotes the determinant of the S-matrix. From the definitions given above, the elements of the scattering transfer matrix for a lossless two-port are rational functions, and if the two-port is reciprocal as well, the reciprocity condition $S_{12} = S_{21}$ leads to $\det[T] = 1$.

2.2 Canonic Representation of Scattering Matrix and Scattering Transfer Matrix

Scattering matrix can be represented by using three canonic polynomials. For a lossless two-port, the canonic forms of the scattering matrix and the scattering transfer matrix in terms of these polynomials are given by

$$S = \frac{1}{g} \begin{pmatrix} h & \sigma f_* \\ f & -\sigma h_* \end{pmatrix}, \quad T = \frac{1}{f} \begin{pmatrix} \sigma g_* & h \\ \sigma h_* & g \end{pmatrix} \tag{2.12}$$

where $f_* = f(-p)$ means the paraconjugate of a real function. The polynomials f, g and h have the following properties [6,33]:

- $f = f(p), g = g(p),$ and $h = h(p)$ are real polynomials in the complex frequency p.

- g is a strictly Hurwitz polynomial.

- f is monic, i.e., its leading coefficient is equal to unity.

- f, g and h polynomials are related by the condition

$$g\, g_* = h\, h_* + f\, f_* \qquad\qquad (2.13)$$

- σ is a constant $(\sigma = \pm 1)$.

If the two-port is reciprocal, then the polynomial f is either even or odd. In this case, $\sigma = +1$ if f is even, and $\sigma = -1$ if f is odd. As a result, for a lossless reciprocal two-port

$$\sigma = \frac{f_*}{f} = \pm 1 \qquad\qquad (2.14)$$

and the relation (2.13) can be modified as

$$g\, g_* = h\, h_* + \sigma f^2 \qquad\qquad (2.15)$$

2.3 Distributed Networks with Commensurate Lines

At microwave frequencies, since the conventional lumped elements have realization problems, distributed networks composed of transmission lines are employed. Distributed circuit design with transmission line elements is a well known topic in the literature.

In distributed network synthesis, most approaches are based on the use of single length of transmission lines which are called unit elements (UE). Originally due to Richards [34], most of the design methods for microwave filters and matching networks employ finite homogenous transmission lines of commensurable lengths as ideal UEs. Here by commensurate, it must be understood that all line lengths in the

network are multiples of the UE length. If one uses the following transformation, the distributed networks composed of commensurate lengths of transmission lines (UEs) could be analyzed or synthesized as lumped element networks [34]

$$\lambda = \tanh p\tau \qquad\qquad (2.18)$$

where τ is the delay of the transmission line, p is the usual complex frequency variable ($p = \sigma + j\omega$) and λ is called as Richards variable ($\lambda = \Sigma + j\Omega$). Under this transformation, the mapping of the λ-plane onto p-plane is periodic. As a result, the frequency response of a distributed network consisting of commensurate transmission lines is periodic with respect to the original real frequency ω.

It is important to express that the right half plane (RHP) and the left half plane (LHP) in the p-domain are directly mapped onto the corresponding ones in λ-domain and vice versa. Namely; $\{\operatorname{Re} p > 0 \leftrightarrow \operatorname{Re} \lambda > 0\}$ and $\{\operatorname{Re} p < 0 \leftrightarrow \operatorname{Re} \lambda < 0\}$. Therefore, all the realizability conditions which are based on the RHP criteria are kept the same in the λ-domain.

The short circuited transmission lines can be regarded as inductors and the open circuited transmission lines as capacitors (if the length of the line is shorter than quarter wavelength) in λ domain under Richards transformation (Figure 2.3). So driving point impedance functions of the networks containing short circuited or open circuited transmission lines positive real rational functions of λ. Eventually, synthesis methods of lumped reactance two-ports can be used for the networks composed of such commensurate transmission lines. A cascade connected

transmission line has no lumped counterpart and therefore must be treated separately. Therefore, the two-port equivalent of a transmission line in λ-domain is taken as a new element called the Unit Element (UE).
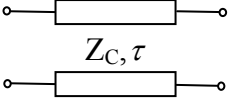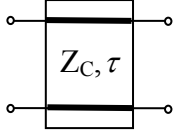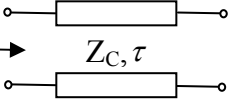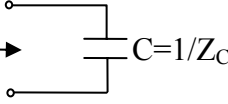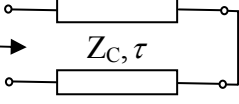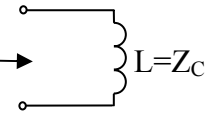
Original frequency domain (p)	Richards domain ($\lambda = \tanh p\tau$)
Transmission Line (TL) Z_C, τ	Unit Element (UE) Z_C, τ
Open ended TL Z_C, τ Z=Z$_C$coth $p\tau$	λ-Capacitor C=1/Z$_C$ Z=1/ λ C
Short ended TL Z_C, τ Z=Z$_C$tanh $p\tau$	λ-Inductor L=Z$_C$ Z= λ L

Figure 2.3 Transmission line elements and their counterparts in Richards domain [6].

The functions of the networks composed of UEs are obviously the functions of λ. Indeed, the input impedance $Z(\lambda)$ of a UE terminated with an impedance $Z^{'}(\lambda)$ can be given by

$$Z(\lambda) = Z_0 \frac{Z^{'}(\lambda) + \lambda Z_0}{\lambda Z^{'}(\lambda) + Z_0} \qquad (2.19)$$

which is a rational function if $Z^{'}(\lambda)$ is rational. So, the following result can be concluded [6,33]:

- The driving point impedance of a distributed network composed of cascaded UEs is a positive real rational function of λ.

According to the Richards theorem, it can be said that a UE of characteristic impedance $Z_0 = Z(1)$ may always be extracted from the positive real impedance function $Z(\lambda)$ leaving a remainder

$$Z^{'}(\lambda) = Z(1)\frac{Z(\lambda) - \lambda Z(1)}{Z(1) - \lambda Z(\lambda)}$$
(2.20)

which is also a positive real function and the degree of $Z^{'}(\lambda)$ is not higher than that of $Z(\lambda)$ (Figure 2.4). Moreover, if $EvZ(\lambda)\big|_{\lambda=1} = 0$, then the degree of $Z^{'}(\lambda)$ is one less than that of $Z(\lambda)$.

A similar statement of the theorem is also available for the input reflection function [35].
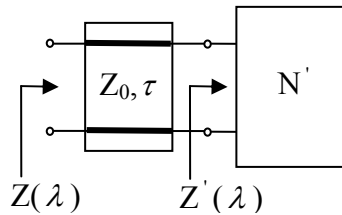
Figure 2.4 Application of Richards theorem.

2.4 Networks with Mixed, Lumped and Distributed Elements

Especially at microwave and millimeter wave frequencies, use of lumped elements alone in the circuit realization presents serious implementation problems, because of the difficulties regarding the physical interconnection of components and the associated parasitic effects. Therefore, it is inevitable to use distributed structures composed of transmission lines between the lumped elements. Since these transmission lines are also considered in the design process, the performance of the network will be better. So it can be concluded that the cascade of reciprocal two-port networks connected by means of equidelay ideal transmission lines constitutes a useful model.

Designing mixed lumped and distributed element networks has gained a great deal of importance for a long time in the literature. But, a complete design theory for the mixed element networks still does not exist. Although some classical network concepts have been extended to cover some classes of mixed element two-ports, the problem of approximation and synthesis of arbitrary mixed element networks could not be resolved completely.

In literature, a special interest has been devoted to the mixed element networks composed of lumped reactances and ideal uniform lossless transmission. That is, the structure of interest consists of cascaded lossless lumped two-ports connected with ideal transmission lines (UEs) [6].

Microwave filters and matching networks composed of this kind of cascaded structures have obviously the properties of both lumped and distributed networks and offer advantages over those designed with lines or lumped elements alone. One of the most important advantages is the harmonic filtering property of the mixed structure. Furthermore, the required physical circuit interconnections are provided by nonredundant transmission line elements which also contribute to the filtering performance of the structure.

2.5 Two-variable Characterization of Cascaded Lumped and Distributed Two-ports

In many engineering problems, multivariable complex functions can be used to describe system functions. A typical example can be given as designing microwave lossless two-ports composed of mixed lumped-distributed elements. For example, a microwave filter or a matching network may include equal length transmission lines as well as lumped elements. In this case, description of the distributed sections can be made in terms of Richards variable λ, ($\lambda = \tanh p\tau$), whereas the lumped sections are described in terms of the complex frequency variable p. In mathematical terms, description of lossless two-ports constructed with lumped and

equal length transmission lines can be made by using complex two-variable functions. In fact, since the complex variables p and λ are not independent, the problem is actually a single variable one. However, if one assumes that p and λ are independent variables, then the problem can be treated using multivariable functions [38].

A lossless two-port composed of cascade connected simple lumped sections and equal length distributed sections can be described in terms of two-variable scattering parameters. Let us represent the scattering matrix of the lossless two-port as $S(p,\lambda)$ and the scattering transfer matrix as $T(p,\lambda)$. The canonic form of the matrices $S(p,\lambda)$ and $T(p,\lambda)$ can be expressed in terms of two-variable polynomials $f(p,\lambda)$, $g(p,\lambda)$ and $h(p,\lambda)$ [39];

$$S(p,\lambda) = \frac{1}{g(p,\lambda)}\begin{bmatrix} h(p,\lambda) & \sigma f(-p,-\lambda) \\ f(p,\lambda) & -\sigma h(-p,-\lambda) \end{bmatrix}$$

(2.22)

$$T(p,\lambda) = \frac{1}{f(p,\lambda)}\begin{bmatrix} \sigma g(-p,-\lambda) & h(p,\lambda) \\ \sigma h(-p,-\lambda) & g(p,\lambda) \end{bmatrix} \qquad (2.23)$$

The canonic polynomials satisfy the following properties;
- g, h and f are real polynomials of the complex variables p and λ.
- g is a scattering Hurwitz polynomial, [39-41], i.e.
    1. $g(p,\lambda) \neq 0$ for $\mathrm{Re}\{p,\lambda\} > 0$,
    2. $g(p,\lambda)$ is relatively prime with $g(-p,-\lambda)$.
- f is monic and σ is a constant $(|\sigma| = 1)$.
- f, g and h are related by
    $$g(p,\lambda)g(-p,-\lambda) = h(p,\lambda)h(-p,-\lambda) + f(p,\lambda)f(-p,-\lambda) \qquad (2.24)$$
- If the two-port includes cascaded UEs, then f is defined as
    $$f(p,\lambda) = f(p)f(\lambda) = f(p)(1-\lambda^2)^{n_\lambda/2} \qquad (2.25)$$
    where n_λ is the number of UEs.

Chapter 3
Gradient Method Based Mixed Modeling

For many communications engineering applications, circuit models for measured data obtained from physical devices or subsystems is inevitable. In practice, class of problems, which demand circuit models for the measured data, may be categorized as follows.

Problems of Type-I "Characterization": *The* c*haracterization or assessment of the electrical behavior of physical devices utilized in communication systems such as minimum noise figure level, maximum power transfer capability etc.* For this category, the model for the device or the system is essential [42].

Problems of Type-II "Design": The design of an analog/digital communication system such as antenna matching networks, microwave amplifiers for mobile or wireless communication systems etc. For these problems, depending on the design method, linear or non-linear circuit models for active and passive devices or sub-systems may be required [43].

Problems of Type-III "Simulation": *Fast simulation of high-speed/high-frequency analog/digital communication sub-systems to be manufactured on VLSI chips.* In this category, commercially available simulation packages such as Spice, Super Compact etc., are employed. Depending on the complexity of the integrated circuits, simulation time may take several days. Therefore, in these type of problems, it is usually preferred to come up with circuit models for interconnects and active and passive devices to speed up the numerical computations [44-47].

It will be proper to clearly identify the above categories by examples.

In designing high-speed/high-frequency communication systems, one of the major issues is to determine the physical limitations of the commercially available devices for power transfer. The passive one-port device is regarded as a dissipative complex termination. This termination may be described by measured either immittance or reflectance data over the frequencies of interest. Precise theoretical power transfer limitations of a physical device may be determined by accessing the Analytic Gain Bandwidth Theory [1,11,42]. In this case, circuit models for the passive terminations are essential. This is a typical Type-I problem.

The design of a single stage microwave amplifier which employs an active device is a typical Type-II problem. In this problem, one has to determine the optimum source and the load impedances of the active device to optimize the performance of the amplifier. Performance optimization may involve the maximization of the flat transducer power gain (TPG) while minimizing the input voltage standing wave ratio (VSWR) and the noise figure over the prescribed frequency band. For this purpose, the optimum source and the load impedances are computed point by point. Eventually, one has to model the resulting source and the load impedances accordingly to end-up with the front-end and the back-end matching networks as shown in Figure 3.1. Hence, the design of the microwave amplifier for optimum terminations is completed.
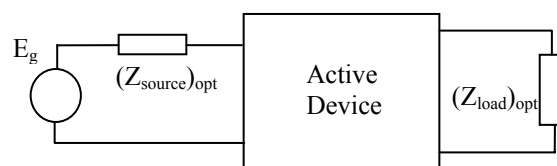
Figure 3.1.a Single stage microwave amplifier.
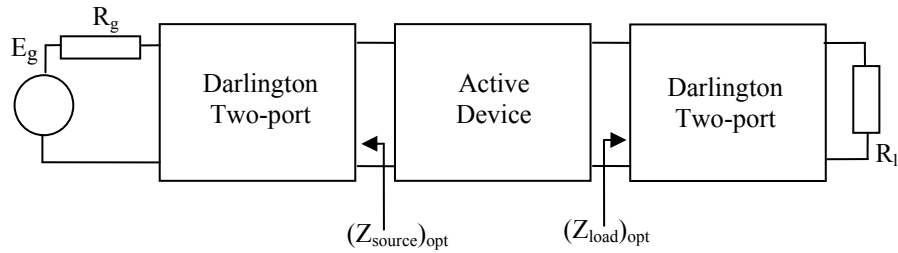
Figure 3.1.b Front-end and back-end matching networks of the amplifier.

Utilizations of circuit model tools are also very important to run fast simulation packages such as ADS, HFSS, Touch Stones, Super-Compact, Microwave Office, Sonnet etc. Simulation of very large networks, those consisting of a large number of nodes is a serious problem in the computer-aided design of integrated circuits. Circuits of this size can typically require several days of CPU time on a work-station for an elegant simulation. However, in many applications, high accuracy in simulation is not required. For problems that require less precision, circuit models can be used. So circuit models for interconnects and solid-state devices become essential to enhance the capability of the commercially available computer packages employed for analysis, design and simulation of Very Large Scale Integrated (VLSI) Circuits, a typical Type-III problem.

There are several modeling techniques available in the literature, which utilize only one type of elements, lumped or distributed, in the circuit topology [48-51].

In practice, however, especially in the microwave discrete, hybrid or monolithic integrated circuit (MIC) designs; the physical realization of ideal lumped and distributed network elements presents serious implementation problems. For a complete characterization of MIC layouts, it is therefore essential to model all the physical parameters and the possible parasitic effects inherent to the implementation process, and to take them into account in the design procedure. This would in turn require the treatment of mixed, lumped and distributed elements in the network design.

In the past, there had been considerable interest in using lumped elements together with transmission lines in the design of microwave circuits. It has long been recognized that mixed element structures incorporating both lumped and distributed circuit elements offer many practical and theoretical advantages over those designed with transmission lines or lumped elements alone. An analytic treatment of the design problem with mixed, lumped and distributed elements, which has not yet been solved analytically, requires the characterization of the mixed element structures using transcendental or multivariable functions.

Therefore, in this thesis, the problem will be defined as:

To model the given reflectance data utilizing two kinds of elements namely, lumped and distributed circuit elements which constitutes a lossless two port in resistive termination. This two-port is called the Darlington equivalent of the physical device [28], Figure 3.2.
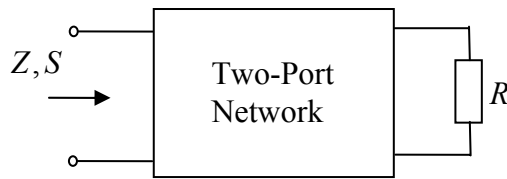
Figure 3.2 Darlington equivalent network.

In the next sections, gradient or steepest descent method is summarized. Then, the proposed methods to model physical devices using mixed lumped and distributed elements are presented. In models, ladder networks connected with unit elements and cascade connected separate lumped and distributed network topologies are used.

3.1 Gradient Method (Steepest Descent Method) [52]

For solving systems of nonlinear equations, Newton's method can be used. Newton's method for approximating the solution p to the single nonlinear equation

$$f(x) = 0 \qquad\qquad (3.1)$$

requires an initial approximation p_0 to p and generates a sequence defined by

$$p_k = p_{k-1} - \frac{f(p_{k-1})}{f'(p_{k-1})}, \qquad \text{for } k \geq 1.$$

(3.2)

Also Newton's method can be modified to find the vector solution $\mathbf{p}$ to the vector equation

$$\mathbf{F(x)} = \mathbf{0}$$

(3.3)

with an initial approximation vector $\mathbf{p}^{(0)}$, where

$$\mathbf{F}(x_1, x_2, \ldots, x_n) = (f_1(x_1, x_2, \ldots, x_n), f_2(x_1, x_2, \ldots, x_n), \ldots, f_n(x_1, x_2, \ldots, x_n))$$
$$i = 1, 2, \ldots, n.$$

,

(3.4)

The advantage of Newton's method for solving systems of nonlinear equations is its speed of convergence once a sufficiently accurate approximation is known. A weakness of the method is that an accurate initial approximation to the solution is needed to ensure convergence. The method of steepest descent (or gradient method) will generally converge only linearly to the solution, namely any starting value will give convergence. The method of gradient determines a local minimum for a multivariable function.

Gradient method for finding a local minimum for an arbitrary function $g(x_1, x_2, \ldots, x_n) = F(f_i(x_1, x_2, \ldots, x_n)), \quad i = 1, 2, \ldots, n$ can be described as follows;

- Evaluate g at an initial approximation $\mathbf{p}^{(0)} = (p_1^{(0)}, p_2^{(0)}, \ldots, p_n^{(0)})$.
- Determine a direction from $\mathbf{p}^{(0)}$ that results in a decrease in the value of g.
- Move an appropriate amount in this direction and call the new value $\mathbf{p}^{(1)}$.
- Repeat the steps with $\mathbf{p}^{(0)}$ replaced by $\mathbf{p}^{(1)}$.

Before describing how to choose the correct direction and the appropriate distance to move in this direction, let's extend the definition "a differentiable single-variable function can have a relative minimum only when the derivative is zero" to multivariable functions:

Let us define the gradient of g at $\mathbf{x} = (x_1, x_2, \ldots, x_n)$, $\nabla g(\mathbf{x})$, by

$$\nabla g(\mathbf{x}) = \left(\frac{\partial g(\mathbf{x})}{\partial x_1}, \frac{\partial g(\mathbf{x})}{\partial x_2}, \ldots, \frac{\partial g(\mathbf{x})}{\partial x_n} \right) \tag{3.5}$$

The gradient for a multivariable function is analogous to the derivative of a single variable function in the sense that a differentiable multivariable function can have a relative minimum at $\mathbf{x}$ only when the gradient at $\mathbf{x}$ is the zero vector. A standard result from the calculus of multivariable functions states that the direction of greatest decrease in the value of g at $\mathbf{x}$ is the direction given by $-\nabla g(\mathbf{x})$.

The object is to reduce $g(\mathbf{x})$ to its minimal value of zero, so given the initial approximation $\mathbf{p}^{(0)}$, one chooses

$$\mathbf{p}^{(1)} = \mathbf{p}^{(0)} - \alpha \nabla g\left(\mathbf{p}^{(0)}\right) \tag{3.6}$$

for some constant $\alpha > 0$.

The problem now reduces to choosing α so that $g\left(\mathbf{p}^{(1)}\right)$ will be significantly less than $g\left(\mathbf{p}^{(0)}\right)$. To determine an appropriate choice for the value of α, one considers the single variable function

$$h(\alpha) = g\left(\mathbf{p}^{(0)} - \alpha \nabla g\left(\mathbf{p}^{(0)}\right)\right) \tag{3.7}$$

The value of α that minimizes h is the value needed for (3.6).

Finding a minimal value for *h* directly would require differentiating *h* and then solving a root-finding problem to determine the critical points of *h*. This procedure is generally too costly. So, if it is possible to get an acceptable solution, it is generally selected as a number between 0 and 1 without finding the exact value of *h*. Now let us apply gradient method to obtain mixed lumped and distributed models for numerically defined passive devices.

3.2 Mixed Modeling via Gradient Method

Assume $S(j\omega)$ is the given reflection coefficient data and $S_{11}(j\omega, j\tan(\omega\tau)) = \dfrac{h(j\omega, j\tan(\omega\tau))}{g(j\omega, j\tan(\omega\tau))}$ is the calculated reflection coefficient of the mixed model. It is desired to have $S(j\omega) = S_{11}(j\omega, j\tan(\omega\tau))$ at the end of the modeling process. So let us define the error between given and calculated reflection coefficients as

$$\varepsilon(j\omega) = S(j\omega) - S_{11}(j\omega, j\tan(\omega\tau)) \tag{3.8}$$

This equation also can be written as

$$\varepsilon(j\omega) = S(j\omega) - S_{11}(j\omega, j\tan(\omega\tau)) = S(j\omega) - \frac{h(j\omega, j\tan(\omega\tau))}{g(j\omega, j\tan(\omega\tau))} \tag{3.9}$$

Let us now write module square of the error

$$|\varepsilon(j\omega)|^2 = \varepsilon(-j\omega)\varepsilon(j\omega)$$
$$= \left(S(-j\omega) - \frac{h(-j\omega, -j\tan(\omega\tau))}{g(-j\omega, -j\tan(\omega\tau))} \right) \left(S(jw) - \frac{h(j\omega, j\tan(\omega\tau))}{g(j\omega, j\tan(\omega\tau))} \right) \tag{3.10}$$

At this step, if gradient method is used to obtain the correct $h(s) = \sum_{k=0}^{n_s} h_k s^k$ values, where n_s specifies the total number of elements in the two-port and the variable $s = \alpha + j\beta$ refers to either the variable p which is associated with the lumped elements or the variable λ which is associated with the cascaded connection of commensurate transmission lines or UEs, then according to (3.6)

$$
\begin{aligned}
h_{i+1}(j\beta) &= h_i(j\beta) - \gamma \, \nabla_{h_i} \left(|\varepsilon_i(j\omega)|^2 \right) \\
&= h_i(j\beta) - \gamma \, \frac{\partial |\varepsilon_i(j\omega)|^2}{\partial h_i(j\beta)}
\end{aligned}
\tag{3.11}
$$

where γ is the step size of the process.

Since the real part of $h(j\beta)$ is an even function and the imaginary part is an odd function, then, the real and the imaginary parts of $h(j\beta)$ are given by

$$
h_R(\beta) = \sum_{k=0}^{m} (-1)^k h_{2k} \beta^{2k}
\tag{3.12a}
$$

where $m = \dfrac{n_s}{2}$ if n_s is even. $m = \dfrac{n_s - 1}{2}$ if n_s is odd, and

$$
h_x(\beta) = \sum_{k=1}^{m} (-1)^{k-1} h_{2k-1} \beta^{2k-1}
\tag{3.12b}
$$

where $m = \dfrac{n_s}{2}$ if n_s is even. $m = \dfrac{n_s + 1}{2}$ if n_s is odd.

Since $h_R(\beta_i)$ and $h_x(\beta_i)$ are numerically specified by (3.12), one can immediately determine the unknown real coefficients of the numerator polynomial $h(s)$ employing the even-odd linear interpolation technique described below over the selected frequencies.

$h(s)$ polynomial can be written as,

$$h(s) = h_0 + h_1 s + h_2 s^2 + \ldots + h_{n_s} s^{n_s}$$
(3.13)

Let us substitute $s = j\beta$ in (3.13), then

$$
\begin{aligned}
h(j\beta) &= h_0 + h_1 j\beta + h_2 (j\beta)^2 + \ldots + h_{n_s} (j\beta)^{n_s} \\
&= (h_0 - h_2 \beta^2 + h_4 \beta^4 - \ldots (-1)^k h_{2k} \beta^{2k}) \\
&\quad + j(h_1 \beta - h_3 \beta^3 + h_5 \beta^5 - \ldots (-1)^{l-1} h_{2l-1} \beta^{2l-1}) \\
&= h_R(\beta) + j h_X(\beta)
\end{aligned}
$$
(3.14)

where $k = 0,1,\ldots,\dfrac{n_s}{2}$ if n_s is even, $k = 0,1,\ldots,\dfrac{n_s - 1}{2}$ if n_s is odd, $l = 1,2,\ldots,\dfrac{n_s}{2}$ if n_s is even, $l = 1,2,\ldots,\dfrac{n_s + 1}{2}$ if n_s is odd.

Unknown coefficients of $h(s)$ polynomial $\{h_0, h_1, h_2, \ldots, h_{n_s}\}$ are obtained by solving the following linear equation sets over n selected frequencies,

$$
\begin{bmatrix}
1 & -\beta_1^2 & \beta_1^4 & \cdots & (-1)^k \beta_1^{2k} \\
1 & -\beta_2^2 & \beta_2^4 & \cdots & (-1)^k \beta_2^{2k} \\
\vdots & \cdots & & \ddots & \vdots \\
1 & -\beta_n^2 & \beta_n^4 & \cdots & (-1)^k \beta_n^{2k}
\end{bmatrix}
\begin{bmatrix}
h_0 \\ h_2 \\ \vdots \\ h_{2k}
\end{bmatrix}
=
\begin{bmatrix}
h_R(\beta_1) \\ h_R(\beta_2) \\ \vdots \\ h_R(\beta_n)
\end{bmatrix}
$$
(3.15a)

$$
\begin{bmatrix}
\beta & -\beta_1^3 & \beta_1^5 & \cdots & (-1)^{l-1} \beta_1^{2l-1} \\
\beta & -\beta_2^3 & \beta_2^5 & \cdots & (-1)^{l-1} \beta_2^{2l-1} \\
\vdots & \cdots & & \ddots & \vdots \\
\beta & -\beta_n^3 & \beta_n^5 & \cdots & (-1)^{l-1} \beta_n^{2l-1}
\end{bmatrix}
\begin{bmatrix}
h_1 \\ h_3 \\ \vdots \\ h_{2l-1}
\end{bmatrix}
=
\begin{bmatrix}
h_X(\beta_1) \\ h_X(\beta_2) \\ \vdots \\ h_X(\beta_n)
\end{bmatrix}
$$
(3.15b)

After forming $h(s)$ polynomial, $g(s)$ polynomial can be obtained by using losslessness equation, $G(-s^2) = g(s)g(-s) = h(s)h(-s) + f(s)f(-s)$. Briefly, $|g(j\beta)|^2$ describes an even polynomial in the phony variable β such that

$$G(\beta^2) = G_0 + G_1\beta^2 + G_2\beta^4 + \ldots G_{n_\beta}\beta^{2n_\beta} \rangle 0 \quad ; \forall \beta \tag{3.16}$$

Coefficients $\{G_0, G_1, G_2, \ldots G_{n_\beta}\}$ can easily be found by any linear or non linear interpolation or curve fitting method as described by [49]. Then, replacing β^2 by $-s^2$, one can extract $g(s)$ from $G(-s^2) = g(s)g(-s)$ by explicit factorization. In this step, obviously the roots of $G(-s^2)$ is computed and then, $g(s)$ is constructed on the Left Half Plane (LHP) roots of $G(-s^2)$ as a strictly Hurwitz polynomial.

At this point, polynomial pairs $h(p), g(p)$ and $h(\lambda), g(\lambda)$ are obtained, which are describing the lumped section of the mixed model and the distributed part of the mixed model, respectively. After synthesizing these polynomial pairs, lumped and distributed element values are reached. According to the desired mixed network structure, transfer scattering matrices of the components are multiplied and as a result, transfer scattering matrix of the mixed network is obtained. So two-variable polynomials of the mixed structure ($h(p, \lambda)$ and $g(p, \lambda)$) are obtained.

The iterative process in (3.11) is stopped when $\varepsilon(j\omega) = S(j\omega) - S_{11}(j\omega, j\tan(\omega\tau)) = S(j\omega) - \dfrac{h(j\omega, j\tan(\omega\tau))}{g(j\omega, j\tan(\omega\tau))}$ is small enough.

In general, in (3.11) numerical derivatives must be calculated. But in the following sections, for two special cases (ladder networks connected with UEs and cascaded separate lumped and distributed networks), the derivatives are calculated analytically and the results are used in the process. So there is no need to calculate numerical derivatives.

3.2.1 Mixed Models with Ladder Networks Connected with Unit Elements

In this part, circuit topology for the mixed models is selected as the ladder networks connected with unit elements. Consider the generic form of a lossless two-port formed with cascade connections of series inductances [L], Unit Elements [UE] and shunt capacitors [C] as shown in Figure 3.3. In this figure, distributed elements are regarded as equal length (or commensurate) transmission lines with constant delay τ.
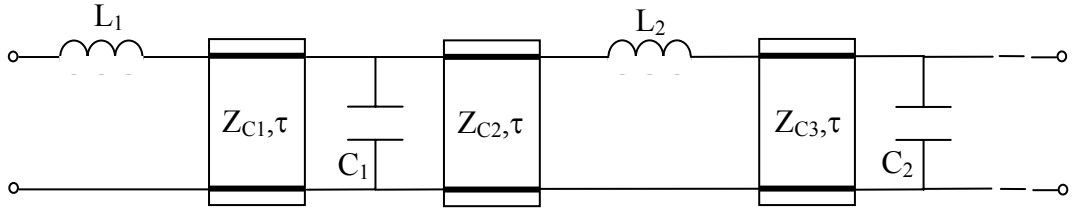
Figure 3.3 Low-pass ladder network connected with unit elements.

The scattering matrix describing the mixed element two-port can be expressed in the Belevitch canonical form as,

$$S(p,\lambda) = \frac{1}{g(p,\lambda)}\begin{pmatrix} h(p,\lambda) & \sigma f(-p,-\lambda) \\ f(p,\lambda) & -\sigma h(-p,-\lambda) \end{pmatrix} \tag{3.17}$$

where $f(p,\lambda)$ is a monic real polynomial consist of transmission zeros and it is given by

$$f(p,\lambda) = (1-\lambda^2)^{n_\lambda/2} \tag{3.18a}$$

$$g(p,\lambda) = \sum_{i=0}^{n_\lambda} g_i(p)\lambda^i \text{ and } h(p,\lambda) = \sum_{i=0}^{n_\lambda} h_i(p)\lambda^i \tag{3.18b}$$

31

are real polynomials in the complex variables p and λ, ($\lambda = \tanh p\tau$, τ being the fixed delay length of unit elements), with $g_i(p) = \sum_{j=0}^{n_p} g_{ij} p^j$ and $h_i(p) = \sum_{j=0}^{n_p} h_{ij} p^j$; n_p and n_λ are being the total number lumped and distributed elements respectively, $g(p,\lambda)$ is a Scattering Hurwitz polynomial, σ is a constant; $|\sigma| = 1$.

Since the two-port under consideration is lossless, scattering matrix of (3.17) must satisfy the paraunitary or so called losslessness condition. That is,

$$S(p,\lambda)S(p,\lambda)^+ = I \tag{3.19}$$

In this expression, $I = \begin{pmatrix} 1 & 0 \\ 0 & 1 \end{pmatrix}$ is the unit matrix and "$+$"designates the dagger operation which takes the transpose and the complex conjugate of a matrix under consideration. In terms of the canonic polynomials, paraunitary condition yields that

$$g(p,\lambda)g(-p,-\lambda) = h(p,\lambda)h(-p,-\lambda) + f(p,\lambda)f(-p,-\lambda) \tag{3.20}$$

The polynomials $g(p,\lambda)$ and $h(p,\lambda)$ with partial degrees n_p and n_λ can be expressed in the matrix form such that

$$g(p,\lambda) = \overline{\mathbf{p}}^T \Lambda_{\mathbf{g}} \overline{\lambda} \text{ and } h(p,\lambda) = \overline{\mathbf{p}}^T \Lambda_{\mathbf{h}} \overline{\lambda} \tag{3.21a}$$

where $\overline{\mathbf{p}}^T = \begin{bmatrix} 1 & p & p^2 \cdots p^{n_p} \end{bmatrix}$, $\overline{\lambda}^T = \begin{bmatrix} 1 & \lambda & \lambda^2 \cdots \lambda^{n_\lambda} \end{bmatrix}$.

$$\Lambda_g = \begin{bmatrix} g_{00} & g_{01} & \cdots & g_{0n_\lambda} \\ g_{10} & g_{11} & \cdots & g_{1n_\lambda} \\ \vdots & \vdots & \ddots & \vdots \\ g_{n_p 0} & g_{n_p 1} & \cdots & g_{n_p n_\lambda} \end{bmatrix} \quad \Lambda_h = \begin{bmatrix} h_{00} & h_{01} & \cdots & h_{0n_\lambda} \\ h_{10} & h_{11} & \cdots & h_{1n_\lambda} \\ \vdots & \vdots & \ddots & \vdots \\ h_{n_p 0} & h_{n_p 1} & \cdots & h_{n_p n_\lambda} \end{bmatrix} \tag{3.21b}$$

Since the first column represents the lumped part of the mixed network and the first row represent the distributed part of the mixed structure, Λ_h and Λ_g in (3.21) can be written in the following form with $h_{00} = 0$ and $g_{00} = 1$ (assuming a transformerless model),

$$\Lambda_h = \begin{array}{|c|c|} \hline 0 & h_D(\lambda) \\ \hline h_L(p) & h_C(p,\lambda) \\ \hline \end{array} \qquad \Lambda_g = \begin{array}{|c|c|} \hline 1 & g_D(\lambda) \\ \hline g_L(p) & g_C(p,\lambda) \\ \hline \end{array}$$

or in mathematical terms,

$$h(p,\lambda) = h_L(p) + h_{R1}(p,\lambda) \tag{3.22a}$$

$$h(p,\lambda) = h_D(\lambda) + h_{R2}(p,\lambda) \tag{3.22b}$$

where $h_{R1}(p,\lambda) = h_D(\lambda) + h_C(p,\lambda)$ and $h_{R2}(p,\lambda) = h_L(\lambda) + h_C(p,\lambda)$.

Now let us calculate the derivative in (3.11) for the lumped and distributed parts of the mixed network,

$$\frac{\partial |\varepsilon(j\omega)|^2}{\partial h_L(j\omega)} = \frac{\partial}{\partial h_L(j\omega)} \varepsilon(-j\omega)\varepsilon(j\omega)$$

$$= \frac{\partial}{\partial h_L(j\omega)} \left[\left(S(-j\omega) - \frac{h(-j\omega,-j\tan(\omega\tau))}{g(-j\omega,-j\tan(\omega\tau))} \right) \left(S(jw) - \frac{h(j\omega,j\tan(\omega\tau))}{g(j\omega,j\tan(\omega\tau))} \right) \right]$$

$$= \frac{\partial}{\partial h_L(j\omega)} \left[\left(S(-j\omega) - \frac{h_L(-j\omega) + h_{R1}(-j\omega,-j\tan(\omega\tau))}{g(-j\omega,-j\tan(\omega\tau))} \right) \\ \left(S(jw) - \frac{h_L(j\omega) + h_{R1}(j\omega,j\tan(\omega\tau))}{g(j\omega,j\tan(\omega\tau))} \right) \right]$$

$$= -\left(S(-j\omega) - \frac{h_L(-j\omega) + h_{R1}(-j\omega,-j\tan(\omega\tau))}{g(-j\omega,-j\tan(\omega\tau))} \right) \frac{1}{g(j\omega,j\tan(\omega\tau))}$$

$$= \frac{-\varepsilon(-j\omega)}{g(j\omega,j\tan(\omega\tau))}$$

$$\frac{\partial |\varepsilon(j\omega)|^2}{\partial h_D(j\tan(\omega\tau))} = \frac{\partial}{\partial h_D(j\tan(\omega\tau))}\varepsilon(-j\omega)\varepsilon(j\omega)$$

$$= \frac{\partial}{\partial h_D(j\tan(\omega\tau))}\left[\left(S(-j\omega) - \frac{h(-j\omega,-j\tan(\omega\tau))}{g(-j\omega,-j\tan(\omega\tau))}\right)\left(S(jw) - \frac{h(j\omega,j\tan(\omega\tau))}{g(j\omega,j\tan(\omega\tau))}\right)\right]$$

$$= \frac{\partial}{\partial h_D(j\tan(\omega\tau))}\left[\left(S(-j\omega) - \frac{h_D(-j\tan(\omega\tau)) + h_{R2}(-j\omega,-j\tan(\omega\tau))}{g(-j\omega,-j\tan(\omega\tau))}\right)\left(S(jw) - \frac{h_D(j\tan(\omega\tau)) + h_{R2}(j\omega,j\tan(\omega\tau))}{g(j\omega,j\tan(\omega\tau))}\right)\right]$$

$$= -\left(S(-j\omega) - \frac{h_D(-j\tan(\omega\tau)) + h_{R2}(-j\omega,-j\tan(\omega\tau))}{g(-j\omega,-j\tan(\omega\tau))}\right)\frac{1}{g(j\omega,j\tan(\omega\tau))}$$

$$= \frac{-\varepsilon(-j\omega)}{g(j\omega,j\tan(\omega\tau))}$$

If these derivatives are substituted in (3.11), the following iterative processes for lumped and distributed parts of the mixed network are obtained, respectively,

$$h_{i+1}(j\omega) = h_i(j\omega) + \gamma\,\frac{\varepsilon(-j\omega)}{g(j\omega,j\tan(\omega\tau))} \tag{3.23a}$$

$$h_{i+1}(j\tan(\omega\tau)) = h_i(j\tan(\omega\tau)) + \gamma\,\frac{\varepsilon(-j\omega)}{g(j\omega,j\tan(\omega\tau))} \tag{3.23b}$$

As a result, these expressions can be used as an iterative process to obtain the suitable $h(p)$ and $h(\lambda)$ polynomials, then by using the losslessness equation (2.13), $g(p)$ and $g(\lambda)$ polynomials can be reached, after selecting $f(p)$ and $f(\lambda)$ polynomials. Then by synthesizing the polynomials for lumped and distributed parts of the mixed model, transfer scattering matrices (T matrices) for each component can be formed. After multiplying these T matrices in the desired connection order, $h(p,\lambda)$ and $g(p,\lambda)$ two-variable polynomials for the mixed model are obtained. Namely, input reflection expression $S_{11}(p,\lambda) = \frac{h(p,\lambda)}{g(p,\lambda)}$ for the desired mixed model that fits the given numerical reflection data is reached.

3.2.2 Mixed Models with Cascaded Lumped and Distributed Networks

In this section, a different network topology is presented to model passive one-port devices. Referring to Figure 3.4, the model is considered as the cascade connections of two lossless two ports namely [L] and [D]. The two port [L] consists of all the possible transmission zeros of the device in the form of lumped circuit elements therefore it is reciprocal whereas, the two port [D] is considered to reflect the physical size of the device (such as an antenna) in the form of tandem connection of equal length transmission lines or unit elements (UE). Obviously, [D] is also reciprocal.
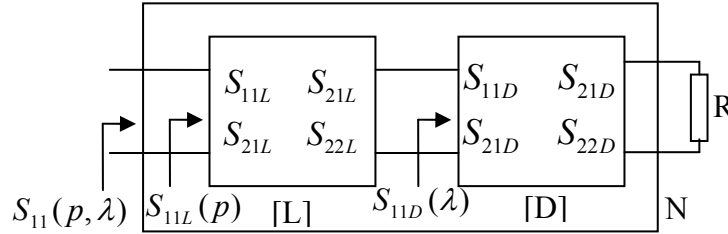
Figure 3.4 Cascade connected lumped and distributed networks.

In this case, two variable input reflection coefficient $S_{11}(p,\lambda)$ of the device is expressed in terms of the scattering parameters of [L] and [D] such that [53]

$$S_{11}(p,\lambda) = S_{11L}(p) + \frac{S_{21L}^2(p)S_{11D}(\lambda)}{1 - S_{22L}(p)S_{11D}(\lambda)} \qquad (3.24)$$

In (3.24), $S_{11L}(p) = \dfrac{h_L(p)}{g_L(p)}$, $S_{21L}(p) = \dfrac{f_L(p)}{g_L(p)}$, $S_{22L}(p) = \dfrac{f_L(-p)h_L(-p)}{f_L(p)g_L(p)}$ (3.25a)

$S_{11D}(\lambda) = \dfrac{h_D(\lambda)}{g_D(\lambda)}$, $S_{21D}(\lambda) = \dfrac{f_D(\lambda)}{g_D(\lambda)}$, $S_{22D}(\lambda) = \dfrac{f_D(-\lambda)h_D(-\lambda)}{f_D(\lambda)g_D(\lambda)}$ (3.25b)

$f_D(\lambda) = (1-\lambda^2)^{n_\lambda/2}$

$f(p,\lambda)$ is a real polynomial which includes all the transmission zeros of the device under consideration. In a mixed element structure constructed by cascade connection of n_p lumped and n_λ distributed elements, the polynomial $f(p,\lambda)$ is given by

$$f(p,\lambda) = \prod_{i=1}^{n} f_i(p)f_i(\lambda) \tag{3.26}$$

where $f_i(p)$ and $f_i(\lambda)$ define the transmission zeros of individual lumped and distributed subsections appearing in the cascade structure and $n = Max_{g_{ij} \neq 0}\{i+j\}$; $i = 0,1,\ldots,n_p$, $j = 0,1,\ldots,n_\lambda$. In general, the transmission zeros can be located anywhere in p and λ planes. From (3.26), it can immediately deduced that the transmission zeros of each subsection in the cascade structure have to arise in multiplication form. In other words, it can be assumed that $f(p,\lambda)$ of the entire mixed element structure is in product separable form as

$$f(p,\lambda) = f_L(p)f_D(\lambda)$$

If one only considers the transmission zeros on the imaginary axis $j\omega$ and $j\Omega$, then, $f_L(p)$ will be a real even or odd polynomial, and $f_D(\lambda)$ in general will have the form

$$f_D(\lambda) = f_0(\lambda)(1-\lambda^2)^{n_\lambda/2}$$

A practical form of $f(p,\lambda)$ can be obtained by disregarding the finite imaginary axis zeros in $f_L(p)$ and $f_D(\lambda)$ (except those at dc) as follows,

$$f(p,\lambda) = p^{k_1}\lambda^{k_2}(1-\lambda^2)^{n_\lambda/2}$$

where k_1 and k_2 designate the total number of transmissions zeros at dc, if these are also excluded, then

$$f(p,\lambda) = (1-\lambda^2)^{n_\lambda/2}$$

For example, for wideband antennas, it is practical to assume all the transmission zeros located at DC and infinity. Therefore, one can choose the following form for $f_L(p)$

$$f_L(p) = p^k \text{ which yields } \frac{f_L(-p)}{f_L(p)} = (-1)^k \qquad (3.27)$$

It should be noted that once the numerator polynomials $h_L(p) = \sum_{j=0}^{n_p} h_{jL} p^j$ and $h_D(\lambda) = \sum_{j=0}^{n_\lambda} h_{jD} \lambda^j$ are initialized, then the complete scattering parameters of [L] and [D] can be determined from the losslessness conditions of $G_L(p^2) = g_L(p)g_L(-p) = h_L(p)h_L(-p) + f_L(p)f_L(-p)$ and

$G_D(\lambda^2) = g_D(\lambda)g_D(-\lambda) = h_D(\lambda)h_D(-\lambda) + f_D(\lambda)f_D(-\lambda)$. In this regard, strictly Hurwitz denominator polynomials $g_L(p)$ and $g_D(\lambda)$ are constructed on the left half plane zeros of $G_L(p^2)$ and $G_D(\lambda^2)$, respectively. Hence, the full scattering parameters of [L] and [D] are generated as in (3.25) which in turn yield the analytic form of the device reflection coefficient as expressed by (3.24). All the above explanation leads us to propose the following numerical approach to build the antenna models.

Let $\varepsilon(j\omega) = S(j\omega) - S_{11}(j\omega, j\tan(\omega\tau))$ be the error function defined as the difference between the analytic form and the given reflection coefficient of the device. Obviously, $|\varepsilon(j\omega)|^2$ is a function of both h_L and h_D. In the mean time, the scattering coefficients $S_{11L}(p) = \frac{h_L(p)}{g_L(p)}$ and $S_{22L}(-p) = (-1)^k \frac{h_L(p)}{g_L(-p)}$ are a function

of h_L. Similarly, $S_{11D}(\lambda) = \dfrac{h_D(\lambda)}{g_D(\lambda)}$ is a function of h_D. These functional relations can

be expressed as

$$|\varepsilon|^2 = \varepsilon\varepsilon^* = F(S_{11L}, S_{22L}^*, S_{11D}) ; \ S_{11L} = F(h_L) , S_{11D} = F(h_D) , S_{22L}^* = F(h_L) \quad (3.28)$$

where (*) represents the complex conjugate of a complex number.

Taking the partial derivatives of $\dfrac{\partial \varepsilon\varepsilon^*}{\partial h_L} = \varepsilon^* \dfrac{\partial \varepsilon}{\partial h_L} + \varepsilon \dfrac{\partial \varepsilon^*}{\partial h_L}$ and $\dfrac{\partial \varepsilon\varepsilon^*}{\partial h_D} = \varepsilon^* \dfrac{\partial \varepsilon}{\partial h_D} + \varepsilon \dfrac{\partial \varepsilon^*}{\partial h_D}$,

one can end up with

$$\frac{\partial |\varepsilon|^2}{\partial h_L} = \frac{1}{g_L} W_1 \ \text{such that} \ W_1 = \varepsilon^* + \frac{\varepsilon}{|g_L|^2} \frac{(S_{21L}^2)^* |S_{11D}|^2}{(1 - S_{22L}^* S_{11D}^*)^2} \qquad (3.29a)$$

and

$$\frac{\partial |\varepsilon|^2}{\partial h_D} = \frac{1}{g_D} W_2 \ \text{such that} \ W_2 = \varepsilon^* \frac{S_{21L}^2}{(1 - S_{22L} S_{11D})^2} \qquad (3.29b)$$

In order to find the best fit between the analytic form and the given reflection coefficients of the device, the amplitude square of the error must be minimized at each frequency point. In this case, the gradient method may be employed to determine the numerator polynomials h_L and h_D from the initialized values of $h_{L0}(j\omega)$ and $h_{D0}(j\tan(\omega\tau))$ as follows.

$$
\begin{aligned}
h_{L(i+1)} &= h_{L(i)} - \gamma \frac{\partial |\varepsilon|^2}{\partial h_{L(i)}} \\
h_{D(i+1)} &= h_{D(i)} - \gamma \frac{\partial |\varepsilon|^2}{\partial h_{D(i)}}
\end{aligned}
\qquad (3.30a)
$$

or

$$h_{L(i+1)} = h_{L(i)} - \gamma \frac{1}{g_{L(i)}} W_{1(i)}$$

$$h_{D(i+1)} = h_{D(i)} - \gamma \frac{1}{g_{D(i)}} W_{2(i)}$$

(3.30b)

In (3.30), the index i designates the iteration count starting at $i = 0$. Certainly, different variants of gradient method may be employed to minimize the error at each frequency.

By using these expressions (3.30), again an iterative process can be defined to obtain the suitable $h(p)$ and $h(\lambda)$ polynomials, then by using the losslessness equation (2.13), $g(p)$ and $g(\lambda)$ polynomials can be reached, after selecting $f(p)$ and $f(\lambda)$ polynomials. Then the expressions given in (3.25) can be formed. So after obtaining the scattering parameter expression for lumped and distributed parts of the mixed model, (3.24) can be used to form the expression for input reflection expression for the desired mixed model.

Chapter 4

Numerical Aspects

In Chapter 3, the proposed mixed modeling procedures via gradient or steepest descent method are explained. Two different circuit topologies are examined. Here, the algorithms, flow charts and numerical aspects for the proposed procedures are given.

4.1 Gradient Method Based Mixed Modeling Algorithm for Ladder Networks Connected with Unit Elements

Inputs:

- $\omega_k; \quad k = 1,2,..,N_\omega$: Given sample frequencies.

- N_ω : Total number of sample frequencies.

- $S(j\omega_k) = R(\omega_k) + jX(\omega_k); \quad k = 1,2,..,N_\omega$: Given reflection coefficient data.

- n_λ : Total number of distributed elements in the mixed model.

- n_p : Total number of lumped elements in the mixed model.

To be able to determine the number of lumped and distributed elements in the model, the designer can use the proposed method in [50]. Here, a single variable modeling method with optimum number of elements (n) is described. This optimum number is calculated by using the difference table method. After obtaining the necessary number of elements in the single variable model, the same number of elements can be used in the mixed model. So the designer can

decide the number of lumped or distributed elements in the mixed model, and the number of the other type elements can be calculated as $n - n_p$ or $n - n_\lambda$.

- $f_D(\lambda)$: A monic polynomial constructed on the transmission zeros of distributed part. It is noted that for cascaded connection of UEs $f_D(\lambda) = (1 - \lambda^2)^{n_\lambda / 2}$ is selected.

- $f_L(p)$: A monic polynomial constructed on the transmission zeros of lumped part.

These transmission zeros can be located by observing the graph of $|S_{21}(j\omega_k)|^2 = 1 - |S(j\omega_k)|^2$.

- $h_{00}, h_{01}, h_{02}, ..., h_{0n\lambda}$ and $h_{00}, h_{10}, h_{20}, ..., h_{np0}$: Initial values for the first row and the first column of Λ_h matrix.

To generate the initial values of the unknown coefficients, the designer can built single variable models, namely lumped and distributed models. Then from the lumped model, $h_{00}, h_{10}, h_{20}, ..., h_{np0}$ coefficients and from the distributed model, $h_{00}, h_{01}, h_{02}, ..., h_{0n\lambda}$ coefficients can be initialized.

- δ : The stopping criteria for the sum of the square errors. For many practical problems it is sufficient to choose $\delta = 10^{-3}$.

Computational Steps:

Step 1: $i = 0$ and start the iterations for the gradient method.

Step 2: By using the initial coefficients $h_{00}, h_{01}, h_{02}, ..., h_{0n\lambda}$ and $h_{00}, h_{10}, h_{20}, ..., h_{np0}$, compute the strictly Hurwitz denominator polynomials $g_D(\lambda)$ and $g_L(p)$ employing the losslessness conditions as described in (3.19).

Step 3: Synthesize lumped and distributed sections of the mixed model and obtain component values.

Step 4: By using the component values, form transfer scattering matrices as described below;

a) If the component is a unit element with characteristics impedance Z_C, then $g(\lambda), h(\lambda)$ and $f(\lambda)$ polynomials can be written as

$$g(\lambda) = \frac{Z_C^2 + 1}{2Z_C} \lambda + 1 \quad h(\lambda) = \frac{Z_C^2 - 1}{2Z_C} \lambda \quad f(\lambda) = \left(1 - \lambda^2\right)^{1/2}$$

b) If the component is a series inductor with the value L, then $g(p), h(p)$ and $f(p)$ polynomials are

$$g(p) = \frac{L}{2} p + 1 \quad h(p) = \frac{L}{2} p \quad f(p) = 1$$

c) If the component is a shunt capacitor with the value C, then $g(p), h(p)$ and $f(p)$ polynomials are

$$g(p) = \frac{C}{2} p + 1 \quad h(p) = -\frac{C}{2} p \quad f(p) = 1$$

Transfer scattering matrices for the components can be formed by using these polynomials and equation (2.12).

Step 5: According to the desired connection order, multiply the transfer scattering matrices of the components and obtain transfer scattering matrix of the mixed model as (2.23) and $g(p, \lambda), h(p, \lambda)$ and $f(p, \lambda)$ two-variable polynomials.

Step 6: Compute the error $\varepsilon_i(j\omega_k) = S(j\omega_k) - \dfrac{h_i(j\omega_k, j\tan(\omega_k \tau))}{g_i(j\omega_k, j\tan(\omega_k \tau))}$ over the given

frequencies. Here τ is the normalized delay length of the distributed elements and can be calculated as $\tau = (\pi/2)/\omega_e$, which corresponds to a delay length of 90^0 at the frequency $\omega_e = 1.2\omega_{max}$.

Step 7: Compute the sum of the square errors $\delta_i = \displaystyle\sum_{k=1}^{N_\omega} \varepsilon_i^2(j\omega_k)$. If $\delta_i \le \delta$, set

$S_{11}(p, \lambda) = \dfrac{h_i(p, \lambda)}{g_i(p, \lambda)}$ and stop. Otherwise go to the next step.

Step 8: Compute the complex quantities over the sample frequencies for the given initials,

$$h_{i+1}(j\omega_k) = h_i(j\omega_k) + \gamma \frac{\varepsilon_i(-j\omega_k)}{g_i(j\omega_k, j\tan(\omega_k \tau))},$$

$$h_{i+1}(j\tan(\omega_k\tau)) = h_i(j\tan(\omega_k\tau)) + \gamma \, \frac{\varepsilon_i(-j\omega_k)}{g_i(j\omega_k, j\tan(\omega_k\tau))} \, .$$

Step 9: Separate the real and the imaginary parts of

$$h_{i+1}(j\omega_k) = h_{R(i+1)}(\omega_k) + jh_{X(i+1)}(\omega_k) \qquad \text{and}$$

$$h_{i+1}(j\tan(\omega\tau)) = h_{R(i+1)}(\tan(\omega\tau)) + jh_{X(i+1)}(\tan(\omega\tau))$$

Step 10: Using the real and imaginary parts of the above equations find the

coefficients of the polynomials $h_{i+1}(\lambda) = \sum\limits_{l=0}^{n_\lambda} h_{0l}\lambda^l$ and $h_{i+1}(p) = \sum\limits_{l=0}^{n_p} h_{l0}p^l$ by means of

even-odd linear interpolation routine described in (3.18).

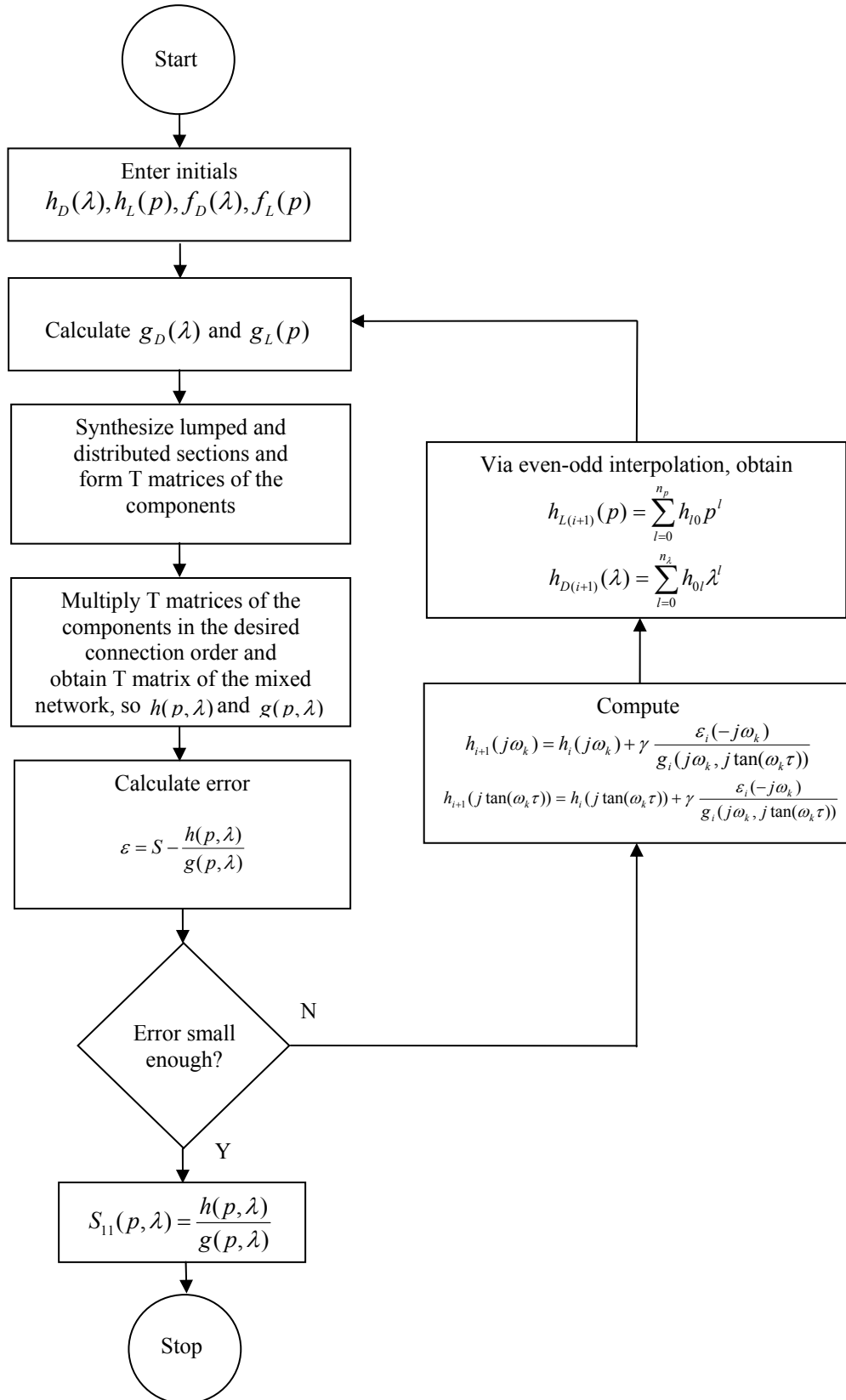**Step 11:** Set $i = i+1$ and go to Step 2.

Figure 4.1 Flowchart for gradient method based mixed modeling algorithm for ladder networks connected with unit elements.

4.2 Gradient Method Based Mixed Modeling Algorithm for Cascaded Separate Lumped and Distributed Networks

Inputs:

- ω_k; $k = 1,2,..,N_\omega$: Given sample frequencies.

- N_ω: Total number of sample frequencies.

- $S(j\omega_k) = R(\omega_k) + jX(\omega_k)$; $k = 1,2,..,N_\omega$: Given reflection coefficient data.

- n_λ: Total number of distributed elements of the prototype [D].

- n_p: Total number of lumped elements of the prototype [L].

n_p and n_λ can be calculated as described in section 4.1.

- $f_D(\lambda)$: A monic polynomial constructed on the transmission zeros of [D]. It is noted that for cascaded connection of UEs $f_D(\lambda) = (1 - \lambda^2)^{n_\lambda/2}$ is selected.

- $f_L(p)$: A monic polynomial constructed on the transmission zeros of [L].

These transmission zeros can be located as described in section 4.1.

- $h_{0D}, h_{1D}, h_{2D},..., h_{n\lambda D}$ and $h_{0L}, h_{1L}, h_{2L},..., h_{npL}$: Initial values for the numerator polynomials $h_D(\lambda)$ and $h_L(p)$ of the input reflection coefficients $S_{11D}(\lambda) = \dfrac{h_D(\lambda)}{g_D(\lambda)}$ and $S_{11L}(p) = \dfrac{h_L(p)}{g_L(p)}$ [D] and [L], respectively.

Initial values for the unknown coefficients $h_{0D}, h_{1D}, h_{2D},..., h_{n\lambda D}$ and $h_{0L}, h_{1L}, h_{2L},..., h_{npL}$ can be generated as described in section 4.1.

- δ: The stopping criteria for the sum of the square errors. For many practical problems it is sufficient to choose $\delta = 10^{-3}$.

Computational Steps:

Step 1: Set $i = 0$ and start the iterations for the gradient method.

Step 2: By using the initial coefficients $h_{0D}, h_{1D}, h_{2D},..., h_{n\lambda D}$ and $h_{0L}, h_{1L}, h_{2L},..., h_{npL}$, compute the strictly Hurwitz denominator polynomials $g_{D(i)}(\lambda)$ and $g_{L(i)}(p)$ employing the losslessness conditions of [D] and [L] as described in (3.19).

Step 3: Construct $S_{11D(i)}(\lambda) = \dfrac{h_{D(i)}(\lambda)}{g_{D(i)}(\lambda)}$ and $S_{11L(i)}(p) = \dfrac{h_{L(i)}(p)}{g_{L(i)}(p)}$ of [D] and [L].

Step 4: By cascading [L] and [D], generate the input reflectance S_{11} of the composite

structure. $S_{11(i)}(p,\lambda) = \dfrac{h_{(i)}(p,\lambda)}{g_{(i)}(p,\lambda)} = S_{11L(i)}(p) + \dfrac{S_{21L(i)}^2(p)S_{11D(i)}(\lambda)}{1 - S_{22L(i)}(p)S_{11D(i)}(\lambda)}$.

Step 5: Compute the error $\varepsilon_i(j\omega_k) = S(j\omega_k) - \dfrac{h_i(j\omega_k, j\tan(\omega_k\tau))}{g_i(j\omega_k, j\tan(\omega_k\tau))}$ over the given

frequencies. Here τ is the normalized delay length of the distributed elements and

can be calculated as $\tau = (\pi/2)/\omega_e$, which corresponds to a delay length of 90^0 at the

frequency $\omega_e = 1.2\omega_{\max}$.

Step 6: Compute the sum of the square errors $\delta_i = \sum\limits_{k=1}^{N_\omega} \varepsilon_i^2(\omega_k)$. If $\delta_i \leq \delta$, set

$S_{11}(p,\lambda) = \dfrac{h_i(p,\lambda)}{g_i(p,\lambda)}$ and stop. Otherwise go to the next step.

Step 7: Compute the complex quantities over the sample frequencies for the given

initials,

$W_{1(i)} = \varepsilon_i^* + \dfrac{\varepsilon_i}{|g_{L(i)}|^2} \dfrac{(S_{21L(i)}^2)^* |S_{11D(i)}|^2}{(1 - S_{22L(i)}^* S_{11D(i)}^*)^2}$; $W_{2(i)} = \varepsilon_i^* \dfrac{S_{21L(i)}^2}{(1 - S_{22L(i)}S_{11D(i)})^2}$ and generate the

complex quantities $\quad h_{L(i+1)} = h_{L(i)} + \dfrac{1}{g_{L(i)}}W_{1(i)}$ and $\quad h_{D(i+1)} = h_{D(i)} + \dfrac{1}{g_{D(i)}}W_{(i)}$ point by

point.

Step 8: Separate the real and the imaginary parts of

$h_{i+1}(j\omega_k) = h_{R(i+1)}(\omega_k) + jh_{X(i+1)}(\omega_k)$

and $h_{i+1}(j\tan(\omega\tau)) = h_{R(i+1)}(\tan(\omega\tau)) + jh_{X(i+1)}(\tan(\omega\tau))$.

Step 9: Using the real and imaginary parts of the above equations find the

coefficients of the polynomials $h_{i+1}(\lambda) = \sum\limits_{l=0}^{n_\lambda} h_{0l}\lambda^l$ and $h_{i+1}(p) = \sum\limits_{l=0}^{n_p} h_{l0}p^l$ by means of

any linear interpolation routine.
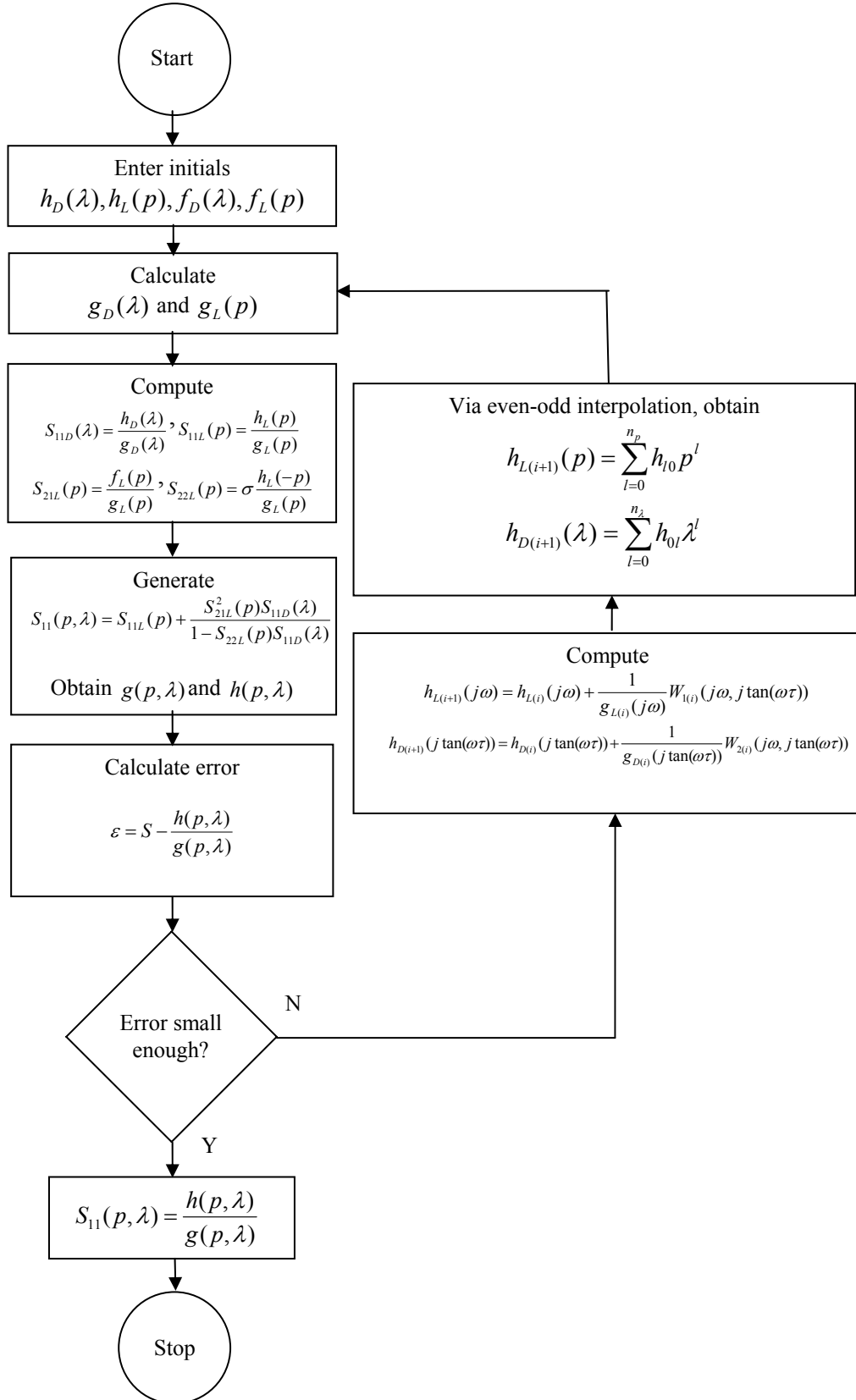
Step 10: Set $i = i+1$ and go to Step 2.

Start

Enter initials
$h_D(\lambda), h_L(p), f_D(\lambda), f_L(p)$

Calculate
$g_D(\lambda)$ and $g_L(p)$

Compute
$$S_{11D}(\lambda) = \frac{h_D(\lambda)}{g_D(\lambda)}, \quad S_{11L}(p) = \frac{h_L(p)}{g_L(p)}$$
$$S_{21L}(p) = \frac{f_L(p)}{g_L(p)}, \quad S_{22L}(p) = \sigma \frac{h_L(-p)}{g_L(p)}$$

Generate
$$S_{11}(p, \lambda) = S_{11L}(p) + \frac{S_{21L}^2(p) S_{11D}(\lambda)}{1 - S_{22L}(p) S_{11D}(\lambda)}$$

Obtain $g(p, \lambda)$ and $h(p, \lambda)$

Calculate error
$$\varepsilon = S - \frac{h(p, \lambda)}{g(p, \lambda)}$$

Error small enough?

N

Via even-odd interpolation, obtain
$$h_{L(i+1)}(p) = \sum_{l=0}^{n_p} h_{l0} p^l$$
$$h_{D(i+1)}(\lambda) = \sum_{l=0}^{n_\lambda} h_{0l} \lambda^l$$

Compute
$$h_{L(i+1)}(j\omega) = h_{L(i)}(j\omega) + \frac{1}{g_{L(i)}(j\omega)} W_{1(i)}(j\omega, j\tan(\omega\tau))$$
$$h_{D(i+1)}(j\tan(\omega\tau)) = h_{D(i)}(j\tan(\omega\tau)) + \frac{1}{g_{D(i)}(j\tan(\omega\tau))} W_{2(i)}(j\omega, j\tan(\omega\tau))$$

Y

$$S_{11}(p, \lambda) = \frac{h(p, \lambda)}{g(p, \lambda)}$$

Stop

Figure 4.2 Flowchart for gradient method based mixed modeling algorithm for cascaded lumped and distributed networks.

Chapter 5

Applications

In this chapter, mixed modeling applications are given by using the proposed modeling method. First, two different mixed models of a monopole antenna are generated, then given lumped element Butterworth and Chebyshev filters are transformed to the mixed element counterparts. Finally, an amplifier with mixed elements is obtained from the amplifier with lumped elements.

5.1 Antenna Modeling

In this part, by using the proposed mixed modeling method, a short monopole antenna is modelled. The topologies used in the mixed models are ladder networks connected with unit elements and cascaded separate lumped and distributed networks.

5.1.1 Antenna Model with Ladder Networks Connected with Unit Elements

In this example, a model for the data that belongs to a short monopole antenna, employed for military communication purpose, is generated. Data for the antenna is provided over 20MHz to 100MHz. The reflectance data for the antenna is given in Table 5.1 over a normalized frequency band of [0.2 to 1].

Table 5.1 Reflectance data for the monopole antenna.

Frequency (ω)	Re (S)	Im (S)
0.20	0.9170	-0.3112
0.30	0.5545	-0.5446
0.40	-0.1111	0
0.45	0.3289	0.4698
0.50	0.6437	0.3325
0.55	0.7828	0.2270
0.60	0.8686	0.1248
0.65	0.9040	0.0528
0.70	0.9189	-0.0187
0.75	0.9233	-0.0831
0.80	0.9214	-0.1415
0.90	0.9019	-0.2566
1.00	0.8288	-0.3767

Naturally, the antenna does not propagate any power at dc. Therefore, $f(p,\lambda)$ is selected as $f(p,\lambda) = p^2(1-\lambda^2)$. From $f(p,\lambda)$ expression, $n_p = 2$ and $n_\lambda = 2$. Namely, the model will contain two lumped and two distributed elements with $\tau = \pi/(4 \cdot 1.2 \cdot \omega_c) = 0.6545$ where ω_c designates the upper edge or the cut-off frequency of pass-band. This delay length corresponds to the half of the quarter wavelength at 100 MHz. In this case the unknown real coefficients $\{h_{00}, h_{10}, h_{20}, h_{21}, h_{22}\}$ of the polynomial $h(p,\lambda)$ are chosen as the free parameters of the problem and determined in such a way that the antenna data is best fit to $S_{11}(jw, j\tan(\omega\tau))$. Eventually, $S_{11}(p,\lambda)$ is generated as

$$S_{11}(p,\lambda) = \frac{h(p,\lambda)}{g(p,\lambda)}$$

where

$$h(p,\lambda) = \begin{bmatrix} 0.5667 & 0.3551 & 0 \\ -0.2089 & 2.3621 & 1.3802 \\ 1.8854 & -0.1678 & -0.4699 \end{bmatrix} \quad g(p,\lambda) = \begin{bmatrix} 0.5667 & 0.3551 & 0 \\ 0.5706 & 2.8506 & 1.3802 \\ 2.1342 & 2.9182 & 1.1049 \end{bmatrix}$$

and it is synthesized as depicted in Figure 5.1 [54].
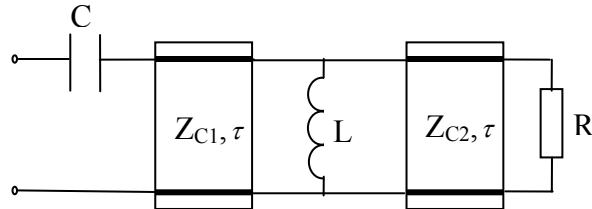
Figure 5.1 Antenna model with ladder networks connected with unit elements
(Z_{C1}=1.5082, Z_{C2}=9.5478, τ=0.6545, C=0.68775, L=5.1566, R=16.156).

Consequently, the fit between the analytic form of the reflection coefficient and measured data is given in Figure 5.2. Close examination of Figure 5.2 reveals that the obtained mixed model can be used as an acceptable model of the monopole antenna.
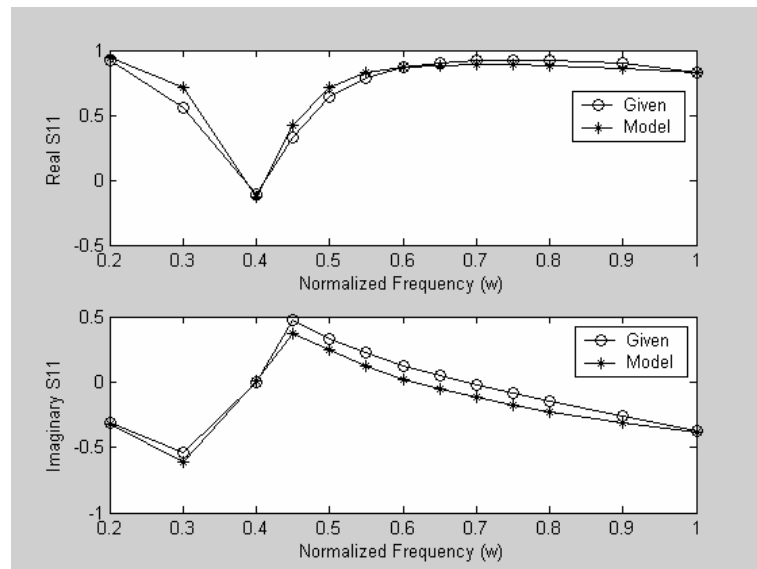
Figure 5.2 Comparison of the given and calculated reflection coefficients.

5.1.2 Antenna Model with Cascaded Separate Lumped and Distributed Networks

In this example, the monopole antenna in section (5.1.1) is modelled by using a mixed model composed of cascade connected lumped and distributed networks. In the lumped circuit [L], only two elements ($n_p = 2$) with single transmission zero at DC are used. In the distributed part [D] of the model, only two sections of unit elements are utilized ($n_\lambda = 2$) with $\tau = 0.6545$. This delay length corresponds to the half of the quarter wavelength at 100 MHz.

For the lumped and the distributed parts of the mixed model, the following polynomials are obtained,

$$h_L(p) = 1.5226p^2 - 0.4782p + 1, \qquad g_L(p) = 1.5226p^2 + 1.1085p + 1$$

$$h_D(\lambda) = -2.7453\lambda^2 + 4.8847\lambda - 0.4782, \qquad g_D(\lambda) = 2.9218\lambda^2 + 5.4509\lambda + 1.1085$$

Finally cascading [L] and [D] it was found

$$h(p,\lambda) = \begin{bmatrix} 1 & 0.3568 & 3.5717 \\ -0.4782 & 4.8847 & -2.7453 \\ 1.5226 & 0.5433 & 5.4383 \end{bmatrix}, \quad g(p,\lambda) = \begin{bmatrix} 1 & 0.3568 & 3.5717 \\ 1.1085 & 5.4509 & 2.9218 \\ 1.5226 & 0.5433 & 5.4383 \end{bmatrix}$$

with $f(p,\lambda) = p(1 - \lambda^2)$.

Synthesis of the above reflection coefficient $S_{11}(p,\lambda) = \dfrac{h(p,\lambda)}{g(p,\lambda)}$ results in the following antenna model (Figure 5.3).
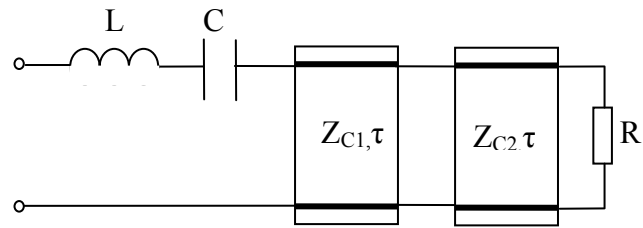
Figure 5.3 Antenna model with cascaded lumped and distributed networks
(L=1.9193, C=0.7933, Z_{C1}=1.4249, Z_{C2}=5.0892, τ=0.6545, R=0.3972).

As a result, the fit between the analytic form of the reflection coefficient and measured data is given in Figure 5.4. It can be seen from Figure 5.4 that the curves of the mixed model fit to the curves formed by using the given antenna data. So also this mixed model can be considered as an acceptable model of the given monopole antenna.
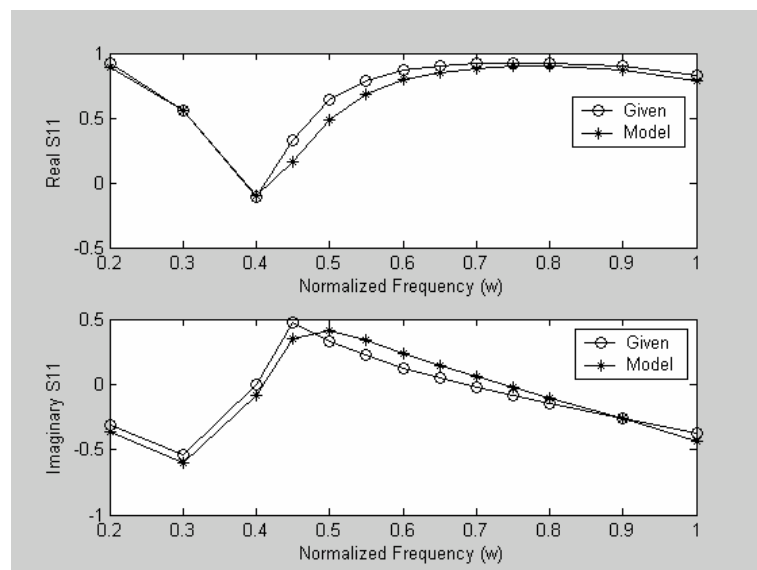
Figure 5.4 Fit between model and the measured data for the monopole antenna.

5.2 Transformation from a Lumped Element Filter to a Mixed Element Filter via Modeling

In this part, mixed element counterparts of a lumped element Butterworth and a lumped element Chebyshev filter are obtained by using the proposed mixed element modeling method.

5.2.1 Mixed Model of a Lumped Element Butterworth Filter

In this example, a two-lumped-element Butterworth filter is transformed to a mixed counterpart. Given lumped filter and its input reflection coefficient calculation are given in Figure 5.5 and Table 5.2, respectively. Mixed model contains two-lumped and two-distributed elements. Since the lumped filter has a low-pass nature, $f(p,\lambda)$ is selected as

$$f(p,\lambda) = f(p)f(\lambda) = 1 \cdot (1 - \lambda^2).$$

In this example, ladder networks connected with unit elements approach will be utilized.
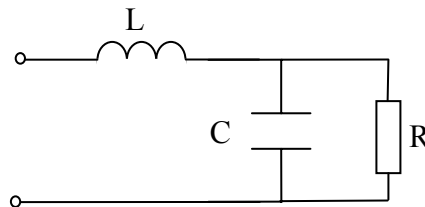
Figure 5.5 Two-lumped-element Butterworth filter

(L=1.4142, C=1.4142, R=1).

Table 5.2 Reflectance data for the lumped element Butterworth filter.

Frequency (ω)	Re $\{S\}$	Im $\{S\}$	Frequency (ω)	Re $\{S\}$	Im $\{S\}$
0	0	0	0.9	-0.0929	0.6225
0.1	-0.0099	0.0014	1.0	0	0.7071
0.2	-0.0383	0.0113	1.1	0.1031	0.7639
0.3	-0.0812	0.0379	1.2	0.2061	0.7951
0.4	-0.1310	0.0883	1.3	0.3024	0.8057
0.5	-0.1765	0.1664	1.4	0.3886	0.8015
0.6	-0.2040	0.2704	1.5	0.4639	0.7873
0.7	-0.2015	0.3912	1.6	0.5287	0.7669
0.8	-0.1635	0.5137	1.7	0.5841	0.7429

Eventually, $S_{11}(p,\lambda)$ is generated as

$$S_{11}(p,\lambda) = \frac{h(p,\lambda)}{g(p,\lambda)}$$

where

$$h(p,\lambda) = \begin{bmatrix} 0.0319 & -0.1453 & 0.6383 \\ -0.0493 & 1.3167 & 0.6898 \\ 0.4600 & 0.3189 & 0 \end{bmatrix} \quad g(p,\lambda) = \begin{bmatrix} 1.0005 & 2.0867 & 1.1864 \\ 0.9452 & 2.0063 & 0.6898 \\ 0.4600 & 0.3189 & 0 \end{bmatrix}$$

and it is synthesized as depicted in Figure 5.6.
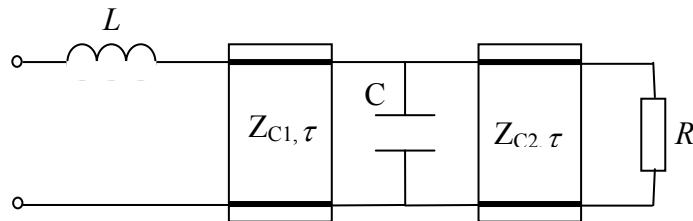
Figure 5.6 Mixed model of the Butterworth filter
(Z_{C1}=1.2800, Z_{C2}=0.72427, τ=0.3850, L=0.92509, C=0.96316, R=1.066).

In Figure 5.7, reflection coefficients of the given lumped Butterworth filter and the obtained mixed model are drawn on the same graph.
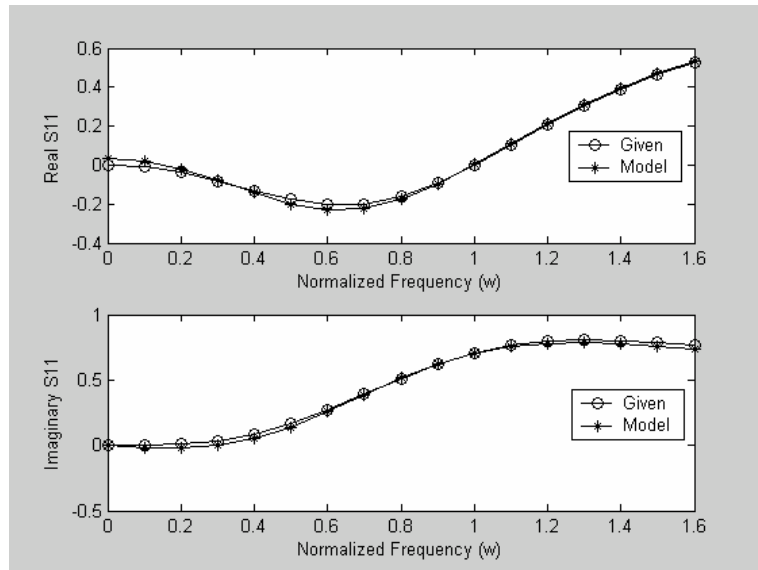
Figure 5.7 Reflection coefficients of the lumped Butterworth filter and the mixed model.

In Figure 5.8, transducer power gain curves (TPG) are given for comparison purpose. So the mixed element Butterworth filter is obtained from the lumped element one via proposed modeling method.
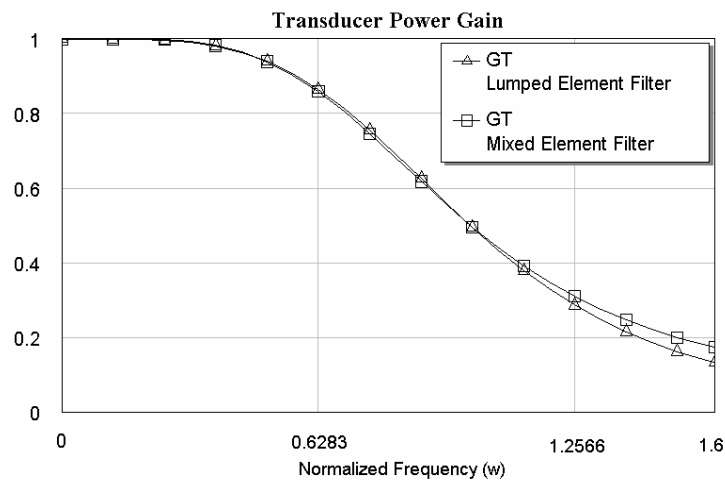
Figure 5.8 Transducer power gain curves for Butterworth filters.

5.2.2 Mixed Model of a Lumped Element Chebyshev Filter

In this example, a three-lumped-element Chebyshev filter (π type network) is transformed to a mixed element counterpart. Given lumped filter and its input reflection coefficient calculation are given in Figure 5.9 and Table 5.3, respectively.
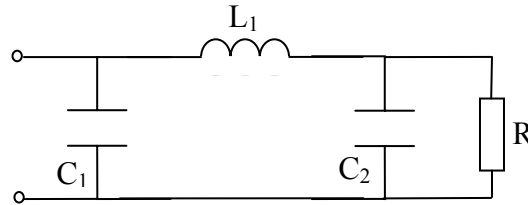
Figure 5.9 Three-lumped-element Chebyshev filter
(L_1=1.0967, C_1=1.5963, C_2=1.5963, R=1).

Table 5.3 Reflectance data for the lumped element Chebyshev filter.

Frequency (ω)	Re $\{S\}$	Im $\{S\}$
0.1	-0.0218	-0.1005
0.2	-0.0797	-0.1775
0.3	-0.1556	-0.2165
0.4	-0.2285	-0.2141
0.5	-0.2795	-0.1751
0.6	-0.2909	-0.1092
0.7	-0.2441	-0.0340
0.8	-0.1212	0.0146
0.9	0.0684	-0.0314
1.0	0.2327	-0.2337
1.1	0.2354	-0.5272
1.2	0.0787	-0.7525
1.3	-0.1229	-0.8541

In the mixed model, ladder networks connected with Unit Elements structure is used. Since the lumped filter has a low-pass nature, $f(p,\lambda)$ is selected as

$$f(p,\lambda) = f(p)f(\lambda) = 1 \cdot (1 - \lambda^2) = 1 - \lambda^2.$$

Eventually, $S_{11}(p,\lambda)$ is generated as

$$S_{11}(p,\lambda) = \frac{h(p,\lambda)}{g(p,\lambda)}$$

where

$$h(p,\lambda) = \begin{bmatrix} 0 & -1.6947 & 1.2298 \\ -0.2198 & 0.1055 & -3.0018 \\ -0.4011 & -1.3409 & 0 \end{bmatrix} \quad g(p,\lambda) = \begin{bmatrix} 1 & 2.8358 & 1.5851 \\ 0.9223 & 2.2429 & 3.0018 \\ 0.4011 & 1.3409 & 0 \end{bmatrix}$$

and it is synthesized as depicted in Figure 5.10.
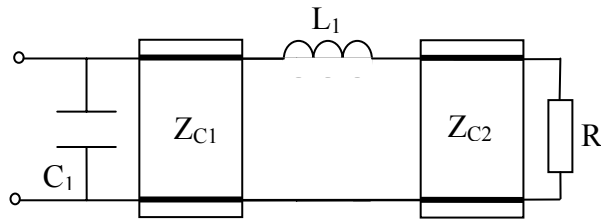
Figure 5.10 Mixed model of the Chebyshev filter
(L_1=0.70268, C_1=1.1419, Z_{C1}=0.84203, Z_{C2}=0.29913, $\tau = 0.5035$, R=1).

In Figure 5.11 and in Figure 5.12, input reflection coefficient and transducer power gain performances for the given lumped filter and for the obtained mixed model are given, respectively. It can be seen form Figure 5.12 that TPG curve of the mixed element filter fits to the TPG curve of the lumped element filter. As a result, by using the proposed method, a lumped element Chebyshev filter is transformed to the mixed element type.
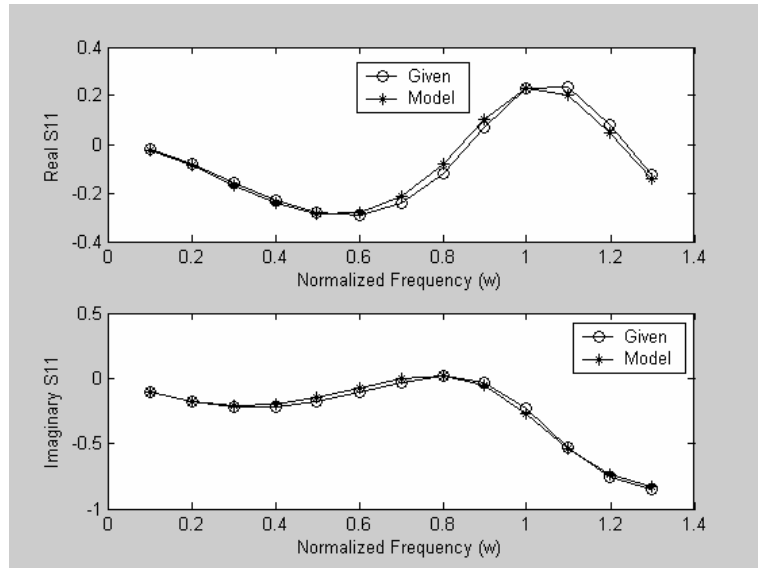
Figure 5.11 Reflection coefficients of the Chebyshev filter and the mixed model.
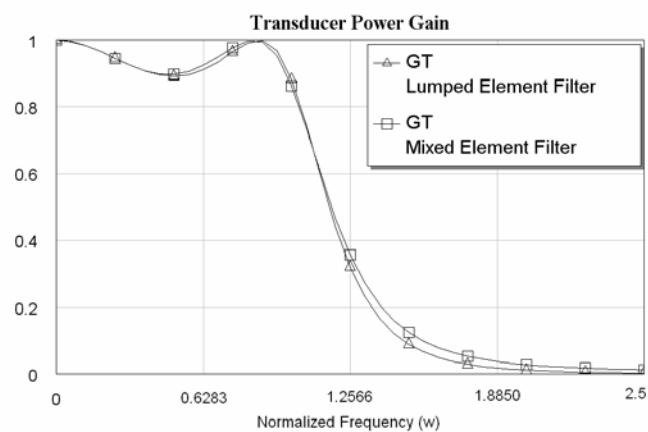
Figure 5.12 Transducer power gain curves for Chebyshev filters.

5.3 A Single Stage Microwave Amplifier Design via Modeling

In [6], a single stage microwave amplifier with HFET2001 is designed. In the matching networks, lumped elements have been used. Here these lumped matching networks are replaced by mixed element counterparts. The new mixed element matching networks are obtained via modeling by using ladder networks connected

58

with unit elements. In Table 5.4, scattering parameters of HFET2001 and in Figure 5.13, microwave amplifier designed in [6] are given.

Table 5.4 Scattering parameters of HFET2001.

Frequency(GHz)	S_{11}	S_{12}	S_{21}	S_{22}
6	0.3719-0.7976i	0.0250+0.0433i	-1.1472+1.6383i	0.6583-0.2660i
7	0.2213-0.8259i	0.0304+0.0459i	-0.8649+1.6974i	0.6247-0.3047i
8	0.0723-0.8268i	0.0361+0.0479i	-0.5893+1.7114i	0.5889-0.3400i
9	-0.0424-0.8089i	0.0369+0.0473i	-0.3586+1.6873i	0.5587-0.3698i
10	-0.1507-0.7755i	0.0378+0.0466i	-0.1429+1.6338i	0.5271-0.3972i
11	-0.2266-0.7411i	0.0374+0.0470i	0.0136+1.5599i	0.5056-0.4242i
12	-0.2970-0.6996i	0.0369+0.0473i	0.1547+1.4719i	0.4827-0.4501i
13	-0.3669-0.6484i	0.0361+0.0479i	0.2861+1.4062i	0.4556-0.4636i
14	-0.4291-0.5906i	0.0353+0.0485i	0.4064+1.3293i	0.4282-0.4756i
15	-0.4956-0.5223i	0.0377+0.0529i	0.5294+1.2473i	0.3971-0.5083i
16	-0.5518-0.4468i	0.0402+0.0573i	0.6399+1.1545i	0.3523-0.5223i
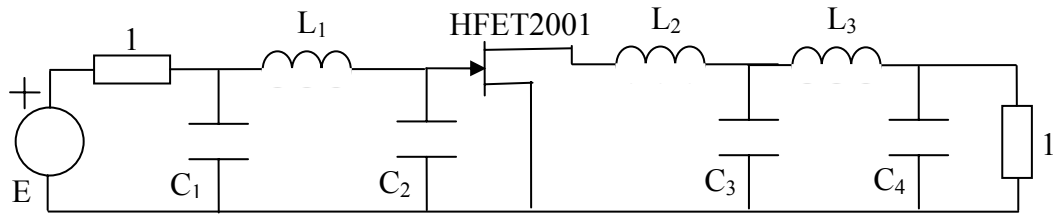
Figure 5.13 Single stage microwave amplifier with lumped elements
(L_1=0.98, L_2=3.23, L_3=1.93, C_1=1.27, C_2=0.06, C_3=1.04, C_4=0.57).

Eventually, $S_{11}^F(p,\lambda)$ and $S_{11}^B(p,\lambda)$ for front-end and back-end matching networks respectively are generated as

$$S_{11}^F(p,\lambda) = \frac{h^F(p,\lambda)}{g^F(p,\lambda)}$$

where

$$h^F(p,\lambda) = \begin{bmatrix} 0.0046 & -0.1585 & -0.3511 \\ -0.0040 & 0.0357 & 0.0480 \\ 0.0009 & 0.0010 & 0 \end{bmatrix} \quad g^F(p,\lambda) = \begin{bmatrix} 1 & 2.0367 & 1.0599 \\ 0.0433 & 0.0876 & 0.0480 \\ 0.0009 & 0.0010 & 0 \end{bmatrix}$$

and it is synthesized as depicted in Figure 5.14.
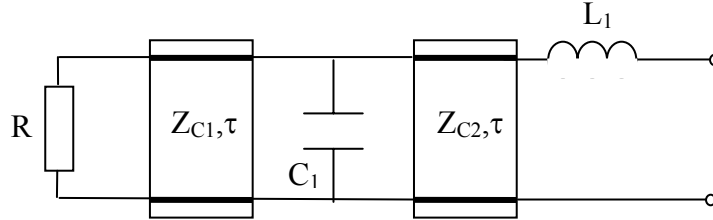
Figure 5.14 Mixed element front-end matching network

(L_1=0.6088, C_1=0.7766, Z_{C1}=1.1062, Z_{C2}=0.7806, τ=0.0065, R=1.0092).

$$S_{11}^B(p,\lambda) = \frac{h^B(p,\lambda)}{g^B(p,\lambda)}$$

where

$$h^B(p,\lambda) = \begin{bmatrix} -0.1364 & 2.6155 & 0.1036 \\ 0.0205 & 0.0345 & 0.2451 \\ 0.0019 & 0.0054 & 0 \end{bmatrix} \quad g^B(p,\lambda) = \begin{bmatrix} 1.0093 & 3.3013 & 1.0053 \\ 0.0698 & 0.1707 & 0.2451 \\ 0.0019 & 0.0054 & 0 \end{bmatrix}$$

and it is synthesized as depicted in Figure 5.15.
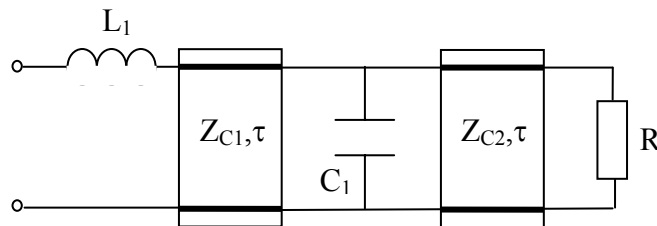
Figure 5.15 Mixed element back-end matching network

(L_1=1.2333, C_1=0.9540, Z_{C1}=2.8900, Z_{C2}=2.2740, τ=0.0065, R=0.7618).

After connecting front-end matching network, active element (HFET2001) and back-end matching network, single stage microwave amplifier is formed, which can be seen in Figure 5.16.
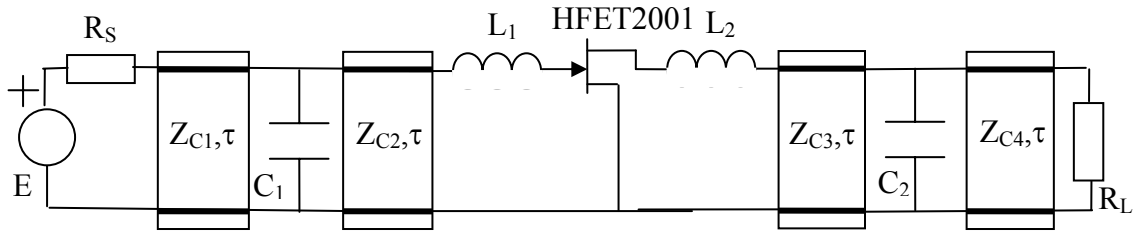
Figure 5.16 Single stage microwave amplifier with mixed elements
(L_1=0.6088, L_2=1.2333, C_1=0.7766, C_2=0.9540, Z_{C1}=1.1062, Z_{C2}=0.7806,
Z_{C3}=2.8900, Z_{C4}=2.2740, τ=0.0065, R_S=1.0092, R_L=0.7618).

To be able to compare transducer power gain curves for lumped and mixed element designs, the graphs are given in Figure 5.17.
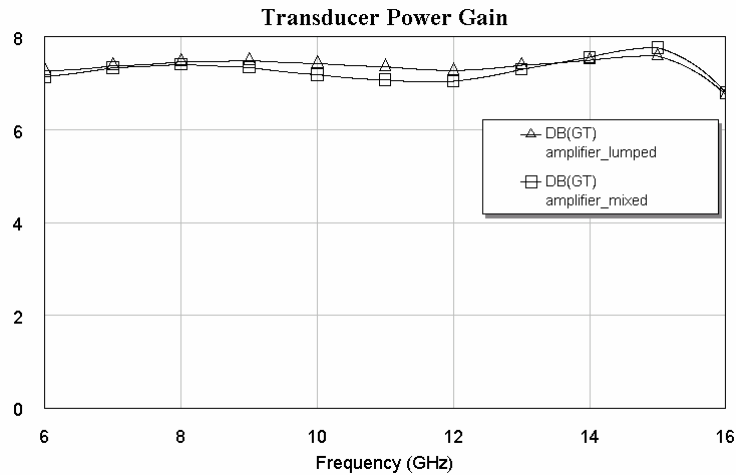
Figure 5.17 Transducer power gain curves for lumped and mixed element amplifiers.

As a result, it can be concluded from Figure 5.17 that almost the same TPG performance is obtained from the mixed element design. So the given lumped element amplifier is successfully transformed to a mixed element amplifier via the proposed modeling method.

Chapter 6
Design and Implementation Issues

In this chapter, first planar transmission lines are summarized. Then, practical issues are covered for the lumped and mixed element circuits examined in Chapter 5. In the implementation process of lumped element circuits, small transmission lines between the lumped elements connecting them degrade the performance of the network. So in this chapter, transducer power gain curves for lumped element circuits are drawn by inserting these lines between lumped elements. But in the mixed element circuits, there is no need to insert such connection lines, since they are already inserted in the design or modeling process. In this chapter, transducer power gain performances of the ideal/practical lumped and mixed element circuits are compared.

6.1 Characteristics of Planar Transmission Lines

Transmission lines are used to carry information or energy from one point to the other in microwave circuits. Also they are used as circuit elements for passive circuits such as filters, impedance transformers, couplers, etc.. Passive elements in conventional microwave circuits can be considered as distributed. Since the size of discrete lumped elements (resistors, inductors and capacitors) used in circuits at lower frequencies become comparable to the wavelength at microwave frequencies. But,if the size of lumped elements are much smaller than the wavelength, they can be used at microwave frequencies.

To be able to use a transmission structure as a circuit element in MICs, the structure should be planar. By planar,it is meant that the characteristics of the element can be

determined from the dimensions in a single plane. Different forms of planar transmission lines have been developed for use in MICs. For example, the strip line, microstrip line, inverted microstrip line, slot line, coplanar waveguide and coplanar strip line are all planar transmission lines. The circuits constructed by using transmission lines have advantages such that light weight, small size, improved performance, reproducibility and low cost as compared to conventional microwave circuits.

In hybrid MIC applications, microstrips, slot lines, coplanar waveguides (CPWs) and coplanar strips (CPSs) have been used, on the other hand in monolithic MICs, microstrip has been used generally, although there is an interest in CPW. A few of the parameters of the four types of lines are compared in Table 6.1. It can be seen from the table that CPWs and CPSs have some advantageous features of microstrip lines and slot lines. Their power-handling capabilities, radiation losses and dispersion behaviour lie in between the corresponding values for microstrip and slot lines.

Table 6.1 Comparison of various MIC lines [55].

Characteristics	Microstrips	Slot Lines	Coplanar Waveguides	Coplanar Strips
Impedance range	20-110	55-300	25-155	45-280
Power-handling capability	High	Low	Medium	Medium
Radiation loss	Low	High	Medium	Medium
Dispersion	Small	Large	Medium	Medium
Enclosure dimensions	Small	Large	Large	Large

Microstip line is one of the most popular types of planar lines, since it can be fabricated and integrated easily with other passive and active microwave devices.

The structure of a microstrip line is shown in Figure 6.1. A conductor of width W is printed on a thin, grounded dielectric substrate of thickness Th and relative permittivity E_r.
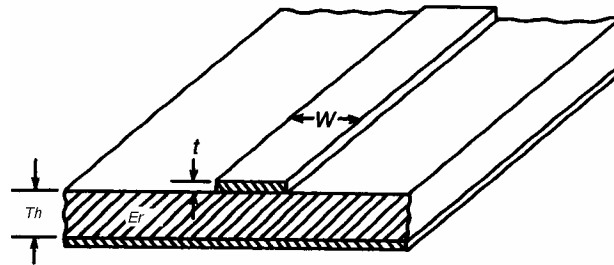
Figure 6.1 Microstrip line configuration [55].

To be able to characterize microstrip lines by using numerical methods, extensive computations must be involved. But for optimization and computer-aided design (CAD) of microstrip circuits, closed-form expressions are necessary. Closed-form expressions for characteristic impedance (Z_C) and and relative permittivity (E_r) can be found in [56-60]. The characteristic impedance and effective dielectric constant versus W/Th is given in Figure 6.2.
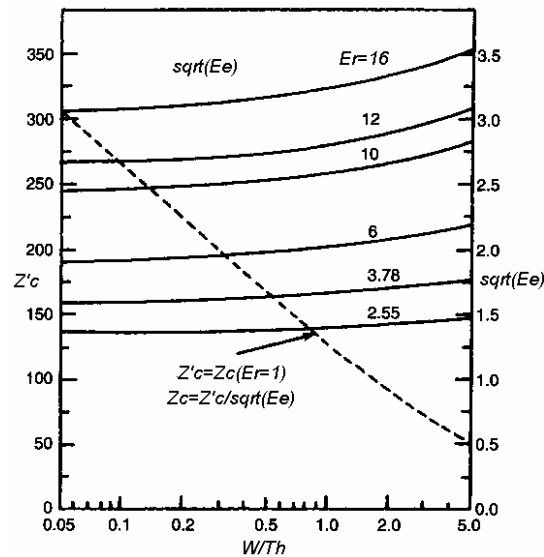
Figure 6.2 Characteristic impedance and effective dielectric constant of microstrip lines [55].

The characteristic impedance and effective dielectric constant expressions are given in Table 6.2.

Table 6.2 Microstrip line characteristics [55].

Parameters	Expressions
Characteristic impedance (Ω)	$Z_C = \begin{cases} \dfrac{\eta_0}{2\pi\sqrt{\varepsilon_e}}\ln\left(\dfrac{8Th}{W'}+0.25\dfrac{W'}{Th}\right) & , \quad \dfrac{W}{Th}\leq 1 \\[4mm] \dfrac{\eta_0}{\sqrt{\varepsilon_e}}\left[\dfrac{W'}{Th}+1.393+0.667\ln\left(\dfrac{W'}{Th}+1.444\right)\right]^{-1} & , \quad \dfrac{W}{Th}\geq 1 \end{cases}$
	$\eta_0 = 120\pi\,\Omega$
	$\dfrac{W'}{Th} = \dfrac{W}{Th}+\dfrac{1.25}{\pi}\dfrac{t}{Th}\left(1+\ln\dfrac{4\pi W}{t}\right), \quad \dfrac{W}{Th}\leq\dfrac{1}{2\pi}$
	$\dfrac{W'}{Th} = \dfrac{W}{Th}+\dfrac{1.25}{\pi}\dfrac{t}{Th}\left(1+\ln\dfrac{2Th}{t}\right), \quad \dfrac{W}{Th}\geq\dfrac{1}{2\pi}$
Effective dielectric constant	$\varepsilon_e = \dfrac{E_r+1}{2}+\dfrac{E_r-1}{2}F\left(\dfrac{W}{Th}\right)-\dfrac{E_r-1}{4.6}\dfrac{t/Th}{\sqrt{W/Th}}$
	$F\left(\dfrac{W}{Th}\right) = \begin{cases} \left(1+12\dfrac{Th}{W}\right)^{-1/2}+0.04\left(1-\dfrac{W}{Th}\right)^2, & \dfrac{W}{Th}\leq 1 \\[4mm] \left(1+12\dfrac{Th}{W}\right)^{-1/2} & , \quad \dfrac{W}{Th}\geq 1 \end{cases}$

6.2 Practical Lumped and Mixed Element Structures

In this section, implementations of the filter and amplifier circuits obtained in Chapter 5 by using the proposed mixed modeling method are examined. Also performance, namely transducer power gain, comparison of the lumped and mixed element implementations is given.

6.2.1 Lumped and Mixed Element Butterworth Filters

In section 5.2.1, after applying the proposed mixed modeling method, mixed element counterpart of the given two-lumped-element Butterworth filter is reached. Let us now construct practical lumped and mixed element Butterworth filters by using the obtained prototype filters.

In the lumped element filter, small pieces of lines are added. These lines correspond to the connections between the lumped elements. The length of the lines are selected as $\lambda/2$, since the input impedance of a transmission line with length of $\lambda/2$ is the termination resistance R. There is no affect of the transmission line at the corresponding frequency to the input impedance, namely to the input reflectance. As one moves away from this frequency at both sides, the affect of the line will increase. So to be able to reduce the affect, this frequency must be selected as the midband frequency of the application.

In this example, suppose that $\lambda/2 = 1mm$ is the desired line lengths. So the corresponding frequency is $150GHz$. If this frequency is placed in the passband, the cut-off frequency of the filter can be selected as $200GHz$.

After frequency and impedance denormalization ($f_n = 200GHz$, $R_n = 50\Omega$), ideal lumped element Butterworth filter shown in Figure 6.3 is obtained.
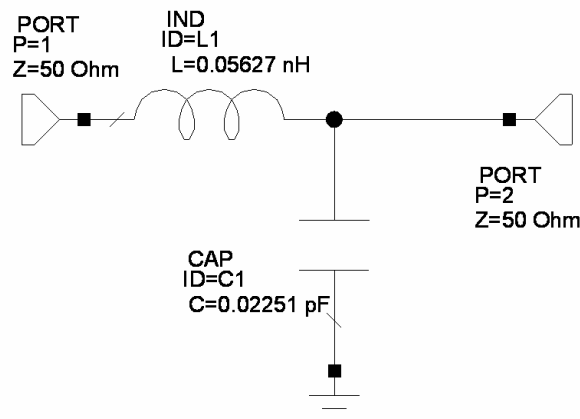
Figure 6.3 Ideal lumped element Butterworth filter ($f_n = 200GHz$, $R_n = 50\Omega$)

(L=0.05627nH, C=0.02251pF, R_S=50Ω, R_L=50Ω).

Transducer power gain for the filter shown in Figure 6.3 is given in Figure 6.4.
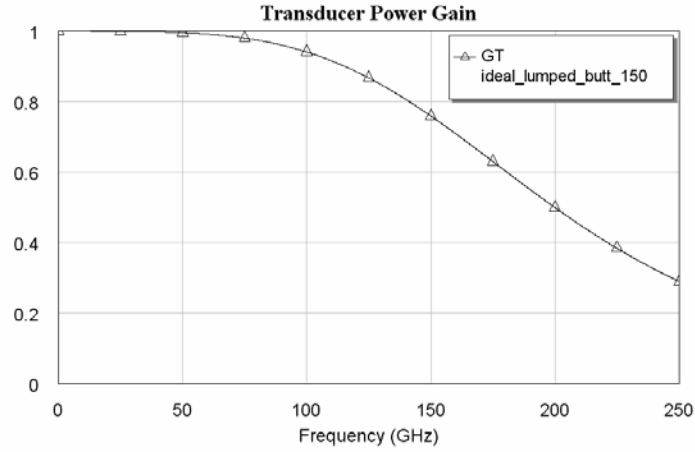
Figure 6.4 Transducer power gain for ideal lumped element Butterwoth filter

$$(f_n = 200GHz , \ R_n = 50\Omega).$$

In Figure 6.5, practical lumped element Butterworth filter is shown. In the circuit, air is selected as the dielectric material, so $E_r = 1$ is used. The height of the material and the thickness of the metal conductor is selected as $Th = 1000\mu m$ and $t = 1\mu m$, respectively. The width of the line is calculated by using AWR-TX Line program to obtain a 50Ω input impedance, since the normalization frequency R_n is 50Ω [61].
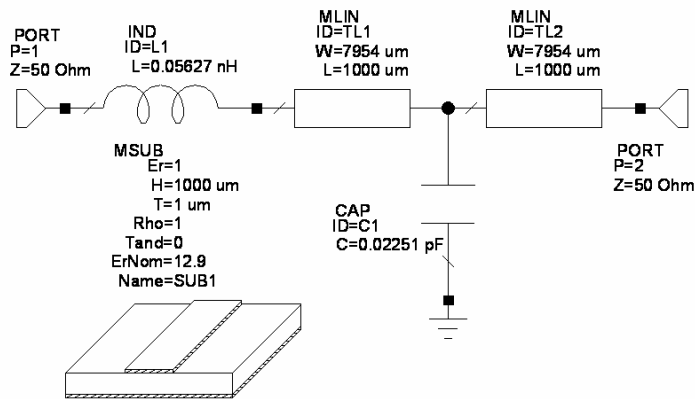
Figure 6.5 Practical lumped element Butterworth filter

$$(f_n = 200GHz , \ R_n = 50\Omega, \ E_r = 1)$$

(L=0.05627nH, C=0.02251pF, TL1=TL2=$7954x1000\mu m$, $E_r = 1$, $Th = 1000\mu m$,

$t = 1\mu m$, R$_S$=50Ω, R$_L$=50Ω).

In Figure 6.6, transducer power gain curve for practical lumped element Butterworth filter can be seen.
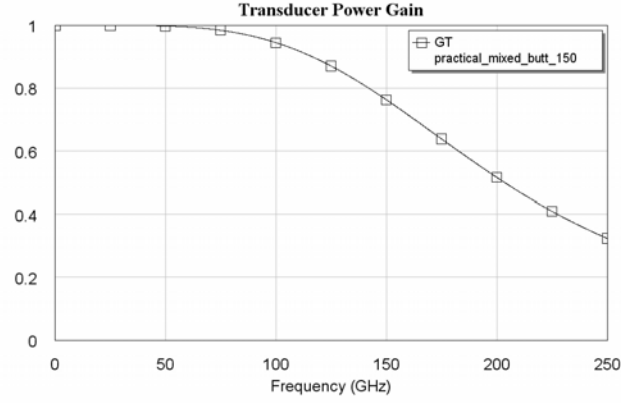

Figure 6.6 Transducer power gain for practical lumped element Butterwoth filter

$$(f_n = 200GHz , \ R_n = 50\Omega, \ E_r = 1).$$

To be able to reduce the line lengths, a dielectric material (GaAs) with $E_r = 12.9$ is used. The height of the material and the thickness of the metal conductor is selected as $Th = 10\mu m$ and $t = 1\mu m$, respectively. The width of the line is calculated by using AWR-TX Line program to obtain a 50Ω input impedance, since the normalization frequency R_n is 50Ω [61].
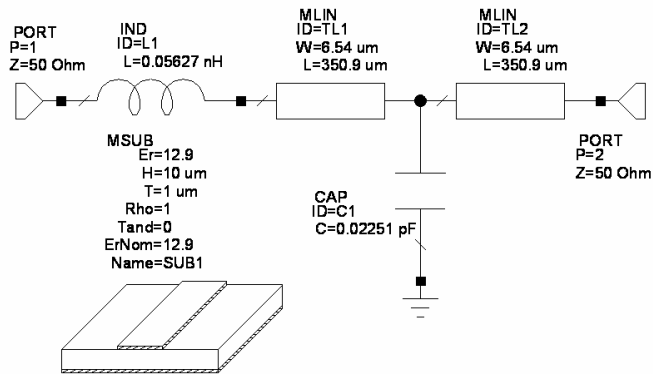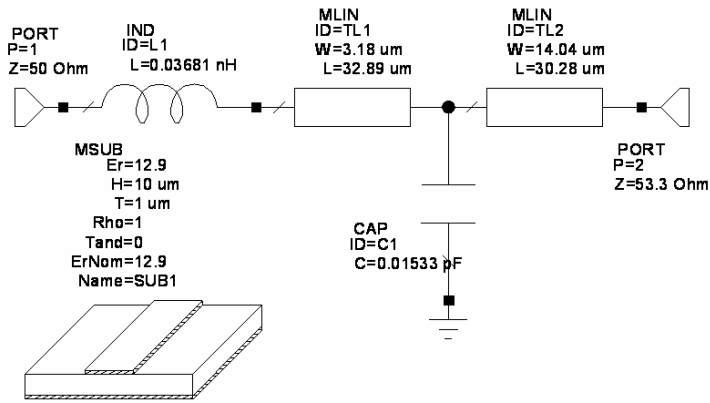

Figure 6.7 Practical lumped element Butterworth filter

$$(f_n = 200GHz , R_n = 50\Omega, E_r = 12.9)$$

(L=0.05627nH, C=0.02251pF, TL1=TL2= $6.54x350.9\mu m$, $E_r = 12.9$, $Th = 10\mu m$,

$t = 1\mu m$, R$_S$=50Ω, R$_L$=50Ω).

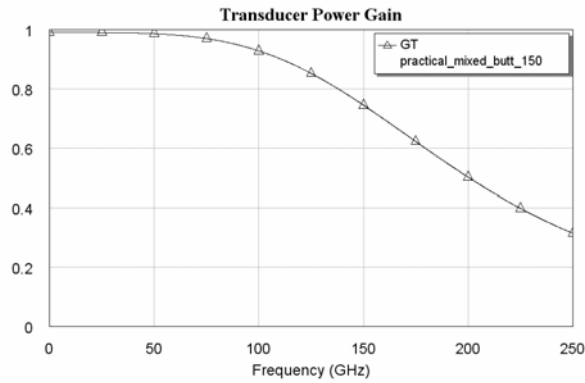In Figure 6.8, transducer power gain curve for practical lumped element Butterworth filter can be seen.
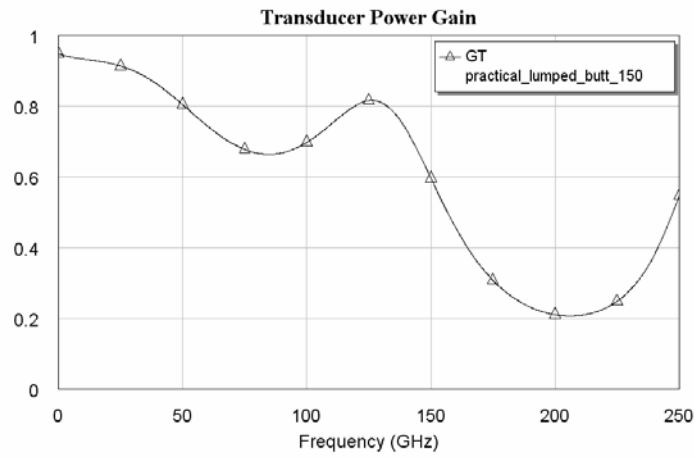
Figure 6.8 Transducer power gain for practical lumped element Butterwoth filter
($f_n = 200GHz$, $R_n = 50\Omega$, $E_r = 12.9$).

Let us now denormalize the obtained mixed element counterpart of the lumped element Butterworth filter. Again $f_n = 200GHz$ and $R_n = 50\Omega$ are used as the denormalization frequency and resistance, respectively. In Figure 6.9, ideal mixed element Butterworth filter is shown.
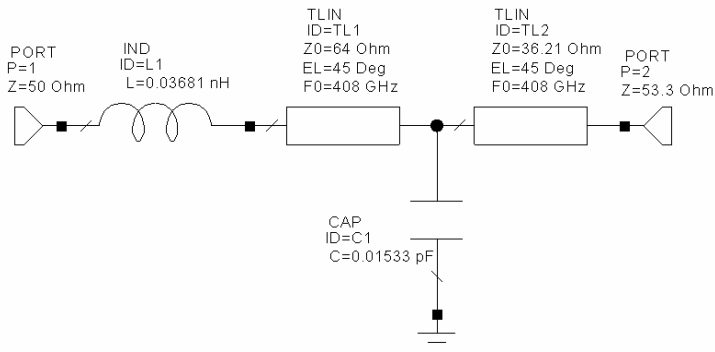
Figure 6.9 Ideal mixed element Butterworth filter ($f_n = 200GHz$, $R_n = 50\Omega$)
(L=0.03681nH, C=0.01533pF, TL1=64Ω, TL2=36.21Ω, R$_S$=50Ω, R$_L$=53.3Ω).

Transducer power gain curve for the filter shown in Figure 6.9 is given in Figure 6.10.

69
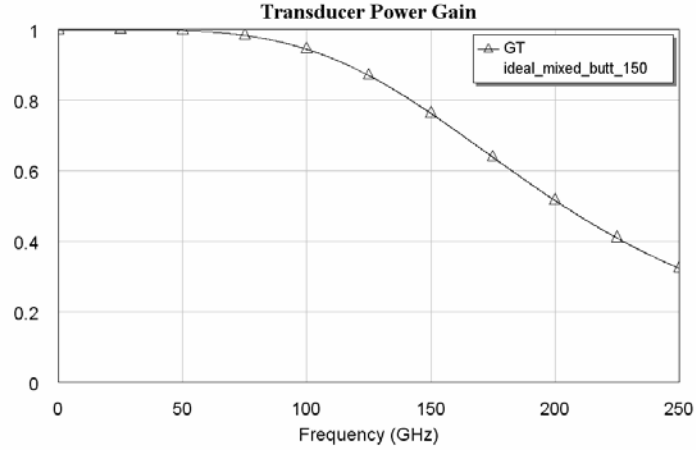
Figure 6.10 Transducer power gain for ideal mixed element Butterwoth filter

$$(f_n = 200GHz , \ R_n = 50\Omega).$$

Practical mixed element Butterworth filter is obtained as seen in Figure 6.11, after calculating the widths and the lengths of the transmission lines seen in Figure 6.9 via AWR-TX Line program [61].
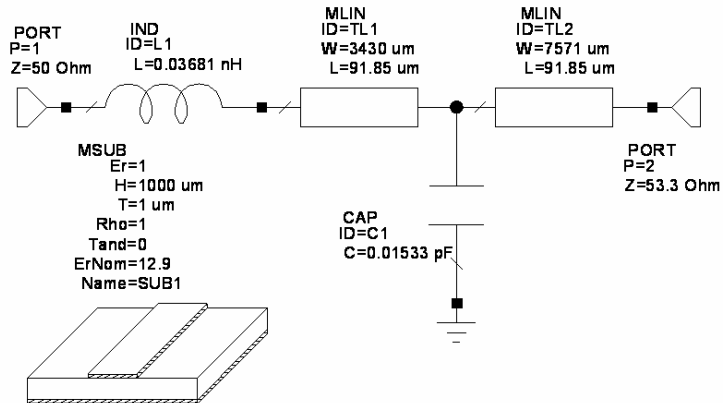
Figure 6.11 Practical mixed element Butterworth filter

$$(f_n = 200GHz , \ R_n = 50\Omega , \ E_r = 1)$$

(L=0.03681nH, C=0.01533pF, TL1=$3429.8x91.848\mu m$, TL2=$7570.8x91.848\mu m$,

$E_r = 1$, $Th = 1000\mu m$, $t = 1\mu m$, R$_S$=50Ω, R$_L$=53.3Ω).

In Figure 6.12, transducer power gain curve for practical mixed element Butterworth filter can be seen.

70

Figure 6.12 Transducer power gain for practical mixed element Butterwoth filter

$$(f_n = 200 GHz , \ R_n = 50 \Omega, \ E_r = 1).$$

Again to be able to reduce the line lengths, a dielectric material (GaAs) with $E_r = 12.9$ is used. The height of the material and the thickness of the metal conductor is selected as $Th = 10 \mu m$ and $t = 1 \mu m$, respectively. The width of the line is calculated by using AWR-TX Line program to obtain a 50Ω input impedance, since the normalization frequency R_n is 50Ω [61].

Figure 6.13 Practical mixed element Butterworth filter

$$(f_n = 200 GHz , \ R_n = 50 \Omega, \ E_r = 12.9)$$

(L=0.03681nH, C=0.01533pF, TL1=$3.18x32.89 \mu m$, TL2=$14.04x30.28 \mu m$,

$E_r = 12.9$, $Th = 10 \mu m$, $t = 1 \mu m$, R$_S$=50Ω, R$_L$=53.3Ω).

In Figure 6.14, transducer power gain curve for practical mixed element Butterworth filter can be seen.

71

Figure 6.14 Transducer power gain for practical mixed element Butterwoth filter
($f_n = 200GHz$, $R_n = 50\Omega$, $E_r = 12.9$).

TPG curves for ideal/practical lumped and mixed element Butterworth filters are given in Figure 6.15 with $E_r = 1$ and Figure 6.16 with $E_r = 12.9$ to be able to compare with each other. It can be seen from the figures that practical mixed element filter responses are very close to the ideal curves, on the other hand practical lumped element filter curves are very different from the ideal ones. Also the circuit size of the mixed element filters is much smaller than the size of the lumped element filters. Transmission line lengths in the mixed element filter is about $90\mu m$ in Figure 6.11 and $30\mu m$ in Figure 6.13, but in the lumped element filter, they are $1000\mu m$ in Figure 6.5 and $350\mu m$ in Figure 6.7.
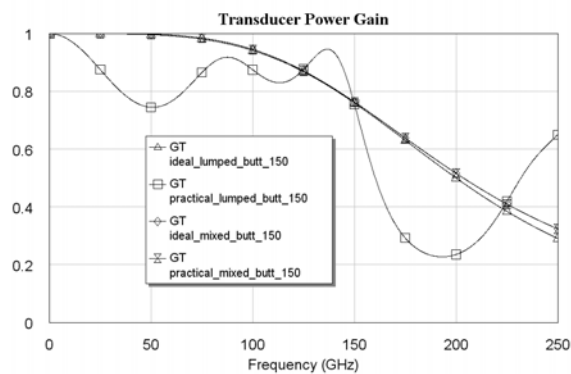
Figure 6.15 Transducer power gain curves for ideal and practical Butterworth filters
($f_n = 200GHz$, $R_n = 50\Omega$, $E_r = 1$).

72
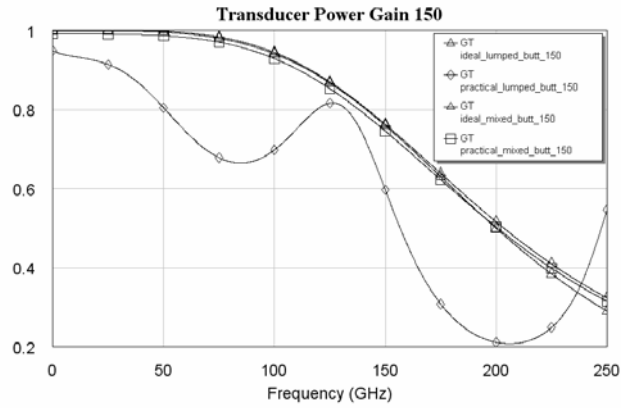
Figure 6.16 Transducer power gain curves for ideal and practical Butterworth filters
($f_n = 200GHz$, $R_n = 50\Omega$, $E_r = 12.9$).

In the previous part, transmission line lengths between the lumped elements were desired to be $\lambda/2 = 1mm$, so the corresponding frequency was $150GHz$. This is very high. If the frequency is reduced to $15GHz$ and the cut-uff frequency to $20GHz$, what are the performances of the lumped and mixed element filters?

In Figure 6.17, obtained ideal lumped element Butterworth filter can be seen in the case of $f_n = 20GHz$, $R_n = 50\Omega$.
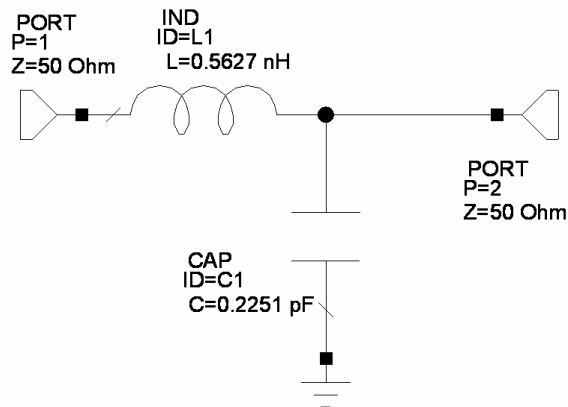
Figure 6.17 Ideal lumped element Butterworth filter ($f_n = 20GHz$, $R_n = 50\Omega$)
(L=0.5627nH, C=0.2251pF, R_S=50Ω, R_L=50Ω).

Transducer power gain curve for the filter shown in Figure 6.17 is given in Figure 6.18.

73
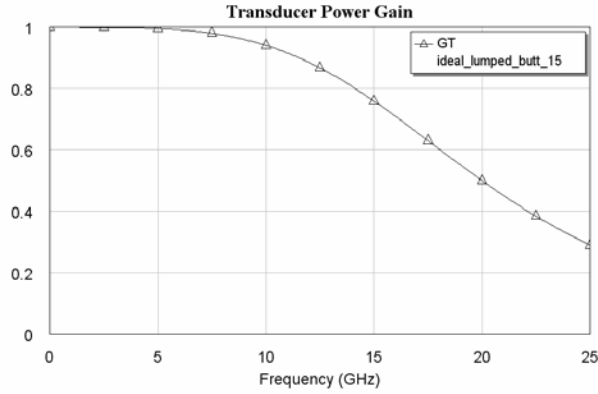
Figure 6.18 Transducer power gain for ideal lumped element Butterwoth filter

$(f_n = 20GHz$, $R_n = 50\Omega)$.

For this case, $\lambda / 2 = 10mm$ length transmission lines must be used between the lumped elements. In the circuit, air is selected as the dielectric material, so $E_r = 1$ is used. The height of the material and the thickness of the metal conductor is selected as $Th = 1000\mu m$ and $t = 1\mu m$, respectively. The width of the line is calculated by using AWR-TX Line program to obtain a 50Ω input impedance, since the normalization frequency R_n is 50Ω [61]. The obtained practical lumped element Butterworth filter is shown in Figure 6.19.
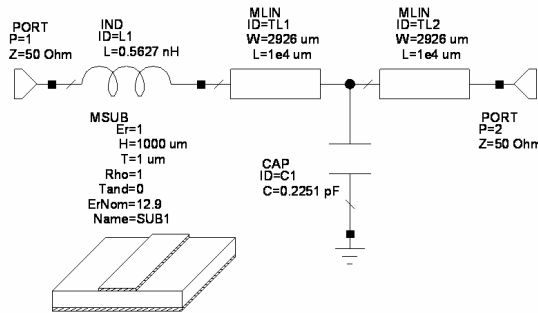
Figure 6.19 Practical lumped element Butterworth filter

$(f_n = 20GHz$, $R_n = 50\Omega$, $E_r = 1)$

(L=0.5627nH, C=0.2251pF, TL1=TL2= $2926x10000\mu m$, $E_r = 1$, $Th = 1000\mu m$,

$t = 1\mu m$, R_S=50Ω, R_L=50Ω).

For practical lumped element Butterworth filter, transducer power gain curve can be seen in Figure 6.20.
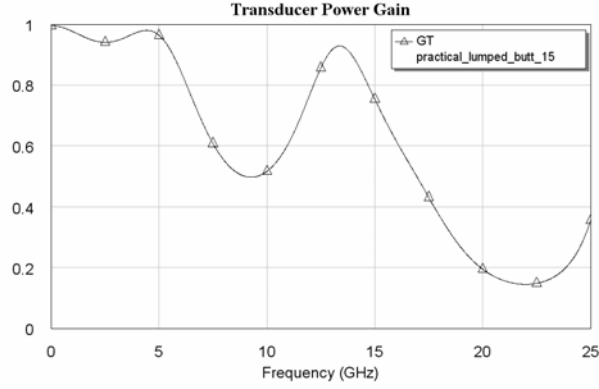
Figure 6.20 Transducer power gain for practical lumped element Butterwoth filter

$(f_n = 20GHz $, $R_n = 50\Omega$, $E_r = 1)$.

To be able to reduce the line lengths, again a dielectric material (GaAs) with $E_r = 12.9$ is used. The height of the material and the thickness of the metal conductor is selected as $Th = 10\mu m$ and $t = 1\mu m$, respectively. The width of the line is calculated by using AWR-TX Line program to obtain a 50Ω input impedance, since the normalization frequency R_n is 50Ω [61]. The obtained practical lumped element Butterworth filter is shown in Figure 6.21.
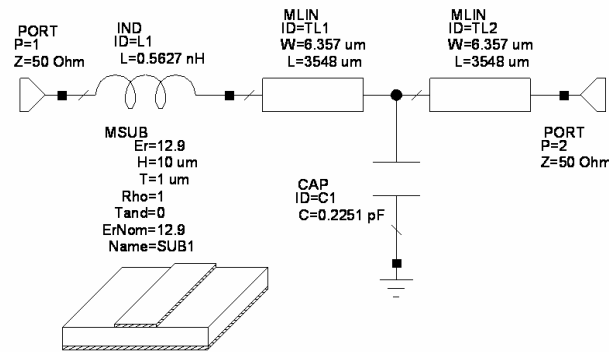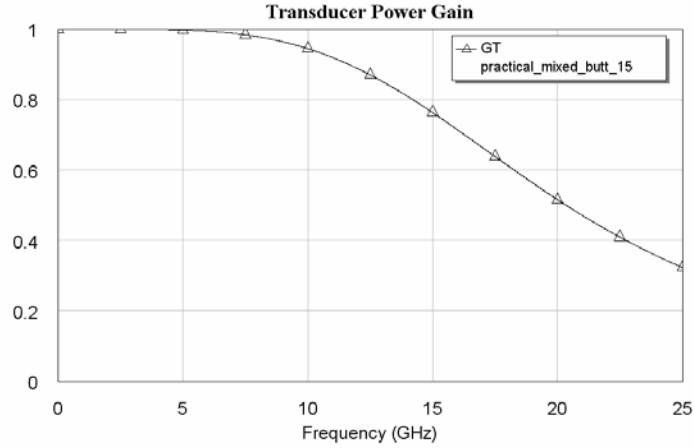

Figure 6.21 Practical lumped element Butterworth filter

$(f_n = 20GHz $, $R_n = 50\Omega$, $E_r = 12.9)$

(L=0.5627nH, C=0.2251pF, TL1=TL2= $6.357x3548\mu m$, $E_r = 12.9$, $Th = 10\mu m$,

$t = 1\mu m$, R$_S$=50Ω, R$_L$=50Ω).

For practical lumped element Butterworth filter, transducer power gain curve can be seen in Figure 6.22.
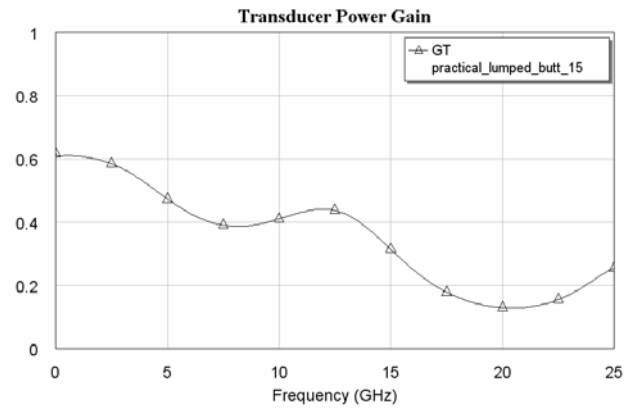
Figure 6.22 Transducer power gain for practical lumped element Butterwoth filter

($f_n = 20GHz$, $R_n = 50\Omega$, $E_r = 12.9$).

Again let us now denormalize the obtained mixed element counterpart of the lumped element Butterworth filter. $f_n = 20GHz$ and $R_n = 50\Omega$ are used as the denormalization frequency and resistance, respectively. In Figure 6.23, ideal mixed element Butterworth filter is shown.
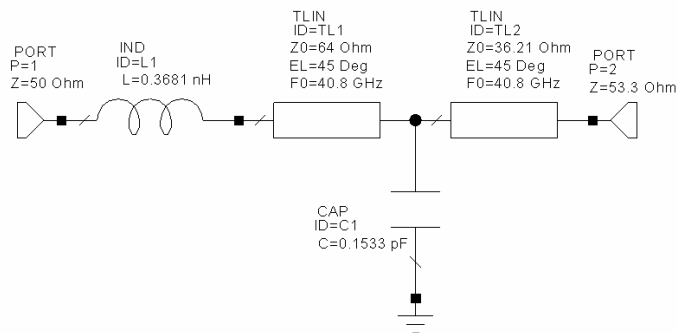
Figure 6.23 Ideal mixed element Butterworth filter ($f_n = 20GHz$, $R_n = 50\Omega$)

(L=0.3681nH, C=0.1533pF, TL1=64Ω, TL2=36.21Ω, R_S=50Ω, R_L=53.3Ω).

In Figure 6.24, transducer power gain curve for the ideal mixed element Butterworth filter can be seen.

76
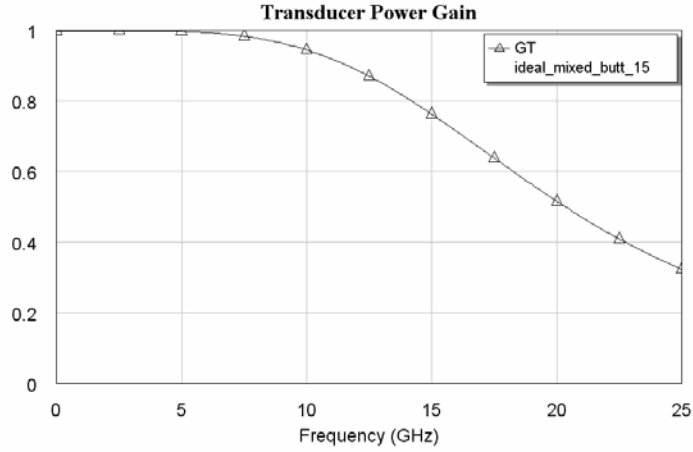
Figure 6.24 Transducer power gain for ideal mixed element Butterwoth filter
$(f_n = 20GHz, R_n = 50\Omega)$.

Practical mixed element Butterworth filter is obtained as seen in Figure 6.25, after calculating the widths and the lengths of the transmission lines seen in Figure 6.23 via AWR-TX Line program [61].
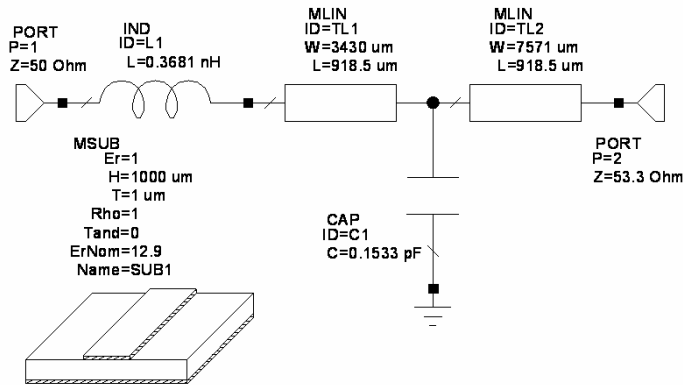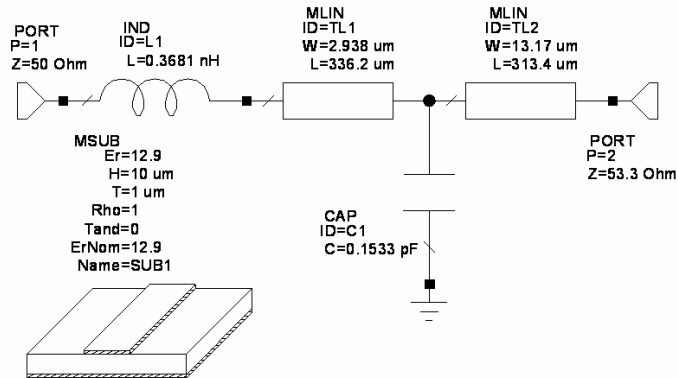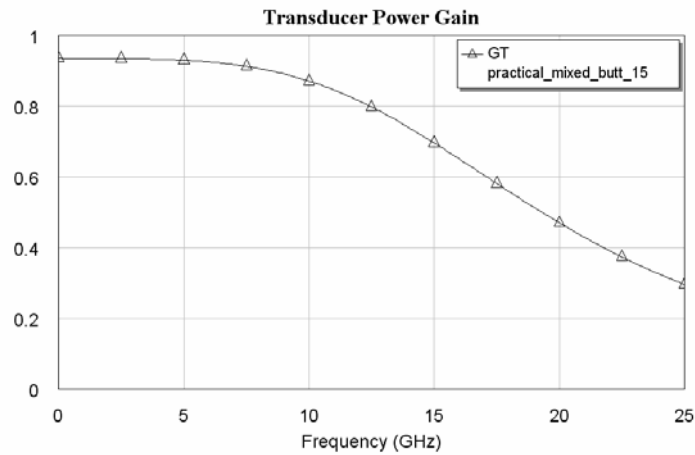

Figure 6.25 Practical mixed element Butterworth filter
$(f_n = 20GHz, R_n = 50\Omega, E_r = 1)$

(L=0.3681nH, C=0.1533pF, TL1=$3429.8x918.48\mu m$, TL2=$7570.8x918.48\mu m$,

$E_r = 1$, $Th = 1000\mu m$, $t = 1\mu m$, R$_S$=50Ω, R$_L$=53.3Ω).

For practical mixed element Butterworth filter, transducer power gain curve is given in Figure 6.26.

Figure 6.26 Transducer power gain for practical mixed element Butterwoth filter

$(f_n = 20GHz,\ R_n = 50\Omega,\ E_r = 1)$.

To be able to reduce the line lengths, again a dielectric material (GaAs) with $E_r = 12.9$ is used. The height of the material and the thickness of the metal conductor is selected as $Th = 10\mu m$ and $t = 1\mu m$, respectively. The width of the line is calculated by using AWR-TX Line program to obtain a 50Ω input impedance, since the normalization frequency R_n is 50Ω [61]. The obtained practical lumped element Butterworth filter is shown in Figure 6.27.

Figure 6.27 Practical mixed element Butterworth filter

$(f_n = 20GHz,\ R_n = 50\Omega,\ E_r = 12.9)$

(L=0.3681nH, C=0.1533pF, TL1=$2.938x336.2\mu m$, TL2=13.17x313.4μm,

$E_r = 12.9$, $Th = 10\mu m$, $t = 1\mu m$, R$_S$=50Ω, R$_L$=53.3Ω).

78

For practical mixed element Butterworth filter, transducer power gain curve is given in Figure 6.28.

Figure 6.28 Transducer power gain for practical mixed element Butterwoth filter

$(f_n = 20GHz$, $R_n = 50\Omega$, $E_r = 12.9)$.

TPG curves for ideal/practical lumped and mixed element Butterworth filters are given in Figure 6.29 with $E_r = 1$ and in Figure 6.30 with $E_r = 12.9$ for comparison. For this case, it can be seen from the figure that practical mixed element filter response again is very close to the ideal curves, on the other hand practical lumped element filter curve is very different from the ideal ones. Also the circuit size of the mixed element filter is much smaller than the size of the lumped element filter. Transmission line lengths in the mixed element filter is about $918\mu m$ in Figure 6.25 and $320\mu m$ in Figure 6.27, but in the lumped element filter, they are $10000\mu m$ in Figure 6.19 and $3550\mu m$ in Figure 6.21.
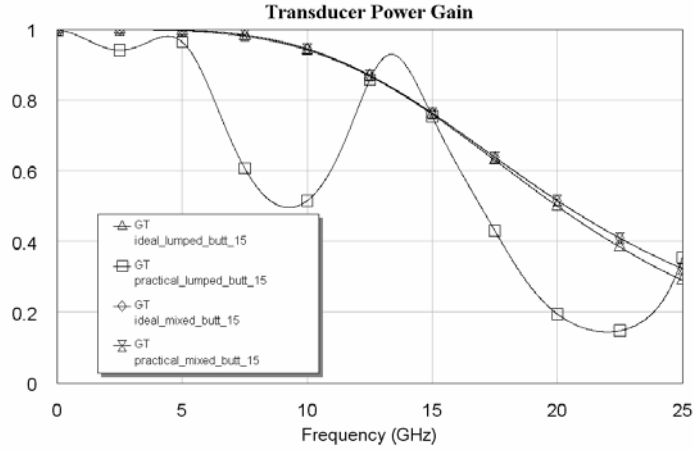
Figure 6.29 Transducer power gain curves for ideal and practical Butterworth filters
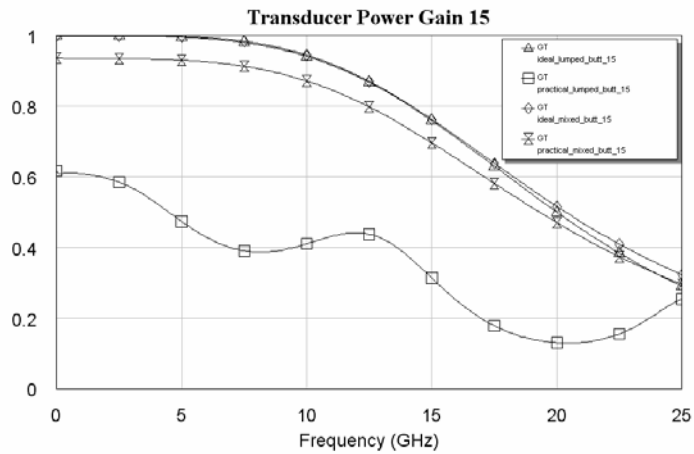
$$(f_n = 20GHz , \ R_n = 50\Omega , \ E_r = 1).$$

Figure 6.30 Transducer power gain curves for ideal and practical Butterworth filters

$$(f_n = 20GHz , \ R_n = 50\Omega , \ E_r = 12.9).$$

6.2.2 Lumped and Mixed Element Chebyshev Filters

In section 5.2.2, after applying the proposed mixed modeling method, mixed element counterpart of the given three-lumped-element Chebyshev filter is reached. Let us now construct practical lumped and mixed element Chebyshev filters by using the obtained prototype filters.

In the lumped element filter, again small pieces of lines are added. These lines correspond to the connections between the lumped elements. The length of the lines are selected as $\lambda/2$.

In this example, again suppose that $\lambda/2 = 1mm$ is the desired line lengths. So the corresponding frequency is $150GHz$. If this frequency is placed in the passband, the cut-off frequency of the filter can be selected as $200GHz$.

After frequency and impedance denormalization ($f_n = 200GHz$, $R_n = 50\Omega$), ideal lumped element Chebyshev filter shown in Figure 6.31 is obtained.
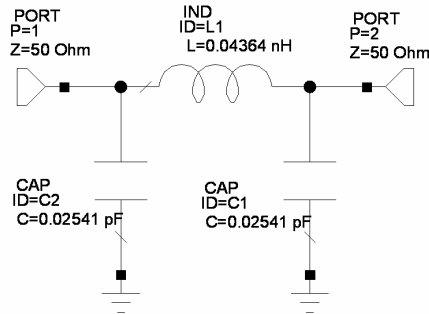
Figure 6.31 Ideal lumped element Chebyshev filter ($f_n = 200GHz$, $R_n = 50\Omega$) (L=0.04364nH, C1=C2=0.02541pF, R$_S$=50Ω, R$_L$=50Ω).

Transducer power gain for the filter shown in Figure 6.31 is given in Figure 6.32
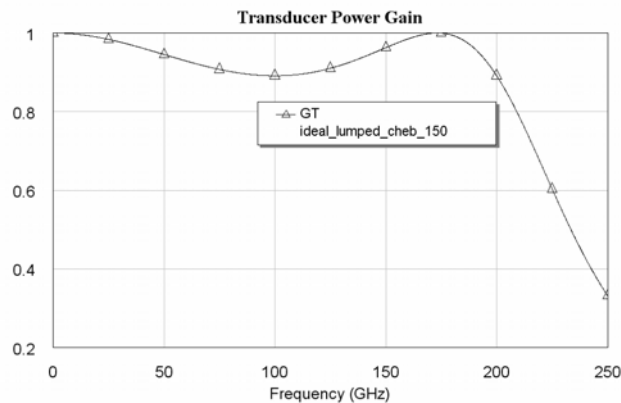
Figure 6.32 Transducer power gain for ideal lumped element Chebyshev filter ($f_n = 200GHz$, $R_n = 50\Omega$).

In Figure 6.33, practical lumped element Chebyshev filter is shown. In the circuit, air is selected as the dielectric material, so $E_r = 1$ is used. The height of the material and the thickness of the metal conductor is selected as $Th = 1000\mu m$ and $t = 1\mu m$, respectively. The width of the line is calculated by using AWR-TX Line program to obtain a 50Ω input impedance, since the normalization frequency R_n is 50Ω [61].
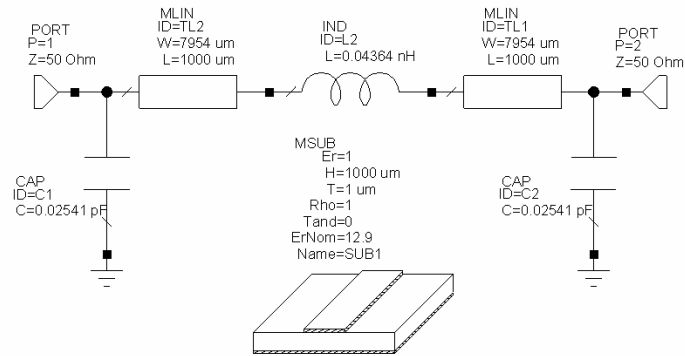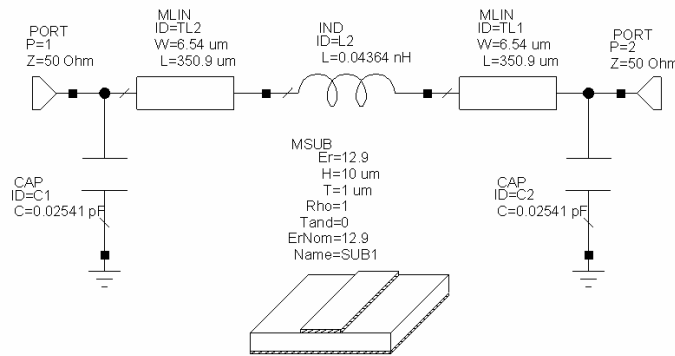

Figure 6.33 Practical lumped element Chebyshev filter

($f_n = 200GHz$, $R_n = 50\Omega$, $E_r = 1$)

(L=0.04364nH, C1=C2=0.02541pF, TL1=TL2=$7954x1000\mu m$, $E_r = 1$,

$Th = 1000\mu m$, $t = 1\mu m$, R$_S$=50Ω, R$_L$=50Ω).

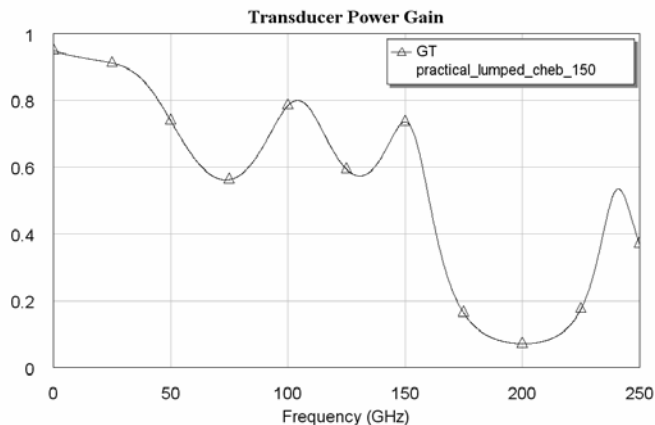In Figure 6.34, transducer power gain curve for practical lumped element Chebyshev filter can be seen.

Figure 6.34 Transducer power gain for practical lumped element Chebyshev filter

($f_n = 200GHz$, $R_n = 50\Omega$, $E_r = 1$).

To be able to reduce the line lengths, a dielectric material (GaAs) with $E_r = 12.9$ is used. The height of the material and the thickness of the metal conductor is selected as $Th = 10\mu m$ and $t = 1\mu m$, respectively. The width of the line is calculated by using AWR-TX Line program to obtain a 50Ω input impedance, since the normalization frequency R_n is 50Ω [61].

Figure 6.35 Practical lumped element Chebyshev filter

$(f_n = 200GHz , \ R_n = 50\Omega, \ E_r = 12.9)$

(L=0.04364nH, C1=C2=0.02541pF, TL1=TL2=$6.54x350.9\mu m$, $E_r = 12.9$,

$Th = 10\mu m$, $t = 1\mu m$, R$_S$=50Ω, R$_L$=50Ω).

In Figure 6.36, transducer power gain curve for practical lumped element Chebyshev filter can be seen.
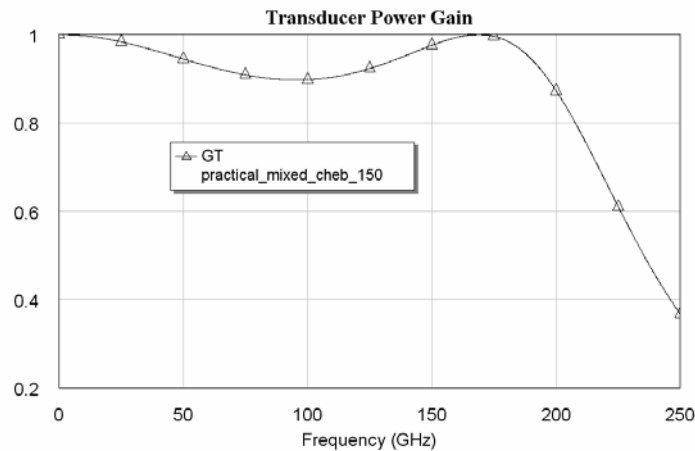

Figure 6.36 Transducer power gain for practical lumped element Chebyshev filter

$(f_n = 200GHz , \ R_n = 50\Omega, \ E_r = 12.9)$.

Let us now denormalize the obtained mixed element counterpart of the lumped element Chebyshev filter. Again $f_n = 200GHz$ and $R_n = 50\Omega$ are used as the denormalization frequency and resistance, respectively. In Figure 6.37, ideal mixed element Chebyshev filter is shown.
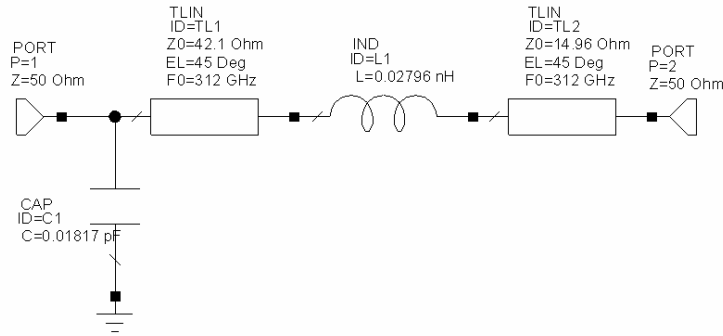
Figure 6.37 Ideal mixed element Chebyshev filter ($f_n = 200GHz$, $R_n = 50\Omega$)

(L=0.02796nH, C=0.01817pF, TL1=42.1Ω, TL2=14.96Ω, R$_S$=50Ω, R$_L$=50Ω).

Transducer power gain curve for the filter shown in Figure 6.37 is given in Figure 6.38.
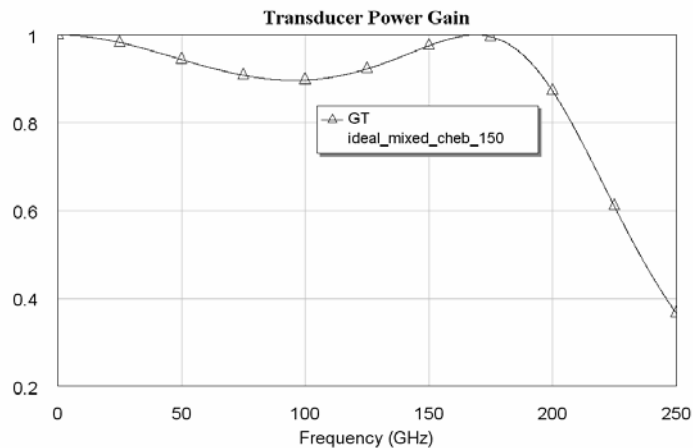
Figure 6.38 Transducer power gain for ideal mixed element Chebyshev filter

($f_n = 200GHz$, $R_n = 50\Omega$).

Practical mixed element Chebyshev filter is obtained as seen in Figure 6.39, after calculating the widths and the lengths of the transmission lines seen in Figure 6.37 via AWR-TX Line program [61].
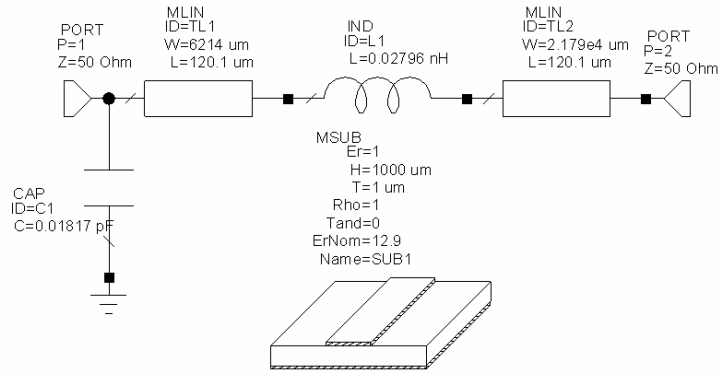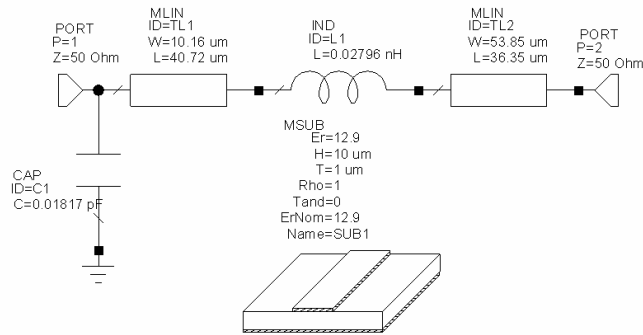
Figure 6.39 Practical mixed element Chebyshev filter

($f_n = 200GHz$, $R_n = 50\Omega$, $E_r = 1$)

(L=0.02796nH, C=0.01817pF, TL1=$6214.3x120.11\mu m$, TL2=$21789x120.11\mu m$,

$E_r = 1$, $Th = 1000\mu m$, $t = 1\mu m$, R$_S$=50Ω, R$_L$=50Ω).

In Figure 6.40, transducer power gain curve for practical mixed element Chebyshev filter can be seen.
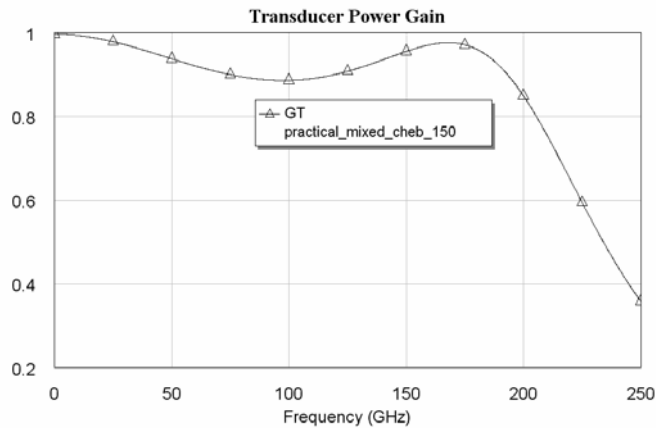

Figure 6.40 Transducer power gain for practical mixed element Chebyshev filter

($f_n = 200GHz$, $R_n = 50\Omega$, $E_r = 1$).

Again to be able to reduce the line lengths, a dielectric material (GaAs) with $E_r = 12.9$ is used. The height of the material and the thickness of the metal conductor is selected as $Th = 10\mu m$ and $t = 1\mu m$, respectively. The width of the line

is calculated by using AWR-TX Line program to obtain a 50Ω input impedance, since the normalization frequency R_n is 50Ω [61].

Figure 6.41 Practical mixed element Chebyshev filter

($f_n = 200GHz$, $R_n = 50\Omega$, $E_r = 12.9$)

(L=0.02796nH, C=0.01817pF, TL1=$10.16x40.72\mu m$, TL2=$53.85x36.35\mu m$,

$E_r = 12.9$, $Th = 10\mu m$, $t = 1\mu m$, R$_S$=50Ω, R$_L$=50Ω).

In Figure 6.42, transducer power gain curve for practical mixed element Chebyshev filter can be seen.

Figure 6.42 Transducer power gain for practical mixed element Chebyshev filter

($f_n = 200GHz$, $R_n = 50\Omega$, $E_r = 12.9$).

TPG curves for ideal/practical lumped and mixed element Chebyshev filters are given in Figure 6.43 with $E_r = 1$ and in Figure 6.44 with $E_r = 12.9$. It can be seen from the figure that practical mixed element filter response is very close to the ideal

86

curves; on the other hand practical lumped element filter curve is very different from the ideal ones. Also the circuit size of the mixed element filter is much smaller than the size of the lumped element filter. Transmission line lengths in the mixed element filter is about $120\mu m$ in Figure 6.39 and $40\mu m$ in Figure 6.41, but in the lumped element filter, they are $1000\mu m$ in Figure 6.33 and $350\mu m$ in Figure 6.35.
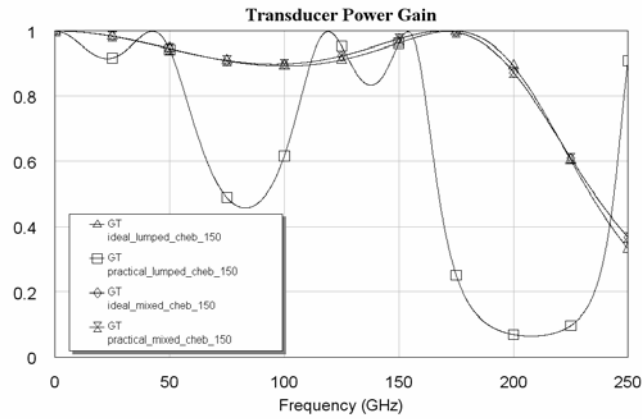

Figure 6.43 Transducer power gain curves for ideal and practical Chebyshev filters ($f_n = 200GHz$, $R_n = 50\Omega$, $E_r = 1$).
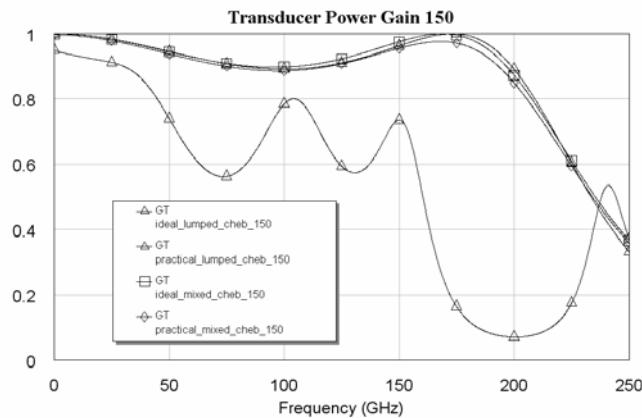
Figure 6.44 Transducer power gain curves for ideal and practical Chebyshev filters ($f_n = 200GHz$, $R_n = 50\Omega$, $E_r = 12.9$).

In the previous part, transmission line lengths between the lumped elements were desired to be $\lambda/2 = 1mm$, so the corresponding frequency was $150GHz$. If the

frequency again is reduced to $15GHz$ and the cut-uff frequency to $20GHz$, what are the performances of the lumped and mixed element filters? In Figure 6.45, obtained ideal lumped element Chebyshev filter can be seen in the case of $f_n = 20GHz$, $R_n = 50\Omega$.
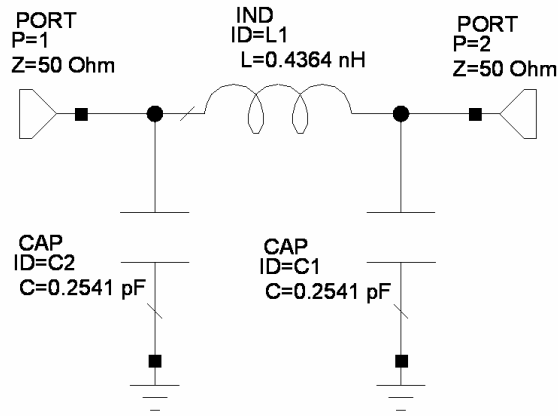

Figure 6.45 Ideal lumped element Chebyshev filter ($f_n = 20GHz$, $R_n = 50\Omega$)

(L=0.4364nH, C=0.2541pF, R$_S$=50Ω, R$_L$=50Ω).

Transducer power gain curve for the filter shown in Figure 6.45 is given in Figure 6.46.
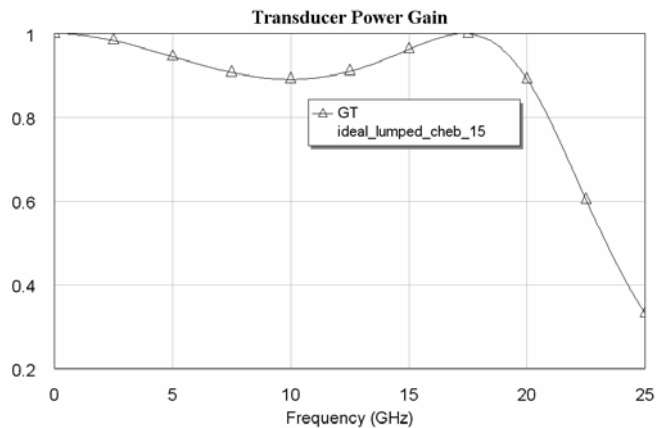
Figure 6.46 Transducer power gain for ideal lumped element Chebyshev filter

($f_n = 20GHz$, $R_n = 50\Omega$).

For this case, $\lambda/2 = 10mm$ length transmission lines must be used between the lumped elements. In the circuit, air is selected as the dielectric material, so $E_r = 1$ is

used. The height of the material and the thickness of the metal conductor is selected as $Th = 1000\,\mu m$ and $t = 1\,\mu m$, respectively. The width of the line is calculated by using AWR-TX Line program to obtain a 50Ω input impedance, since the normalization frequency R_n is 50Ω. The obtained practical lumped element Chebyshev filter is shown in Figure 6.47 [61].
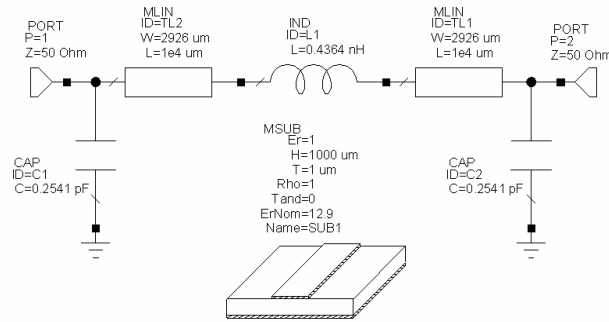

Figure 6.47 Practical lumped element Chebyshev filter

$(f_n = 20GHz,\ R_n = 50\Omega,\ E_r = 1)$

(L=0.4364nH, C=0.2541pF, TL1=TL2= $2926x10000\,\mu m$, $E_r = 1$, $Th = 1000\,\mu m$,

$t = 1\,\mu m$, R$_S$=50Ω, R$_L$=50Ω).

For practical lumped element Chebyshev filter, transducer power gain curve can be seen in Figure 6.48.
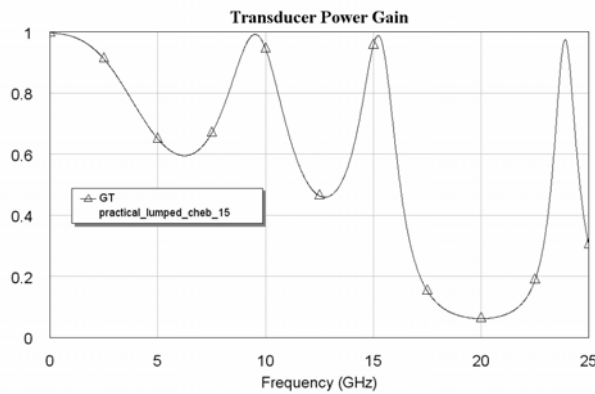

Figure 6.48 Transducer power gain for practical lumped element Chebyshev filter

$(f_n = 20GHz,\ R_n = 50\Omega,\ E_r = 1)$.

To be able to reduce the line lengths, a dielectric material (GaAs) with $E_r = 12.9$ is used. The height of the material and the thickness of the metal conductor is selected as $Th = 10\mu m$ and $t = 1\mu m$, respectively. The width of the line is calculated by using AWR-TX Line program to obtain a 50Ω input impedance, since the normalization frequency R_n is 50Ω [61].
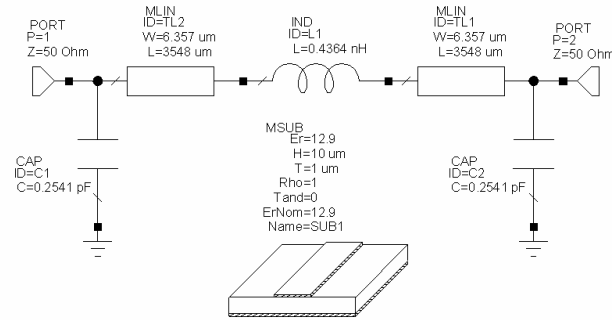

Figure 6.49 Practical lumped element Chebyshev filter

($f_n = 20GHz$, $R_n = 50\Omega$, $E_r = 12.9$)

(L=0.4364nH, C=0.2541pF, TL1=TL2=$6.357x3548\mu m$, $E_r = 12.9$, $Th = 10\mu m$,

$t = 1\mu m$, R$_S$=50Ω, R$_L$=50Ω).

For practical lumped element Chebyshev filter, transducer power gain curve can be seen in Figure 6.50.
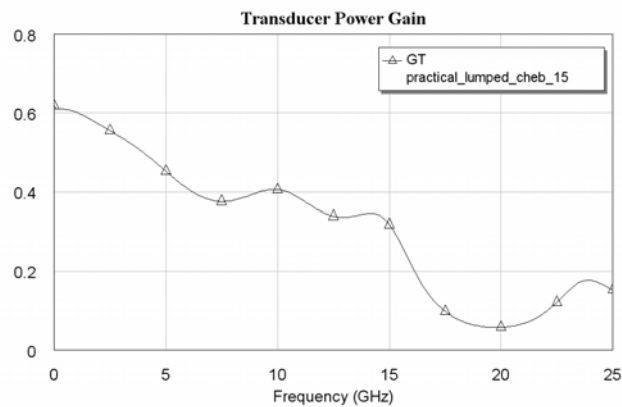

Figure 6.50 Transducer power gain for practical lumped element Chebyshev filter

($f_n = 20GHz$, $R_n = 50\Omega$, $E_r = 12.9$).

Again let us now denormalize the obtained mixed element counterpart of the lumped element Chebyshev filter. $f_n = 20GHz$ and $R_n = 50\Omega$ are used as the denormalization frequency and resistance, respectively. In Figure 6.51, ideal mixed element Butterworth filter is shown.
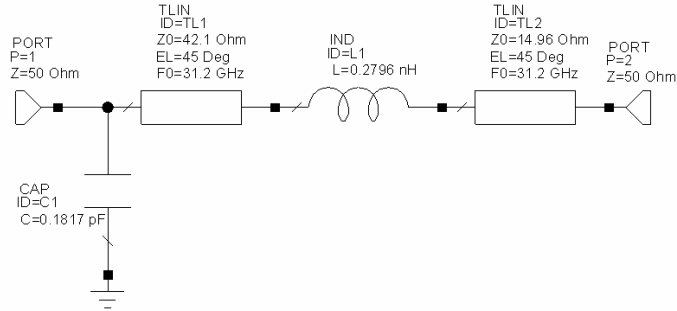

Figure 6.51 Ideal mixed element Chebyshev filter ($f_n = 20GHz$, $R_n = 50\Omega$) (L=0.2796nH, C=0.1817pF, TL1=42.1Ω, TL2=14.96Ω, R$_S$=50Ω, R$_L$=50Ω).

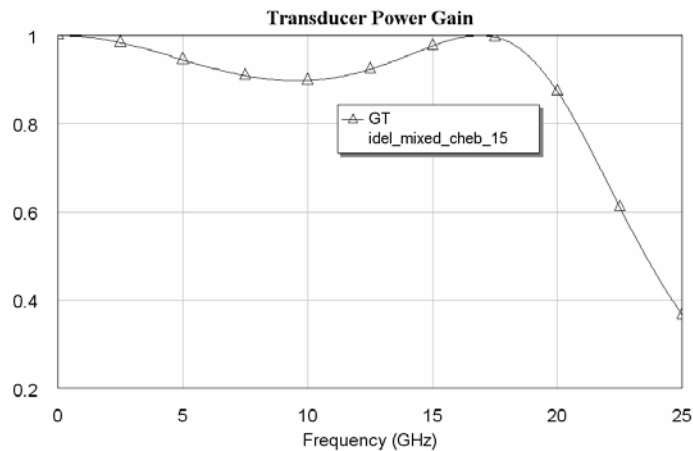In Figure 6.52, transducer power gain curve for the ideal mixed element Chebyshev filter can be seen.

Figure 6.52 Transducer power gain for ideal mixed element Chebyshev filter ($f_n = 20GHz$, $R_n = 50\Omega$).

Practical mixed element Chebyshev filter is obtained as seen in Figure 6.53, after calculating the widths and the lengths of the transmission lines seen in Figure 6.34 via AWR-TX Line program [61].
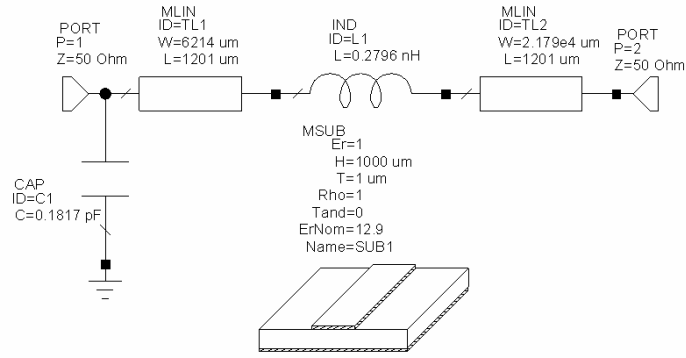
91

Figure 6.53 Practical mixed element Chebyshev filter

$$(f_n = 20GHz , \ R_n = 50\Omega, \ E_r = 1)$$

(L=0.2796nH, C=0.1817pF, TL1=$6214.3x1201.1\mu m$, TL2=$21789x1201.1\mu m$,

$E_r = 1$, $Th = 1000\mu m$, $t = 1\mu m$, R$_S$=50Ω, R$_L$=50Ω).

For practical mixed element Chebyshev filter, transducer power gain curve is given in Figure 6.54.
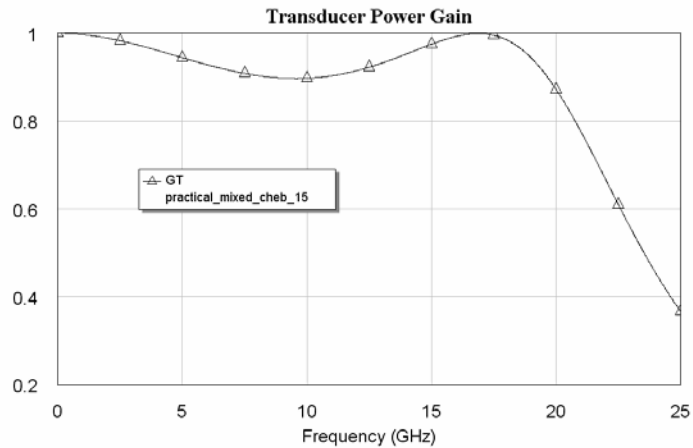

Figure 6.54 Transducer power gain for practical mixed element Chebyshev filter

$$(f_n = 20GHz , \ R_n = 50\Omega, \ E_r = 1).$$

Again to be able to reduce the line lengths, a dielectric material (GaAs) with $E_r = 12.9$ is used. The height of the material and the thickness of the metal conductor is selected as $Th = 10\mu m$ and $t = 1\mu m$, respectively. The width of the line

92

is calculated by using AWR-TX Line program to obtain a 50Ω input impedance, since the normalization frequency R_n is 50Ω [61].
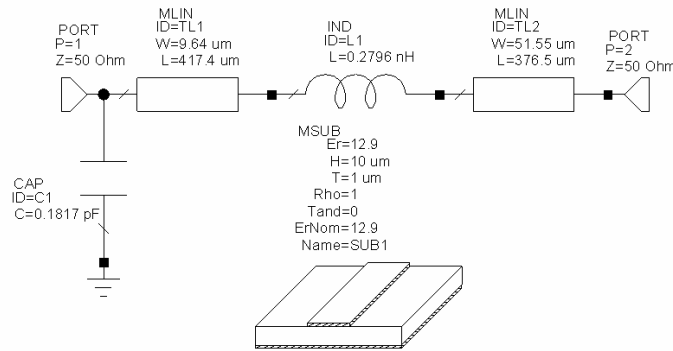

Figure 6.55 Practical mixed element Chebyshev filter

$$(f_n = 20GHz , \ R_n = 50\Omega, \ E_r = 12.9)$$

(L=0.2796nH, C=0.1817pF, TL1=$9.64x417.4\mu m$, TL2=$51.55x376.5\mu m$,

$E_r = 12.9$, $Th = 10\mu m$, $t = 1\mu m$, R_S=50Ω, R_L=50Ω).

For practical mixed element Chebyshev filter, transducer power gain curve is given in Figure 6.56.
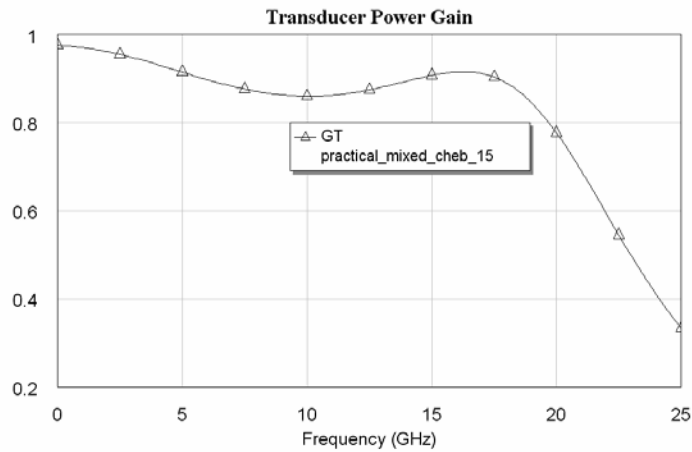

Figure 6.56 Transducer power gain for practical mixed element Chebyshev filter

$$(f_n = 20GHz , \ R_n = 50\Omega, \ E_r = 12.9).$$

TPG curves for ideal/practical lumped and mixed element Chebyshev filters are given in Figure 6.57 with $E_r = 1$ and in Figure 6.58 with $E_r = 12.9$. For this case, it

93

can be seen from the figure that practical mixed element filter response is very close to the ideal curves, but practical lumped element filter curve is very different from the ideal ones. Also the circuit size of the mixed element filter is much smaller than the size of the lumped element filter. Transmission line lengths in the mixed element filter is about $1200 \mu m$ in Figure 6.53 and $400 \mu m$ in Figure 6.55, but in the lumped element filter, they are $10000 \mu m$ in Figure 6.47 and $3550 \mu m$ in Figure 6.49.

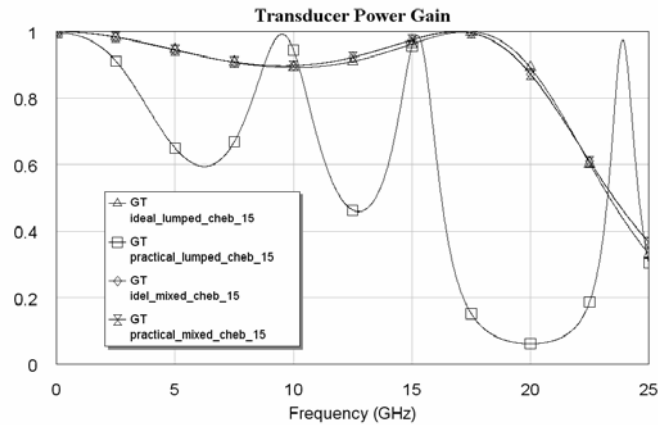Figure 6.57 Transducer power gain curves for ideal and practical Chebyshev filters ($f_n = 20GHz$, $R_n = 50\Omega$, $E_r = 1$).
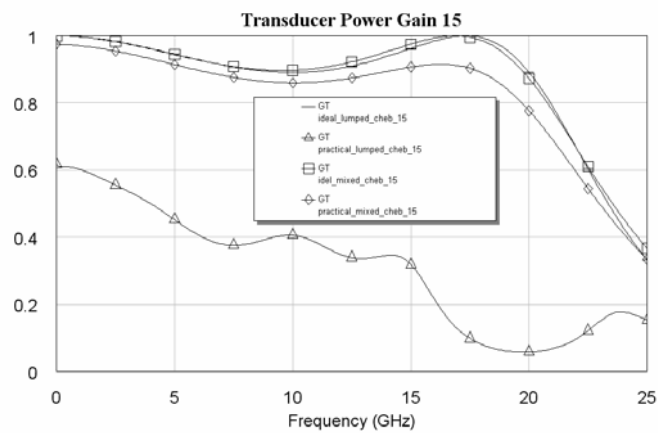

Figure 6.58 Transducer power gain curves for ideal and practical Chebyshev filters ($f_n = 20GHz$, $R_n = 50\Omega$, $E_r = 12.9$).

94

6.2.3 Lumped and Mixed Element Microwave Amplifiers

In section 5.3, after applying the proposed mixed modeling method, mixed element counterpart of the given microwave amplifier is reached. Let us now construct practical lumped and mixed element amplifiers by using the obtained prototype amplifiers.

In the practical lumped element amplifier, again small pieces of lines are added. These lines correspond to the connections of the lumped elements. The length of the lines are selected as $\lambda/2$. According to the Table 5.4, the corresponding frequency can be calculated as $f = \sqrt{f_L f_U} = \sqrt{6 \cdot 16} = 9.7980 GHz$.

After frequency and impedance denormalization ($f_n = 1GHz$, $R_n = 50\Omega$), ideal lumped element amplifier shown in Figure 6.59 is reached.

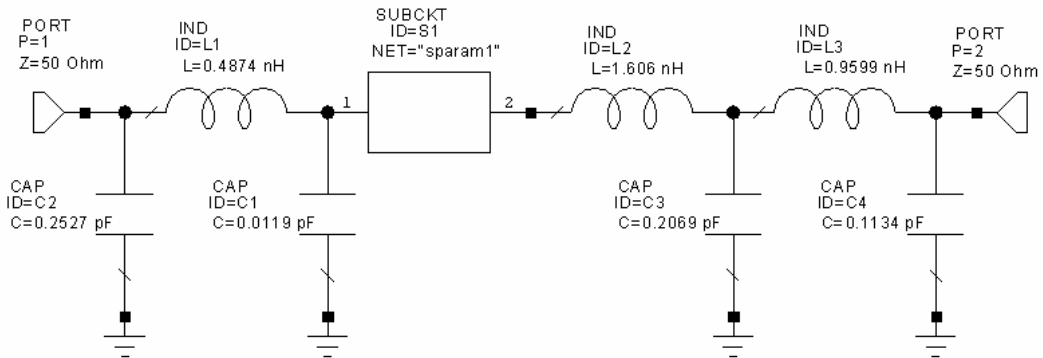Figure 6.59 Ideal lumped element amplifier
(L1=0.4874nH, L2=1.606nH, L3=0.9599nH, C1=0.0119pF, C2=0.2527pF,
C3=0.2069pF, C4=0.1134pF, Rs=50Ω, RL=50Ω).

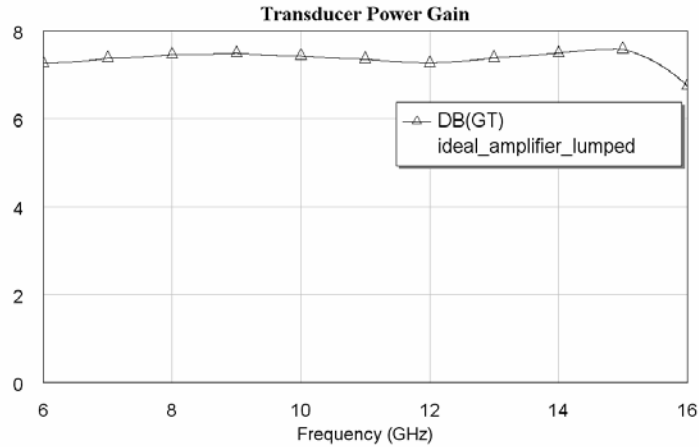Transducer power gain curve for the ideal lumped element amplifier is given in Figure 6.60.

Figure 6.60 Transducer power gain for ideal lumped element amplifier.

If $3744x15299\mu m$ length transmission lines (calculated via AWR-TX Line program [61], the input impedance of this line is 50Ω at $9.7980GHz$ with $\lambda/2$ length) are inserted between the lumped elements, the practical lumped element amplifier circuit seen in Figure 6.61 is obtained. In the circuit, air is selected as the dielectric material, so $E_r = 1$ is used. The height of the material and the thickness of the metal conductor is selected as $Th = 1000\mu m$ and $t = 1\mu m$, respectively. The width of the line is calculated by using AWR-TX Line program to obtain a 50Ω input impedance, since the normalization frequency R_n is 50Ω [61].
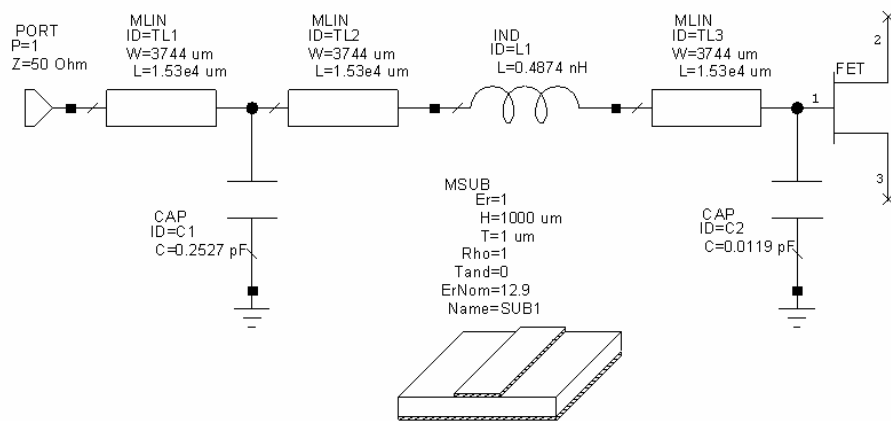

Figure 6.61 a) Practical input matching network of lumped element amplifier, Er=1
(L_1=0.4874nH, C_1=0.2527pF, C_2=0.0119pF, TL$_1$=TL$_2$=TL$_3$=$3744x15299\mu m$, Er=1,
Th=$1000\mu m$, t=$1\mu m$)

96

Figure 6.61 b) Practical output matching network of lumped element amplifier, Er=1
(L$_1$=1.606nH, L$_2$=0.9599nH, C$_1$=0.2069pF, C$_2$=0.1134pF,

TL$_1$=TL$_2$=TL$_3$=TL$_4$=$3744x15299\mu m$, Er=1, Th=$1000\mu m$, t=$1\mu m$, R$_S$=50Ω,

R$_L$=50Ω).

For practical lumped element amplifier, transducer power gain curve can be seen in
Figure 6.62.

Figure 6.62 Transducer power gain for practical lumped element amplifier, Er=1.

The length of the lines is very long, 15,299mm. If it reduced to 2mm, the amplifier
and its transducer power gain curve shown in Figure 6.63 and in Figure 6.64 are
obtained.
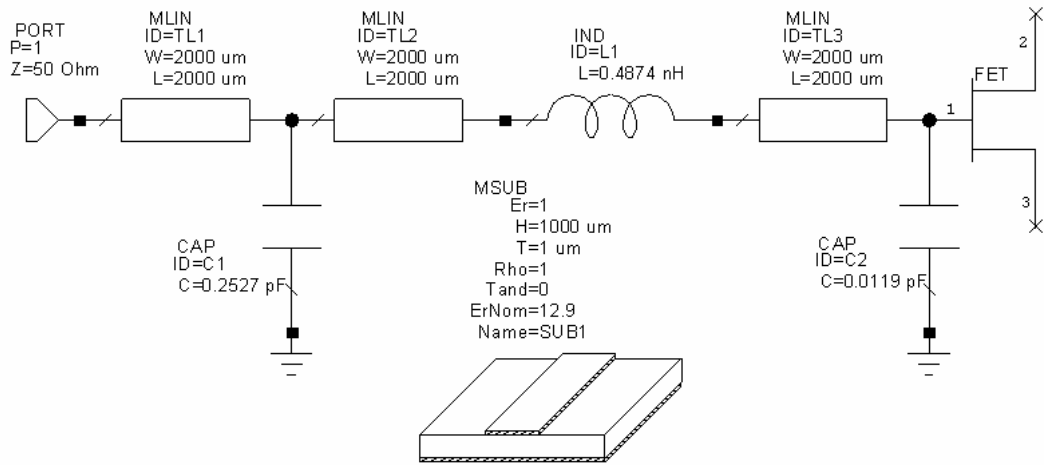
Figure 6.63 a) Practical input matching network of lumped element amplifier, Er=1,

TL=2x2mm, (L$_1$=0.4874nH, C$_1$=0.2527pF, C$_2$=0.0119pF,
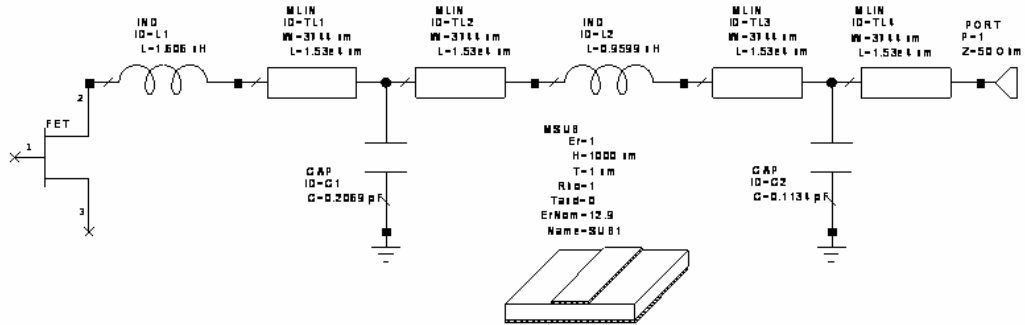
TL$_1$=TL$_2$=TL$_3$=2000x2000μm Er=1, Th=1000μm, t=1μm)

Figure 6.63 b) Practical output matching network of lumped element amplifier, Er=1

(L$_1$=1.606nH, L$_2$=0.9599nH, C$_1$=0.2069pF, C$_2$=0.1134pF,

TL$_1$=TL$_2$=TL$_3$=TL$_4$=2000x2000μm, Er=1, Th=1000μm, t=1μm, R$_S$=50Ω, R$_L$=50Ω).
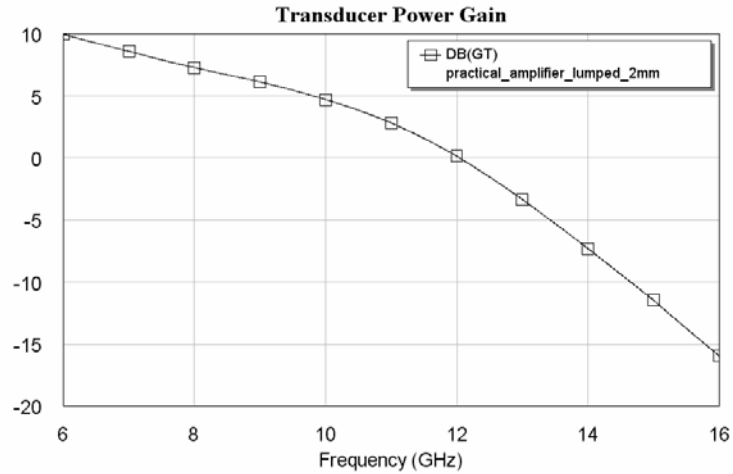
Figure 6.64 Transducer power gain for practical lumped element amplifier, Er=1,
TL=2x2mm.

If $30.011x11293\mu m$ length transmission lines (calculated via AWR-TX Line program [61], the input impedance of this line is 50Ω at $9.7980GHz$ with $\lambda/2$ length) are inserted between the lumped elements, the practical lumped element amplifier circuit seen in Figure 6.65 is obtained. In this case, a dielectric material (RT/Duroid 5880) with $E_r = 2.16$ is used. The height of the material and the thickness of the metal conductor is selected as $Th = 10\mu m$ and $t = 1\mu m$, respectively. The width of the line is calculated by using AWR-TX Line program to obtain a 50Ω input impedance, since the normalization frequency R_n is 50Ω [61].

Figure 6.65 a) Practical input matching network of lumped element
amplifier,Er=2.16 (L₁=0.4874nH, C₁=0.2527pF, C₂=0.0119pF,
TL₁=TL₂=TL₃=$30.01x11293\mu m$, Er=2.16, Th=$10\mu m$, t=$1\mu m$)

Figure 6.65 b) Practical output matching network of lumped element amplifier, Er=2.16 (L_1=1.606nH, L_2=0.9599nH, C_1=0.2069pF, C_2=0.1134pF, TL_1=TL_2=TL_3=TL_4=30.01x11293μm, Er=2.16, Th=10μm, t=1μm, R_S=50Ω, R_L=50Ω).

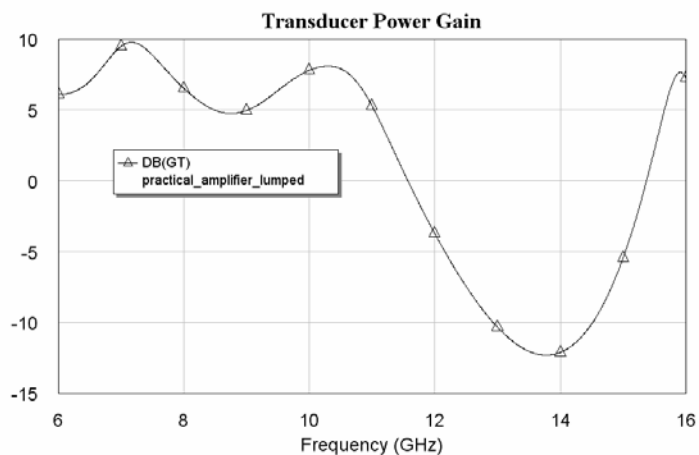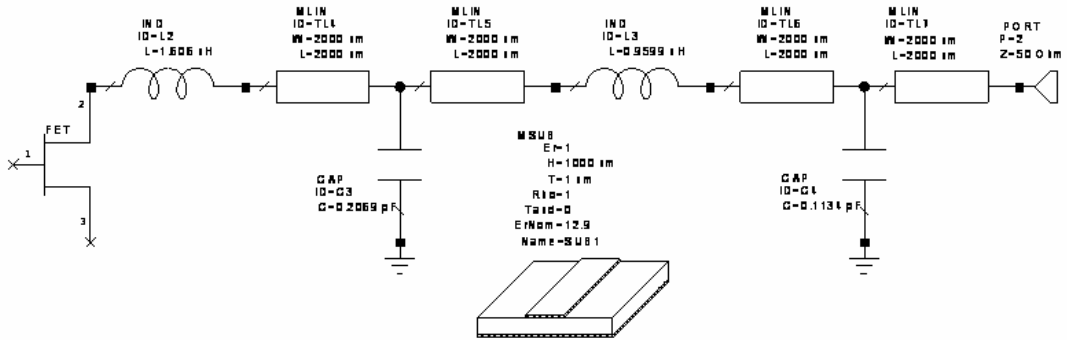For practical lumped element amplifier, transducer power gain curve can be seen in Figure 6.66.
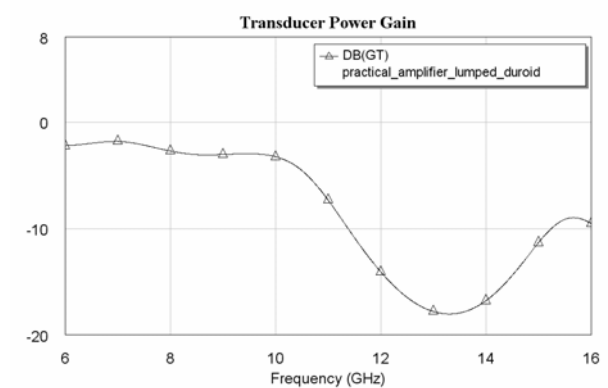
Figure 6.66 Transducer power gain for practical lumped element amplifier, Er=2.16.

Again the length of the lines is very long, 11,293mm. If it reduced to 2mm, the amplifier and its transducer power gain curve shown in Figure 6.67 and in Figure 6.68 are obtained.
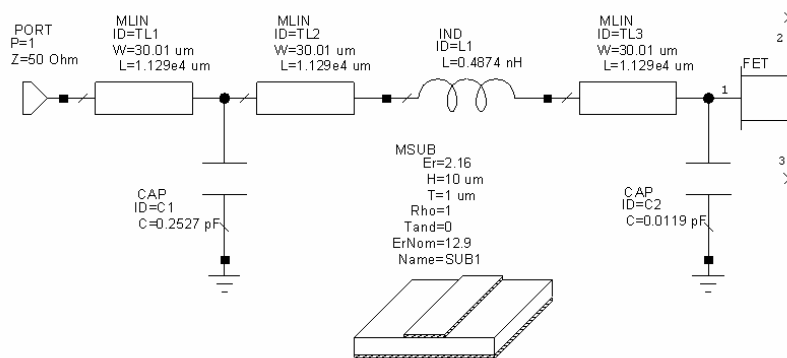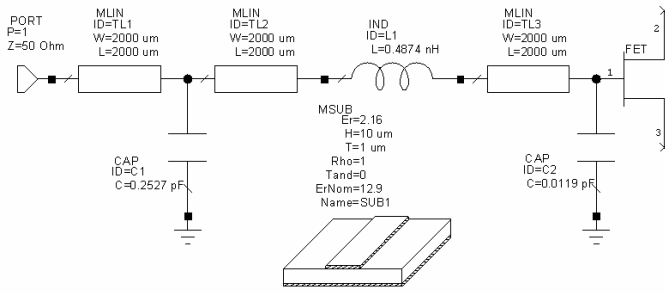
Figure 6.67 a) Practical input matching network of lumped element amplifier,Er=2.16, TL=2x2mm (L_1=0.4874nH, C_1=0.2527pF, C_2=0.0119pF, TL_1=TL_2=TL_3=2x2mm, Er=2.16, Th=10μm, t=1μm)
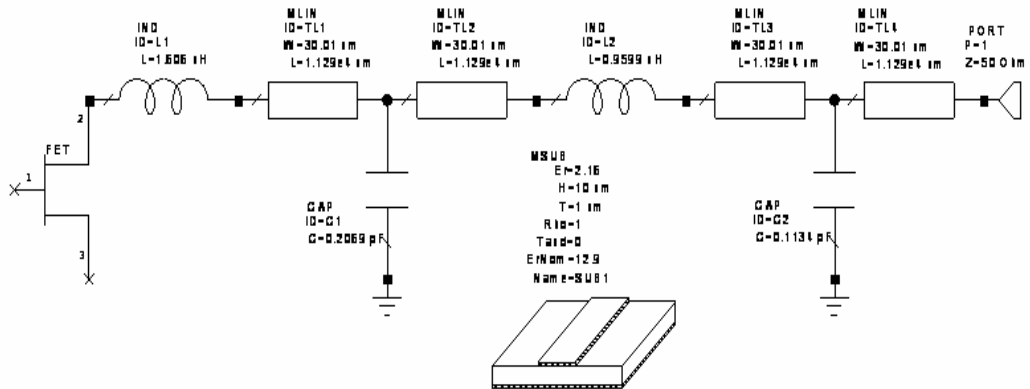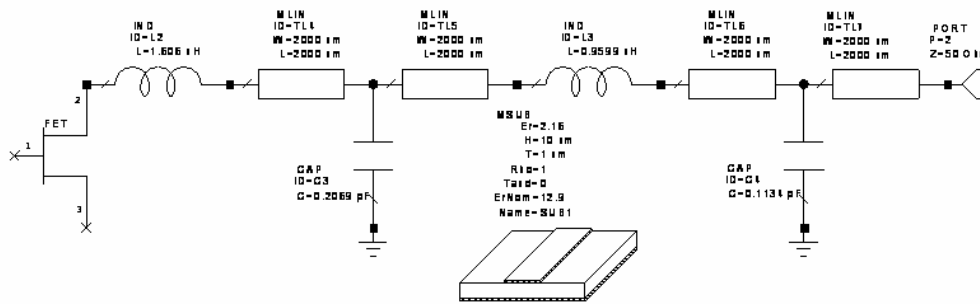

Figure 6.67 b) Practical output matching network of lumped element amplifier,Er=2.16, TL=2x2mm (L_1=1.606nH, L_2=0.9599nH, C_1=0.2069pF, C_2=0.1134pF, TL_1=TL_2=TL_3=TL_4=2x2mm, Er=2.16, Th=10μm, t=1μm, R_S=50Ω, R_L=50Ω).
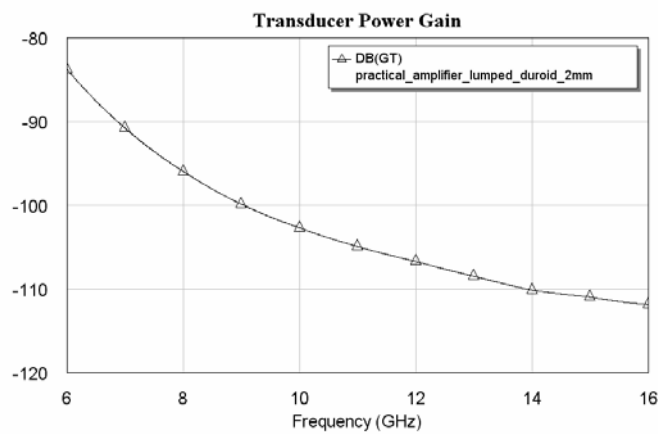
Figure 6.68 Transducer power gain for practical lumped element amplifier, Er=2.16, TL=2x2mm.

Let us now denormalize the obtained mixed element counterpart of the lumped element amplifier. $f_n = 1GHz$ and $R_n = 50\Omega$ are used as the denormalization frequency and resistance, respectively. In Figure 6.69, ideal mixed element amplifier is shown.
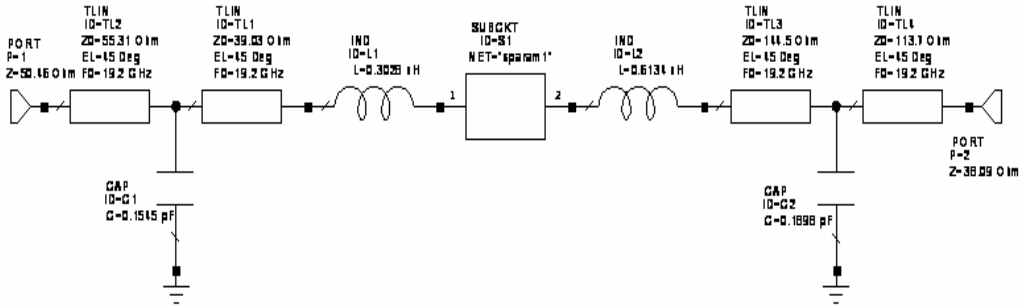
Figure 6.69 Ideal mixed element amplifier
(L1=0.3028nH, L2=0.6134nH, C1=0.1545pF, C2=0.1898pF, TL1=39.03Ω, TL2=55.31Ω, TL3=144.5Ω, TL4=113.7Ω, Rs=50.46Ω, RL=38.09Ω).

Transducer power gain curve for ideal mixed element amplifier is given in Figure 6.70.
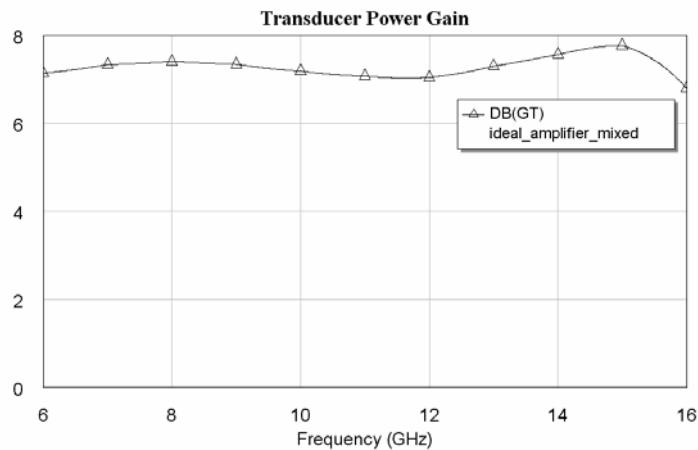
Figure 6.70 Transducer power gain for ideal mixed element amplifier.

Now let us obtain the practical mixed element amplifier circuit. In the circuit, air is selected as the dielectric material, so $E_r = 1$ is used. The height of the material and the thickness of the metal conductor is selected as $Th = 1000\mu m$ and $t = 1\mu m$,

respectively. The dimensions of the lines are calculated by using AWR-TX Line program [61]. As a result, the circuit seen in Figure 6.71 is obtained.
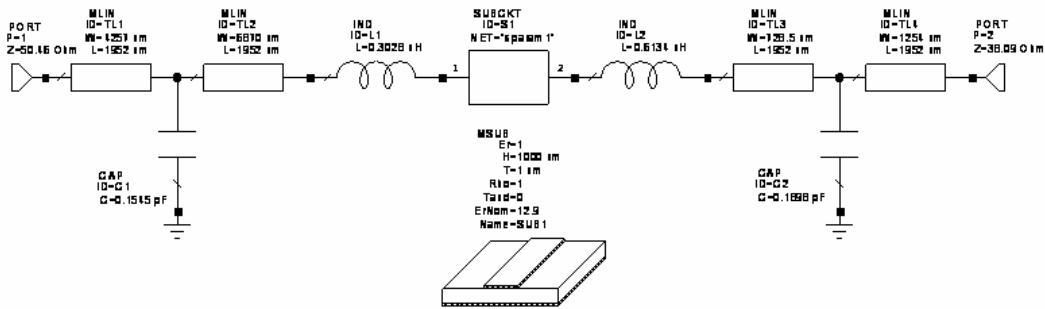
Figure 6.71 Practical mixed element amplifier, Er=1

(L1=0.3028nH, L2=0.6134nH, C1=0.1545pF, C2=0.1898pF,

$TL1 = 4256.7x1951.8\mu m$, $TL2 = 6870x1951.8\mu m$, $TL3 = 728.49x1951.8\mu m$,

$TL4 = 1253.5x1951.8\mu m$, Er=1, Th=$1000\mu m$, t=$1\mu m$, R_S=50.46Ω, R_L=38.09Ω).

In Figure 6.72, transducer power gain curve for the practical mixed element amplifier is given.
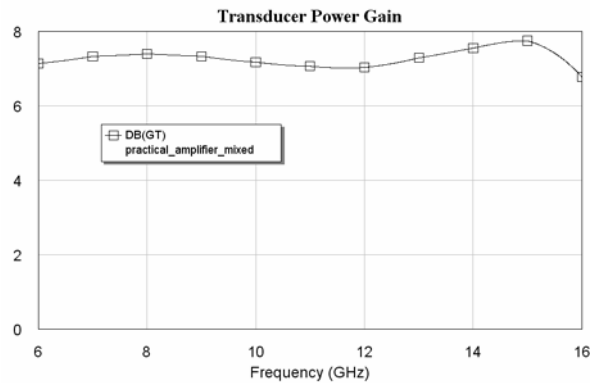
Figure 6.72 Transducer power gain for practical mixed element amplifier. Er=1.

Now let us obtain the practical mixed element amplifier circuit. In this circuit, a dielectric material (RT/Duroid 5880) with $E_r = 2.16$ is used. The height of the material and the thickness of the metal conductor is selected as $Th = 10\mu m$ and $t = 1\mu m$, respectively. The dimensions of the lines are calculated by using AWR-TX Line program [61]. As a result, the circuit seen in Figure 6.73 is obtained.
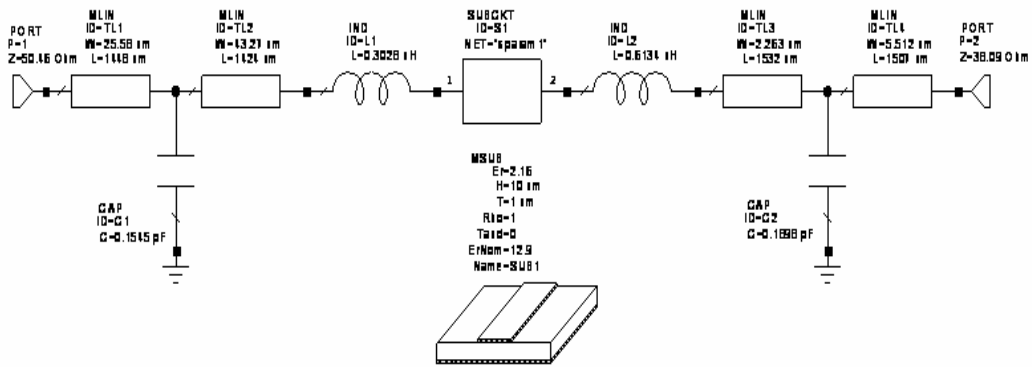
Figure 6.73 Practical mixed element amplifier, Er=2.16

(L1=0.3028nH, L2=0.6134nH, C1=0.1545pF, C2=0.1898pF, TL1=$25.58x1448\mu m$,

TL2=$43.27x1424\mu m$, TL3=$2.263x1532\mu m$, TL4=$5.512x1507\mu m$, Er=2.16,

Th=$10\mu m$, t=$1\mu m$, R_S=50.46Ω, R_L=38.09Ω).

In Figure 6.74, transducer power gain curve for the practical mixed element amplifier is given.
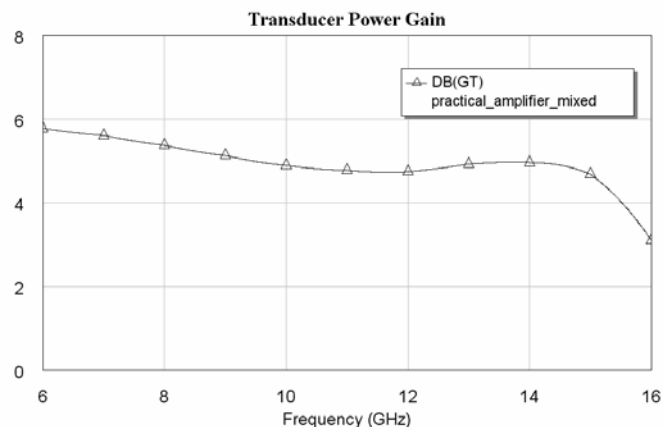
Figure 6.74 Transducer power gain for practical mixed element amplifier, Er=2.16.

TPG curves for ideal/practical lumped and mixed element amplifiers are given in Figure 6.75 with Er=1 and in Figure 6.76 with Er=2.16. It can be seen from the figure that practical mixed element amplifier response is close to the ideal curves, on the other hand practical lumped element amplifier curve is very different from the ideal ones. Also the circuit size of the mixed element filter is much smaller than the

size of the lumped element filter. Transmission line lengths in the mixed element filter is about $1950\mu m$ in Figure 6.71 and $1500\mu m$ in Figure 6.73, but in the lumped element filter, they are $15300\mu m$ in Figure 6.61 and $11290\mu m$ in Figure 6.65.
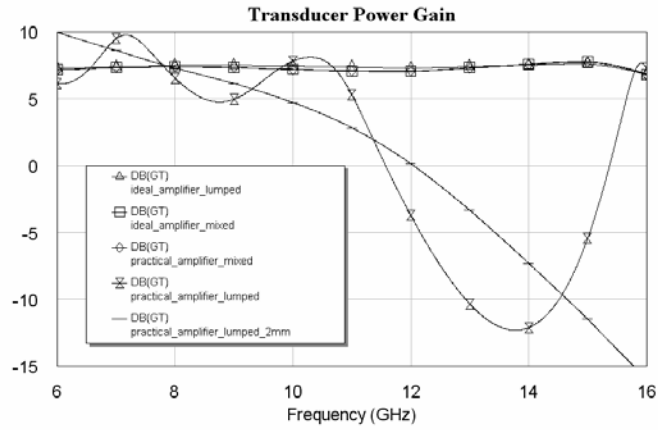
Figure 6.75 Transducer power gain curves for ideal and practical amplifiers, Er=1.
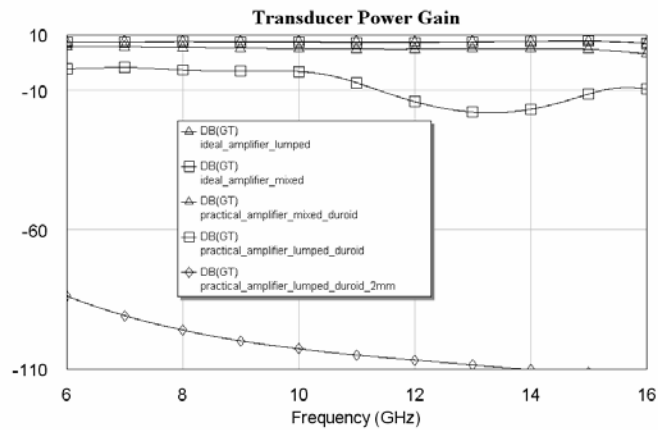
Figure 6.76 Transducer power gain curves for ideal and practical amplifiers,Er=2.16.

Chapter 7
Conclusions

There are several modeling techniques available in the literature, which utilize only one type of elements, lumped or distributed, in the circuit topology [48-51]. In practice however, especially in the microwave discrete or monolithic integrated circuit (MIC) design, the physical realization of ideal lumped and distributed network elements presents serious implementation problems. For a complete characterization of MIC layouts, it is therefore essential to model all the physical parameters and the possible parasitic effects inherent to the implementation process and to take them into account in the design procedure. This would in turn require the treatment of mixed lumped and distributed elements in the network design.

All the modeling methods in the literature use only lumped (or distributed) elements in the models. So in this study, the objective is to develop new modeling methods which use mixed lumped and distributed elements in the models. Therefore, the gap of the literature which covers passive one port models with two kinds of elements has been filled with this thesis.

Also it has been shown in the last chapter of the thesis that the performance of the mixed element circuits is better than that of the lumped element circuits. Since the transmission lines between the lumped elements in the mixed models have been considered as circuit elements, they have been optimized to make the performance better during the modeling or design process. So at the end of the process, the obtained performance curve is very close to the desired one. But since the lines in the lumped element circuits degraded the performance, the obtained curve is very

different from the desired one. Also the size of the mixed element circuits is smaller than that of the lumped element circuits. So by using the proposed method, smaller circuits and better performances have been obtained.

In most of the existing studies, the particular interest is devoted to a special network configuration. But from the technical realization point of view, it is a very useful structure, where in addition to the lumped reactances, the lossless two-port is allowed to contain ideal uniform lossless transmission lines in cascade mode. Therefore, one of the used mixed model topologies in this work is "Ladder Networks Connected with Unit Elements" and the second one is "Cascaded Lumped and Distributed Networks".

At the beginning of the proposed mixed modeling algorithm, user must supply measured reflection data (S) for the device to be modeled and measurement frequencies (ω), then select the transmission zeros locations of the model, namely, $f(p)$ and $f(\lambda)$ polynomials and the degree (namely number of lumped and distributed elements) of the model. Transmission zeros are located by examining $1 - |S|^2$ information and the degree is obtained by using the difference table based method proposed by Yarman and Kılınç in [50].

In the proposed modeling algorithm, input reflection function of the two-variable model has been utilized. It is necessary and sufficient for this kind of functions to be bounded real. In the algorithm, this has been achieved by using a strictly Hurwitz $g(p)$ and $g(\lambda)$ polynomials for lumped and distributed parts of the mixed model, respectively. So it has been guaranteed to obtain a realizable network function at the end of the modeling process.

An iterative process has been defined to obtain the best fit between the given reflectance data S and calculated input reflection function $S_{11}(p,\lambda)$ at each iteration. In this process, gradient (steepest descent) approach has been employed. To get a satisfactory result in a short time or to converge quadratically, initial values are

very important in gradient approach based algorithms. All gradient based methods have the properties that they generally converge only linearly to the solution, namely any starting value will give convergence So to make the convergence time shorter, suitable initial values must be obtained.

For one-variable (only lumped or only distributed elements) gradient based modeling algorithms, suitable initial value generation algorithm has been developed, but for two-variable modeling, this is not possible.

In the thesis, lumped element filters have been transformed to mixed element counterparts by using the proposed algorithm. In literature, there are not coefficient tables to design mixed element filters. So by using the proposed method, it is now possible to form such coefficient tables.

In this work, lossless two-variable models have been examined. Future work is to obtain lossy models and circuit models for active devices.

In this thesis, only two-variable, two-port circuit models have been obtained. I hope the work done in this thesis will be useful to get n-variable and /or m-port circuit models and transformation expressions from lumped/distributed networks to mixed networks and from mixed networks to lumped/distributed networks in the future.

References

[1]   Fano, R. M., "Theoretical Limitations on the Broadband Matching of Arbitrary Impedances", *J. Franklin Ins.* **249**, 57-83 (1950).

[2]   Youla, D. C., "A New Theory of Broadband Matching", *IEEE Trans. Circuit Theory* **11**, 30-50 (1964).

[3]   Chen, W. K., *Broadband Matching Theory and Implementations*, World Scientific, 1988.

[4]   Carlin, H. J., Amstutz, P., "On Optimum Broadband Matching", *IEEE Trans CAS* **28**, 401-405 (1981).

[5]   Yarman, B. S., *Broadband Matching a Complex Generator to a Complex Load*, Ph.D. Thesis, Cornell University, 1982.

[6]   Aksen, A., *Design of Lossless Two-ports with Mixed Lumped and Distributed Elements for Broadband Matching*, Ph.D. Thesis, Ruhr University, 1994.

[7]   Hatley, W. T., *Computer Analysis of Wideband Impedance Matching Networks*, Tech. Report, no:6657-2, Stanford University, Stanford Electronics Laboratories, CA., 1967.

[8]   Bode H., *Network Analysis and Feedback Amplifier Design*, Van Nostrand, NY, 1945.

[9]   Balabanian, N., Bickart, T. A., *Electrical Network Theory*, John Wiley&Sons Inc., 1969.

[10]   Belevitch, V., *Classical Network Theory*, Holden Day, San Francisco, CA., 1968.

[11]   Carlin, H. J., "A New Approach to Gain-Bandwidth Problems", *IEEE Trans. CAS* **23**, 170-175 (1977).

[12]   Youla, D. C., Saito, M., *Interpolation with Positive Real Functions*, Report no PIBMRI-1353-66, Microwave Research Inst., Polytechnic Institute of Brooklyn, 1966.

[13]   Smilen, L. I., *Interpolation on Real Frequency Axis*, Report no PIBMRI-1211-64, Microwave Research Inst., Polytechnic Institute of Brooklyn, 1964.

[14]   Baum., R. F., "A Contribution to the Approximation Problem", *Proc. IRE* **36(7)**, 863-869 (1948).

[15]   Kotiveeriah, P., *Rational Approximation of Frequency Data by Physically Realizable Network Functions*, Ph.D. Thesis, Cornell University, 1972.

[16]   Kody and Stoer, *Rational Chebyshev Approximation Using Interpolation*, Springer Verlag, Numerische Mat.Bd.9, 1966.

[17]   Carlin, H. J., Yarman, B. S., "The Double Matching Problem: Analytic and Real Frequency Solutions", *IEEE Trans. CAS* **30(1)**, 15-28 (1983).

[18]   Yarman, B. S., "A Simplified Real Frequency Technique for Broadband Matching a Complex Generator to a Complex Load", *RCA Review* **43**, 529-541 (1982).

[19]   Yarman, B. S., "Real Frequency Broadband Matching Using Linear Programming", *RCA Review* **43**, 626-654 (1982).

[20]   Beccari, C., "Broadband Matching Using the Real Frequency Technique", *IEEE Trans. CAS* **37**, 212-222 (1984).

[21]   Carlin, H. J., Civalleri, P., "On Flat Gain with Frequency-Dependent Terminations", *IEEE Trans. CAS* **32**, 827-839 (1985).

[22] Youla, D. C., Yarman, B. S., Carlin, H. J., "Double Broadband Matching and Problem of Reciprocal Reactance 2n-port Cascade Decomposition", *Int. J. Circuit Theory and App.* **12**, 269-281 (1984).

[23] Yarman, B. S., "Modern Approaches to Broadband Matching Problems", *Proc. IEE* **132**, 87-92 (1985).

[24] Yarman, B. S., *Geniş Bandlı Empedans Uyumlaştırma Devreleri ve Çok Katlı Mikrodalga Kuvvetlendiricileri Tasarım Yöntemleri*, TÜBİTAK Marmara Bilimsel ve Endüstriyel Araştırma Enstitüsü Elektronik Araştırma Bölümü. Bölüm içi rapor no.UI-85/01, 1985.

[25] Fettweis, A., Pandel, J., "Numerical Solution to Broadband Matching Based on Parametric Representation", *Arch. Elektr. Ubertrangung* **41**, 202-209 (1987).

[26] Yarman, B. S., Fettweis, A., "Computer Aided Double Matching via Parametric Representation of Brune Functions", *IEEE Trans. CAS* **37**, 212-222 (1990).

[27] Yarman, B. S., Aksen, A., "An Integrated Design Tool to Construct Lossless Matching Networks with Mixed Lumped and Distributed Elements", *IEEE Trans. CAS* **39(9)**, 713-723 (1992).

[28] Darlington, S., "Synthesis of Reactance 4 Poles", *MIT J. Mathematics and Physics* **18**, 257-353 (1939).

[29] Yarman, B. S., "Novell Circuit Configurations to Design Loss Balanced 0°-360° Digital Phase Shifters", *Archiv Für Elektronik und Übertragungstechnik* **45(2)**, 1991.

[30] Günel, M. T., *Yeni İki Global Karma Optimizasyon Algoritması ve bu Algoritmaların Mikrodalga Devrelerine Uygulanması*, Ph.D. Thesis, Istanbul Technical University, 1993.

[31] Kılınç, A., *Özgün Veri Modelleme Yöntemleri: Empedans ve Saçılma Parametreli Yaklaşımlar*, Ph.D. Thesis, Istanbul University, 1995.

[32]   Medley, M. W., *Microwave and RF Circuits: Analysis, Synthesis and Design*, Artech House Inc., 1993.

[33]   Sertbaş, A., *Genelleştirilmiş İki-Kapılı, İki-Değişkenli Kayıpsız Merdiven Devrelerin Tanımlanması*, Ph.D. Thesis, Istanbul University, 1997.

[34]   Richards, P. I., "Resistor-Transmission-Line Circuits", *Proc. IRE* **36**, 217-220 (1948).

[35]   Carlin, H. J., "Distributed Circuit Design with Transmission Line Elements", *Proc. IEEE* **3**, 1059-1081 (1971).

[36]   Matthaei, G., Young, L., Jones, E. M. T., *Microwave Filters, Impedance Matching Networks and Coupling Structures*, McGraw-Hill, NY, 1964.

[37]   Levy, R., "A General Equivalent Circuit Transformation for Distributed Networks", *IEEE Trans. Circuit Theory* **12**, 457-458 (1965).

[38]   Koga, T., "Synthesis of a Resistively Terminated Cascade of Uniform Lossless Transmission Lines and Lumped Passive Lossless Two-Ports", *IEEE Trans. Circuit Theory* **18**, 444-455 (1971).

[39]   Fettweis, A., "On the Scattering Matrix and the Scattering Transfer Matrix of Multidimensional Lossless Two-Ports", *Archiv Elektr. Übertrangung* **36**, 374-381 (1982).

[40]   Fettweis, A., "Some Properties of Scattering Hurwitz Polynomials", *Archiv Elektr. Übertragung* **38**, 171-176 (1984).

[41]   Fettweis, A., "A New Approach to Hurwitz Polynomials in Several Variables", *Circuits Systems and Signal Proc* **5**, 405-417 (1986).

[42]   Yarman, B. S., *Broadband Networks*, Wiley Encyclopedia of Electrical and Electronics Engineering, vol.II, pp.589-604, 1999.

[43]   Güneş, F., Çetiner, A., "A Novel Smith Chart Formulation of Performance Characterisation for a Microwave Transistor", *IEE Proc. Circuit Devices and Sys.*, **145(6)**, 419-429 (1998).

[44]   Yu, Q., Wang, J., Kuh, E., "Passive Multipoint Moment Matching Model Order Reduction Algorithm on Multiport Distributed Interconnect Networks", *IEEE Trans. on CAS* **46**, 140-160 (1999).

[45]   Mc Shane, E., Trivedi, M., Xu, Y., Khandewal, P., Mulay, A., Shenai, K., "One Chip Wanders", *IEEE Circ. & Devices, The Optoelectronics Magazine* **14(5)**, 35-42 (1998).

[46]   Sercu, S., Martens, L., "High-Frequency Circuit Modeling of Large Pin Count Packages", *IEEE Trans. on MTT* **45(10)**, 1897-1904 (1997).

[47]   O'Connor, C., "RFIC Receiver Technology for Digital Mobile Phones", *Microwave Journal* **40(7)**, 64-75 (1992).

[48]   Yarman, B. S., Aksen, A., "A Reflectance-Based Computer Aided Modeling Tool for High Speed/High Frequency Communication Systems", *Proc. of IEEE-ISCAS* **4**, 270-273 (2001).

[49]   Yarman, B. S., Aksen, A., Kılınç, A., "Immitance Data Modeling via Linear Interpolation Techniques", *Proc. of IEEE-ISCAS* **3**, 527-530 (2002).

[50]   Yarman, B. S., Kılınç, A., Aksen, A., "Immitance Data Modeling via Linear Interpolation Techniques: A Classical Circuit Theory Approach", *Int. J. of Circuit Theory and Applications* **32**, 537-563 (2004).

[51]   Yarman B. S**.**, Aksen A., Kılınç A., "An Immitance Based Tool for Modeling Passive One-Port Devices by Means of Darlington Equivalents", *Int.J.Electron.Commun.(AEÜ)* **55(6)**, 443-451 (2001)

[52]   Faires J. D., Burden R. L., *Numerical Methods,* Thomson Engineering, 2003.

[53]   Carlin H. J., Civalleri P. P., *Wideband Circuit Design,* Boca Raton: CRC Press LLC, 1998.

[54]   Şengül M., Aksen A., Yarman B. S., "Karışık Toplu ve Dağınık Devre Elemanları İçeren Merdiven Devrelerin Sentezi", *Elektrik-Elektronik-Bilgisayar Mühendisliği 11. Ulusal Kongresi ve Fuarı*, 2005.

[55]   Inder, B., Bhartia, P., *Microwave Solid State Circuit Design*, 2nd Edition, Wiley Interscience, 2003.

[56]   Wheeler, H. A., "Transmission Line Properties of Paralel Strips Separated by a Dielectric Sheet", *IEEE Trans. Microwave Theory Tech.* **13**, 172-185 (1965).

[57]   Wheeler, H. A., "Transmission Line Properties of a Strip on a Dielectric Sheet on a Plane", *IEEE Trans. Microwave Theory Tech.* **25**, 631-647 (1977).

[58]   Schneider, M. V., Glance, B., Bodtmann, W. F., "Microwave and Millimeter Wave Integrated Circuits for Radio Systems", *Bell Syst. Tech. J.* **48**, 1703-1726 (1969).

[59]   Hammerstad, E. O., "Equations for Microstrip Circuit Design", *Proceedings of the European Microwave Conference*, Microwave Exhibitors & Publishers, 268-272 (1975).

[60]   Hammerstad, E. O., "Accurate Models for Microstrip Computer-Aided Design", *Dig. IEEE Int. Microwave Symp.* 407-409 (1980).

[61]   AWR: Microwave   Office   of   Applied   Wave   Research   Inc.: www.appwave.com, 2006.

Curriculum Vitae

Publications

[1] Yarman B.S., Şengül M., Kılınç A., Aksen A., "Circuit Model for Given Reflectance Data Constructed with Mixed Lumped and Distributed Elements", *The Fourth International Workshop on Multidimensional (ND) Systems NDS 2005*, July 10-13 2005, Wuppertal, Germany.

[2] Yarman B.S., Şengül M., Kılınç A., Aksen A., "Reflectance Data Model with Mixed Lumped and Distributed Elements for Wireless Communication Systems", *European Conference on Circuit Theory and Design ECCTD 2005*, 29 August- 1 September 2005, Cork, Ireland.

[3] Şengül M., Aksen A., Yarman B.S., "Karışık Toplu ve Dağınık Devre Elemanları İçeren Merdiven Devrelerin Sentezi", *Elektrik-Elektronik-Bilgisayar Mühendisliği 11. Ulusal Kongresi ve Fuarı*, 22-25 Eylül 2005, Istanbul, Turkey.

[4]   Şengül M., Yarman B.S., "Real Frequency Technique without Optimization", *The Fourth International Conference on Electrical and Electronics Engineering ELECO 2005*, 7-11 December 2005, Bursa, Turkey.

[5]   Şengül M., Trabert J., Blau K., Yarman B.S., Hein M., "Power Transfer Networks at RF Frequencies - Roadmap to Design and Recommendations", *IEEE International Symposium on Circuits and Systems, ISCAS 2006*, Kos, Greece, May 21-24, 2006 (Accepted).

[6]   Yarman B.S., Şengül M., Kılınç A., "Design of Practical Matching Networks with Lumped Elements via Modeling", *IEEE Trans. On Circuits and Systems-I: Regular Papers*, (Submitted).